SEISMIC FRAGILITY ASSESSMENT OF AS-BUILT AND RETROFITTED BRIDGES USING FIBER REINFORCED ELASTOMERIC ISOLATOR

SEISMIC FRAGILITY ASSESSMENT OF AS-BUILT AND RETROFITTED BRIDGES USING FIBER REINFORCED ELASTOMERIC ISOLATOR

By

Seyyed Saber Ale Saheb Fosoul, M.Sc., B.Sc.

A Thesis Submitted to the School of Graduate

Studies in Partial Fulfilment of the Requirements for

the Degree

Doctor of Philosophy

McMaster University

Hamilton, Ontario, Canada

August 2022

Doctor of Philosophy (2022) (Civil Engineering)

McMaster University Hamilton, Ontario

TITLE: **Seismic Fragility Assessment of As-built and Retrofitted Bridges using Fiber Reinforced Elastomeric Isolator**

AUTHOR: **Seyyed Saber Ale Saheb Fosoul, M.Sc., B.Sc.**

SUPERVISOR: **Dr. Michael Tait, P.Eng.**

NUMBER OF PAGES: **xxi, 207**

Abstract

Highway bridges are considered to be one of the most susceptible constituents of transportation networks when they are subjected to severe natural hazards such as earthquakes and environmental exposures like subfreezing temperatures. To facilitate and enhance pre-hazard event mitigation and post-hazard emergency response strategies, probabilistic risk assessment methodologies have attracted increased attention, recently. Seismic fragility assessment is one of the probabilistic techniques which predicts the damage risk of the structure for a given hazard level. While fragility curves can be developed using different methods, such as expert-based, empirical, experimental, analytical, and hybrid, analytical fragility curves are perceived to be the most reliable and least biased technique. Seismic isolation systems are prevalently used in bridge structures to mitigate the damage risk of bridge components against natural hazards. However, the effectiveness of implementing recently emerged isolators such as Stable Unbonded Fiber Reinforced Elastomeric Isolators (SU-FREI) should be examined by developing analytical fragility curves of retrofitted bridges and quantifying the mitigation in the damage probability of different bridge components. In this regard, incorporating the Soil-Structure Interaction (SSI) is critical since the lateral response of bridges relies on the relative stiffness of bridge components, such as columns and isolators and the supporting soil. In addition, all bridge components are exposed to environmental stressors like subfreezing temperature that can alter the seismic response of bridges.

In the first phase of this thesis, a seismic fragility assessment is carried out on an existing multi-span continuous reinforced concrete bridge. Two bridge representations are

developed to simulate the as-built bridge along with its retrofitted counterpart utilizing SU-FREI. An Incremental Dynamic Analysis (IDA) is conducted using 45 synthetic ground motion records developed for eastern Canada and damage limit states are applied to generate fragility curves and determine the probability of damage to different bridge components. Bridges are analyzed in longitudinal and transverse directions, independently, and component- and system-level fragility curves are developed. In the second phase, the previously generated bridge models are expanded to incorporate the SSI effects by introducing the pile groups under piers and abutments. Several interactions including deck-abutment, abutment-embankment, pile-soil, and pile-soil-pile interactions are considered. A significant challenge in this phase is the accurate simulation of the lateral and vertical behavior of pile groups since all pile groups comprised of closely-spaced vertical and battered piles. A ground motion suite consisting of 45 ground motions has been selected, which reflects the seismicity of the bridge site. IDA is conducted to monitor the seismic performance of the bridge from the elastic linear region up to collapse. Fragility curves, which serve as an important decision-support tool have been developed to identify the potential seismic risk of the bridge. In the third phase, a multi-hazard assessment is carried out by conditioning the previously developed bridge models (i.e. monolithic fixed-base, isolated fixed-base, monolithic with SSI, and isolated with SSI) to a range of room and subfreezing temperatures and applying a seismic excitation, simultaneously. The cold temperature behavior of the constitutive materials of different bridge components, namely, concrete, reinforcing steel, rubber, and the supporting soil are studied and reflected in the

bridge models. IDA is performed and damage potential of different bridge components are quantified.

In summary, it is demonstrated that SU-FREI is a competing alternative for seismic isolation of bridges by offering potentially less manufacturing time and cost, lower weight, and easier installation which is an attractive feature for accelerated bridge construction applications. In all three phases, it is shown that the bridges which are isolated using SU-FREI have improved seismic performance in comparison with monolithic bridges by exhibiting lower probability of damage to the primary bridge components like columns and pile caps and transferring the damage to less important components such as abutments at which damage does not cause bridge closure. In addition, it is shown that seismic isolation using SU-FREI can effectively mitigate the seismic demand and damage potential of the constitutive components of a bridge supported by weak soil. While occurrence of seismic events along with an environmental stressor such as cold temperature can drastically jeopardize the functionality of a bridge supported by weak soil, it is demonstrated that seismic isolation using SU-FREI can significantly alleviate the probability of damage to bridge components.

Acknowledgements

I am grateful for the people who have supported me during my academic career. First and foremost, I would like to express my sincere gratitude to my outstanding supervisor, Dr. Michael Tait, for his continuous support, patience, encouragement, and guidance throughout the course of my PhD. His confidence in me from the beginning was stunning. By trusting me with covering his class on a handful of occasions and giving me free rein on my path through my research, he has taught me so much about what it means to be an independent researcher, educator, and a free thinker.

Special thanks are due to my supervisory committee members, Dr. Dimitrios Konstantinidis, Dr. Wael El-Dakhakhni, and Dr. Georgios Balomenos, for their generous encouragement, engagement, insights, and direction. I would like to thank Dr. Shahria Alam for reviewing my work and providing insightful comments as the external examiner.

My gratitude extends to the current and past staff in the Civil Engineering office, Joanne Gadawski, Sarah Sullivan, Tonya Antonecchia, Shannon Krasulja, Bethany Beierema, Morgan Shuker, Amelia Brooke, and Olivia Pare. You have impacted the lives of many other students and faculty as well, in ways that I am sure are not always noticed.

My parents, Nasrin and Mehdi, and my brother, Sadra, have always encouraged me to chase my dreams and to never give up when something is tougher or more difficult than expected. It is because of them and their sacrifices that they made for me that I have been able to follow my passions.

None of this would have been possible without the sacrifices made by and the continuous support of my loving wife, Saba, for which and whom I will be eternally grateful. Her love and confidence in me to finish this project and move forward more strongly than I ever have is testament to why I am so lucky to have her by my side. Together we will accomplish everything we can and will ever dream of.

Finally, I want to acknowledge my love for my daughter, Lianna, who is almost 18 months old at the time of writing, and the motivation that her arrival brought me to push through and finish this chapter of my life.

Co-Authorship

This thesis has been prepared in accordance with the regulations for a 'Sandwich' thesis format or as a compilation of papers stipulated by the Faculty of Graduate Studies at McMaster University. Chapters 2 through 4 have been published or submitted for publication in peer-reviewed journals, for which the numerical work was carried out solely by the author of this thesis. The work was all completed under the supervision, guidance, and review of Dr. Michael Tait. This thesis consists of the following manuscripts in the following chapters:

Chapter 2: Seismic performance assessment of an existing multi-span bridge in eastern Canada retrofitted with fiber reinforced elastomeric isolator
By Saber A. S. Fosoul and Michael Tait
Published in the *Canadian Journal of Civil Engineering*, In press.
doi: 10.1139/cjce-2021-0344

Chapter 3: Soil-pile-structure interaction effects on seismic demands and fragility estimates of a typical Ontario highway bridge retrofitted with fiber reinforced elastomeric isolator
By Saber A. S. Fosoul and Michael Tait
Published in *Soil Dynamics and Earthquake Engineering*, 151, 106967.
doi: https://doi.org/10.1016/j.soildyn.2021.106967

Chapter 4: Seismic fragility analysis of bridge-isolator-foundation-soil systems in subfreezing temperatures
By Saber A. S. Fosoul and Michael Tait
Submitted for review to the journal of *Engineering Structures.*

Contents

List of Tables

List of Figures

1 Introduction

1.1 Problem description and motivation

Highway bridges are perceived to be key components in transportation networks that must retain their functionality before, during, and after earthquakes to facilitate traffic flow, medical services, firefighting, and rescues. Quantifying the seismic behavior of these lifelines is imperative in pre-earthquake planning, and post-earthquake response of transportation systems. Earthquake-induced damage to bridges jeopardizes the immediate recovery efforts and can lead to structural failures, casualties, and socio-economic costs. Although western Canada commonly experiences larger number of seismic events, historic events such as Saguenay (M_s 5.8) and Ungava (M_s 6.3) in 1988 and 1989 raised awareness that seismic hazards extend eastward where seismic evaluation of highway bridges is traditionally neglected due to relatively lower seismicity. Furthermore, modern seismic design standards entail a comprehensive seismic performance assessment of conventionally designed bridges that are not necessarily meet ductile design provisions. Figure 1.1 demonstrates that more than 44% of existing bridges in Ontario have been built prior to 1970, before significant modifications to bridge design philosophies that followed the San Fernando earthquake (Zhang & Huo, 2009). Additionally, Figure 1.2 shows that more than 27% and 78% of the Ontario bridges have not experienced any major or minor rehabilitations, respectively, in the past 40 years. It should be noted that recently updated hazard levels (from 10% to 2% in 50 years probability of exceedance) along with the age and rehabilitation state of the Ontario bridges accentuates the immediate need for seismic evaluation of bridges in this province.

Investigating regional geology of eastern metropolitan areas of Canada reveals that several bridges are located in the regions with weak soil. For example, Ottawa is located on the Ottawa Valley Clay plain and the Russell and Prescott Sand plain, where the former is characterized by relatively thick deposits of sensitive marine clay, silt, and silty clay, and the latter is characterized by a sand mantle about 3 to 5 m thick overlying an extensive deposit of sensitive marine clay deposited within the Champlain Sea basin (Chapman & Putnam, 1984). Moreover, this region falls within the Western Québec (WQ) seismic zone that encompasses urban areas such as Ottawa, Montreal and Cornwall. Two major earthquakes in this zone includes the 1935 Témiscaming event which had a magnitude of 6.2, and the 1944 Cornwall-Massena event which had a magnitude of 5.6. The combined presence of weak supporting soil and seismic active zone underlines the need for nonlinear dynamic analysis of bridge structures in this region to evaluate the efficiency of the seismic performance of these bridges.

As shown in Figure 1.3, most metropolitan cities in Canada will experience subfreezing temperatures in the upcoming years. For example, in densely populated urban areas in eastern Canada, such as Ottawa, the projected average annual coolest minimum temperature may drop to -35ºC where the projected average annual number of -30ºC days may reach 10 to 20 days. Moreover, a historical investigation of the previous earthquakes demonstrates that major seismic events (e.g. the 2001 Nisqually earthquake in Washington, the 2017 central Italy earthquake, and the 2018 Alaska earthquake) occurred in cold wintry conditions. Extremely cold temperature alters the mechanical behavior of materials, namely, concrete, steel, soil, and rubber, and consequently, impacts the seismic

performance of structures. Therefore, continuous exposure of highway bridges to environmental stressors (e.g. subfreezing temperatures) and natural hazards (e.g. earthquakes) entails seismic risk evaluation and upgrading plans to mitigate the potential damage to this infrastructure.

Highway bridges play a pivotal role in facilitating an efficient commerce and commuting system between cities and across the country. However, these lifelines can easily turn into weak links when they are exposed to multitude hazards, such as, aging, earthquakes, and subfreezing temperatures. Probabilistic seismic risk assessment methods are paramount tools for enhancing prehazard and posthazard event mitigation and emergency response strategies of transportation systems. These methods include fragility estimates of bridge components subjected to a range of hazards. This thesis focuses on, first, probabilistic seismic performance assessment of existing bridges in Canada, second, implementing a retrofit method for improving the seismic response of the bridge, third, evaluating the seismic performance of the retrofitted bridge under imposed demands (e.g. presence of sensitive soil domain and earthquake events), and last, assessing the seismic performance of the existing and retrofitted bridges under a combination of natural hazards such as earthquakes, subfreezing temperatures and presence of a weak soil domain.

1.2 Seismic isolation for bridge structures

Seismic isolation is a response modification technique that decreases the seismic demands on bridges by decoupling the superstructure from the input excitation (Buckle, Constantinou, Dicleli, & Ghasemi, 2006; Ghobarah & Ali, 1988; Jangid, 2004; Siqueira, Sanda, Paultre, & Padgett, 2014; Wesolowsky & Wilson, 2003; Xiang & Alam, 2019).

This uncoupling is achieved by introducing a mechanical device with sufficiently large vertical but relatively low lateral stiffness between the superstructure and substructure. As shown in Figure 1.4, a monolithically connected deck-column system maximizes the earthquake-induced shear forces on the supporting columns resulting in plastic hinge formation in the column end zones. However, introducing the isolation system results in a significant decrease in the transferred shear force to the substructure and concentrates the lateral demand in the isolators. In addition to the supplemental damping provided by the isolation system, their relatively low stiffness elongates the fundamental natural vibration period of the bridge system to a value larger than the predominant ground motion periods of earthquake. These desirable characteristics of the isolation system makes them a viable approach for seismic retrofit of existing bridges.

1.2.1 Commonly employed seismic isolators

Seismic isolation systems are typically categorized into sliding and elastomeric where the former is referred to as a medium with sufficiently low coefficient of friction in the horizontal direction and the latter is comprised of intermittent layers of natural or synthetic elastomers and reinforcements (Buckle et al., 2006). Friction pendulum systems are the most common type of sliding system for bridge applications in North America. Depending on the number of sliding surfaces, these systems can be subcategorized into single, double or triple friction pendulum systems. The White River Bridge in Yukon, Canada, is an example of implementing a friction pendulum system to retrofit a bridge in Canada (Yasser M Al-Anany & Tait, 2017b). The majority of bridge isolators in North America are elastomeric-based isolators, such as lead rubber bearings (LRBs) or high-damping rubber

bearings (HDRBs) (J. M. Kelly & Konstantinidis, 2011; Kumar, Whittaker, & Constantinou, 2014). To accommodate relatively high vertical forces, these isolators are reinforced with either steel shims or fiber fabrics to prevent the elastomer layers from experiencing excessive bulging. Steel Reinforced Elastomeric Isolators (SREI) are typically fastened to the upper and lower supports using relatively thick steel end plates. As a result of this bonded behavior, tensile stresses may develop under lateral and rotational deformations resulting in a higher likelihood of delamination, particularly for aged isolators (Angelilli, 2007). The relatively heavy weight of SREI (due to thick end plates and reinforcing steel shims) along with the labor-intensive manufacturing process and high cost prevents these isolators from mass implementation.

Fiber Reinforced Elastomeric isolators (FREI) are a viable alternative to conventional SREI by offering less weight (by eliminating steel shims and end plates), cost-effective manufacturing process (produced in large sheets and waterjet cut to required size) and easy installation (unbonded vs. bonded). Extensive research efforts have demonstrated the superior mechanical properties of FREIs (Dezfuli & Alam, 2013; J. Kelly & Calabrese, 2012; J. M. Kelly, 2002; J. M. Kelly & Takhirov, 2001; Mordini & Strauss, 2008; Toopchi-Nezhad, Tait, & Drysdale, 2008; Van Engelen, Konstantinidis, & Tait, 2016). It should be pointed out that the most recent version of the Canadian Highway Bridge Design Code (CHBDC) (*Canadian Highway Bridge Design Code*, 2019) permits the use of FREI.

1.2.2 Unbonded Fiber-Reinforced Elastomeric Isolators (U-FREI)

A more recent development in the base isolation research introduces FREI in which elastomeric isolators are not attached to the superstructure and substructure and shear

forces are transferred by frictional force. If a FREI is able to maintain a positive tangential stiffness throughout its entire lateral displacement ranges, it is called a Stable Unbonded FREI (SU-FREI) (Pauletta, Cortesia, & Russo, 2015; Toopchi-Nezhad, Tait, & Drysdale, 2008). De Raaf et al. experimentally investigated the lateral stability of U-FREIs using dynamic and monotonic testing in order to evaluate the critical buckling load corresponding to zero lateral tangential stiffness. U-FREIs are found resistant to buckling instability since they were able to undergo large lateral displacements (up to 3.50 t_r, where t_r is the total rubber thickness) under large compressive stresses (up to 18.5 MPa).

Rollover

A unique behavior of SU-FREI that is expected to be observed under large shear strains is rollover. As the SU-FREI is subjected to incremental lateral displacements, conditioned on using an appropriate aspect ratio, the contact faces with the horizontal loading support begin to lift off and a rollover mechanism develops (Toopchi-Nezhad et al., 2008). Aspect ratio, the ratio of the total length (in direction of lateral loading) to the total height of the isolator, is the controlling parameter for maintaining the lateral stability. Van Engelen et al. (Van Engelen, Tait, & Konstantinidis, 2014) have shown that SU-FREI remains stable over a large range of lateral displacements if the aspect ratio is approximately larger than 2.60. For aspect ratios larger than 10, it was found that rollover mechanism can be disregarded, and SU-FREI can be modeled as an element with constant effective stiffness. Figure 1.5 shows that the more rollover continues, the more effective lateral stiffness decreases. At a sufficiently large lateral displacement, the onset of full rollover is observed, and lateral stiffness increases.

Full rollover

A condition in which the vertical faces of isolator attain a full contact with upper and lower loading plates is called full rollover. This unique behavior is critically important in preventing the isolator from experiencing excessive lateral displacements and prevents the occurrence of negative lateral tangential stiffness (de Raaf, Tait, & Toopchi-Nezhad, 2011).

This softening and stiffening regime of SU-FREI implies that they can serve as adaptive seismic devices in order to meet different performance levels, making them an ideal passive control device. At very low displacements (e.g. small service loads), the large initial stiffness of the isolator effectively decreases the vibration transmissibility. In moderate to large displacements (e.g. earthquake, etc.), the isolator operates in its softening regime which maximizes the seismic efficiency of the system by reducing its lateral stiffness. Under large displacements, the stiffening regime controls the excessive displacement of the superstructure and provides a self-restraint mechanism.

SU-FREI under vertical, lateral and rotational loads

Bridge isolators usually experience vertical (e.g. gravity loads), lateral (e.g. seismic loads, traffic loads, creep, shrinkage, thermal expansion/contraction, etc.), rotational (live traffic loads, misalignment during installation, etc.) loads and a combination of these loads throughout their lifetime (AASHTO, 2012; *Canadian Highway Bridge Design Code*, 2019; D. J. Lee, 1994). Several numerical and experimental studies have been conducted in order to scrutinize the response of SU-FREI. Conducting a set of experimental test on SU-FREI

Toopchi-Nezhad et al. (Toopchi-Nezhad et al., 2008) revealed that the vertical stiffness of SU-FREI is sufficiently large and lateral cyclic testing did not degrade the vertical stiffness of the isolator. A 10% increase in the effective damping occurred as a result of a 50% increase in the vertical load. Al-Anany et al. (Y. Al-Anany, Van Engelen, & Tait, 2017) investigated the effect of loading rate as well as lateral displacement on the vertical response of FREI. It is shown that vertical loading frequency has a larger effect on FREI with lower shape factors. Vertical stiffness, compression modulus, vertical frequency, and damping are also shown to be insensitive to lateral offset.

Focusing on bridge applications, the rotational behavior of SU-FREI compared to bonded FREI is investigated both numerically and experimentally by Al-Anany and Tait (Yasser M Al-Anany & Tait, 2015). It is shown that unbonded FREI demonstrates lower stress demand on both the elastomer and the fiber reinforcement with respect to similar bonded FREI. It is concluded that negligible slippage at the top and bottom surfaces occur since the vertical response of both isolators were comparatively similar. Moreover, the unbonded FREI demonstrated a higher rotational capacity (i.e. higher angles of rotation) compared to bonded FREI. In another study by Al-Anany and Tait (Yasser M Al-Anany & Tait, 2017a), viability of FREI as bridge isolators has been investigated through assessing their behavior under different loading scenarios. Results show that while increasing applied vertical load leads to an increase in vertical stiffness, it decreases the lateral stiffness. Moreover, static rotation decreases the vertical stiffness at lower vertical loads (due to lift-off) where it does not affect the vertical stiffness at higher vertical loads. Lateral offset up to 0.5% has no significant effect on vertical behavior. The effect of vertical load, lateral

offset, and static and cyclic rotation on the response of FREI with various geometrical properties has been investigated by Al-Anany and Tait (Yasser M Al-Anany & Tait, 2017b). It is shown that lateral stiffness is directly related to rotation (due to loss of contact and reduction in shear area). In addition, the effect of rotational deformation on the effective lateral stiffness is found to be negligible under large lateral displacements. Finally, the dissipated energy is found to be insensitive to rotation.

Low temperature behavior of SU-FREI is investigated by Sciascetti and Tait (Sciascetti, 2017), where quarter scale SU-FREI is conditioned under a range of subfreezing temperatures and exposure durations. It is shown that while the cold temperature results in stiffening of the FREI, the lateral performance of the FREI remains acceptable.

Research findings have shown superior advantages of FREI in comparison with SREI, including low weight, ease of installation, enhanced damping properties, potential for mass production, lower compressive stress demand and increased seismic isolating efficiency by means of rollover (de Raaf et al., 2011; Foster, 2012; Toopchi-Nezhad, Drysdale, & Tait, 2009; Toopchi-Nezhad et al., 2008; Toopchi-Nezhad, Tait, & Drysdale, 2009). It should be highlighted that using of fabric reinforcement instead of conventional steel shims is permitted in most recent versions of CAN/CSA-S6 (*Canadian Highway Bridge Design Code*, 2019) and AASHTO-LRFD (AASHTO, 2012).

1.3 Seismic risk assessment of bridges

Evaluating the seismic risk assessment of bridges can be conducted by establishing a relationship between different intensity levels and the probability of exceeding certain

damage states. In the context of probabilistic risk analysis, probabilistic seismic demand models (PSDMs) are versatile tools for describing the seismic demand of different bridge components in terms of the earthquake intensity and for deriving analytical fragility functions, accordingly. Developing a PSDM can be performed using a cloud approach, or multi-stripe analysis, both of them employing a nonlinear time history analysis (NLTHA) (Mangalathu & Jeon, 2019). In the cloud approach, the bridge is analyzed using un-scaled ground motion records and the PSDM is established by the linear regression of engineering demand parameters (EDPs) and the intensity measure (IM) in a lognormal space. In the stripe analysis, ground motion records are scaled to the same intensity levels in order to determine the probability distribution of the EDPs. In the IDA approach, monotonically increasing ground motion records are applied to a bridge and probabilistic mean and standard deviation are determined using simple statistical calculations. Unlike the PSDM method, IDA is computationally expensive. However, no priori assumptions are required in IDA for probabilistic distribution of seismic demand (Zhang & Huo, 2009). In addition, IDA demonstrates the performance of the bridge and its constitutive components over a vast range of earthquake intensities including rare and severe ground motions. More importantly, IDA accounts for the effect of record-to-record variability, which is perceived to be the most important source of uncertainty (Dolsek, 2009). Several researchers have used IDA for investigating the seismic performance and reliability of bridges. Zhang et al. (Zhang, Huo, Brandenberg, & Kashighandi, 2008) used IDA to develop fragility curves for six classes of straight bridges in California. Abdel-Mohti and Pekcan (Abdel-Mohti & Pekcan, 2013) developed fragility curves for post-tensioned reinforced concrete box-girder

highway bridges in California using IDA. Tehrani and Mitchell (Tehrani & Mitchell, 2013) applied IDA to investigate the effect of different earthquake types on the seismic performance of a typical highway bridge. Fosoul and Tait (A. S. Fosoul & Tait, 2020, 2021b; Fosoul & Tait, 2021) have investigated the seismic performance of existing and retrofitted bridges utilizing IDA.

1.3.1 Fragility functions

Fragility curves describe the conditional probability of exceedance from a certain damage state for a given ground motion intensity which can be generally expressed as $P [DS_i | IM = y]$ where y is the realized condition of the ground intensity measure (Kevin Rory Mackie & Stojadinović, 2005). The seismic vulnerability of a structure can be described by fragility curves developed using different methodologies, namely, expert based, experimental, empirical, hybrid, and analytical. While the first four approaches deemed to be cumbersome in terms of the amount of information and experience needed for developing fragility curves, the analytical approach is readily feasible by characterizing and quantifying the seismic demand and capacity of a structure. Furthermore, in regions with a low seismicity where the seismic bridge damage records are scarce, such as in the United States (Choi, DesRoches, & Nielson, 2004; Hwang, Jernigan, & Lin, 2000; Nielson & DesRoches, 2007a; Pan, Agrawal, & Ghosn, 2007) or Eastern Canada (Tavares, Padgett, & Paultre, 2012), analytical approaches are advantageous. Moreover, the analytical approach is less biased and is capable of considering all types of uncertainty (Muntasir Billah & Shahria Alam, 2015). Several studies are conducted on the seismic vulnerability of bridge structures (Cardone & Gesualdi, 2012; Hwang et al., 2000; Nielson &

DesRoches, 2007b). However, most of the studies on the existing bridges have been focused on analyzing generic idealized bridges (K. Mackie & Stojadinović, 2003; Yi, Kim, & Kushiyama, 2007) and limited number of fragility curves have been developed for real bridges (Lupoi, Franchin, & Pinto, 2007; Shinozuka, Feng, Lee, & Naganuma, 2000). Similarly, there are a few studies on fragility analysis of isolated bridges (Alam, Bhuiyan, & Billah, 2012; Siqueira et al., 2014).

Assuming a lognormal distribution for both demand and capacity due to their inherent randomness, the bridge component fragility curves can be computed in closed forms as follows:

$$P\,[DS|IM]=\Phi\left[\frac{\ln\left(\frac{S_D}{S_C}\right)}{\sqrt{\beta_{D|IM}^2+\beta_C^2}}\right]$$

where Φ is standard normal cumulative distribution function; S_C and β_C are median and logarithmic standard deviation for capacity; S_D and $\beta_{D|IM}$ are median and logarithmic standard deviation for demand. System-level fragility curves, however, are perceived to be more insightful for evaluating bridge safety in comparison with component fragility curves (Xiang & Alam, 2019). The vulnerability of overall bridge system can be estimated using upper and lower first order bounds of fragility. Given that the system is configured in series, the component fragilities should be combined and implemented in the following expression:

$$\max_{i=1:n}\left[P\left(F_{comp_i}\right)\right]\leq P\left(F_{sys}\right)\leq 1-\Pi_{i=1}^{n}\left[1-P\left(F_{comp_i}\right)\right]$$

where $P(F_{comp\_i})$ and $P(F_{sys})$ are probabilities of damage for component i and the overall system, respectively. It should be pointed out the series configuration of the structural component implies that a failure in every structural component corresponds to the failure of the overall system. The lower bound of fragility represents the case in which the demands placed on the bridge components are fully correlated, whereas the upper bound assumes zero correlation between the bridge components (Xiang & Alam, 2019).

1.3.2 Seismic risk assessment of bridge-isolator-foundation-soil systems

Investigating the seismic performance of bridges with incorporation of the Soil-Structure Interaction (SSI), has long attracted the interest of research community (Kevin R. Mackie, Lu, & Elgamal, 2012; Stefanidou, Sextos, Kotsoglou, Lesgidis, & Kappos, 2017; Xie, Zhang, & Huo, 2018). However, there is no consensus on the impact of this interaction on the seismic performance of bridges. For example, Mylonakis et al. (Mylonakis & Gazetas, 2000) have demonstrated that incorporating SSI does not necessarily lead to smaller response as opposed to the prevailing view in structural engineering that including SSI effects is always beneficial. This is even more complicated for an isolated bridge located on soft soil. Therefore, SSI effects are commonly ignored in the seismic assessment of isolated bridges (Dicleli, Albhaisi, & Mansour, 2005). While several studies have been conducted on incorporating the SSI effects in seismic performance of bridges (Carbonari, Morici, Dezi, Gara, & Leoni, 2017; Elgamal, Yan, Yang, & Conte, 2008; González et al., 2019), a fewer number of studies, in part, have explored the seismic performance of isolated bridges (Yasser M. Al-Anany, Moustafa, & Tait, 2018; Castaldo & Priore, 2018). The complicated multi-parametric nature of bridge-isolator-foundation-soil systems along

with their high degree of nonlinearity and excessively large computational cost has resulted in an inadequate number of studies being conducted on these systems (Dai, Rojas, Shi, & Tan, 2018; Ucak & Tsopelas, 2008; Wang, Padgett, & Dueñas-Osorio, 2012). To alleviate this relatively computational burden, these studies typically utilize simplification techniques such as using a two degree of freedom linear elastic models (Vlassis & Spyrakos, 2001), lumped spring models (Dicleli et al., 2005), and closed-form solutions (Ucak & Tsopelas, 2008) to simulate the SSI effect. However, the standing question is the extent to which these simplification techniques result in biased structural response and how the inherent nonlinearity in the soil domain interacts with the high nonlinearity in the isolation system, particularly, in large seismic events.

1.3.3 Seismic risk assessment of bridge-isolator-foundation-soil systems in subfreezing temperature

The complex problem of bridge-isolator-foundation-soil systems can be even more complicated when multitude hazards (e.g. subfreezing temperature, earthquake, hurricane, etc.) occur simultaneously. Investigating the mechanical behavior of the constitutive bridge materials such as concrete, steel, rubber and soil has demonstrated that in cold temperature: compressive and tensile strength, bond strength, Poisson's ratio, and elastic modulus on concrete will increase (Filiatrault & Holleran, 2001; G. C. Lee, Shih, & Chang, 1988); yield and ultimate tensile strength of steel increases while its ductility decreases (Filiatrault & Holleran, 2001; Whiteley, Armstrong, & Welburn, 1982); soil shear strength and stiffness increases (Sritharan, Suleiman, & White, 2007; Suleiman, Sritharan, & White, 2006); and rubber, as the main constituent of elastomeric isolator, may undergo significant thermal

stiffening (Cardone & Gesualdi, 2012; Murray & Detenber, 1961; Sciascetti & Tait, 2019; Stevenson, 1986). While evaluating the seismic performance of bridges is a multicomponent problem and the effect of subfreezing temperature on all constitutive bridge components must be taken into account, most of studies in this domain are limited to evaluating the performance of the bridge where only the isolation system is conditioned in cold temperatures. Using a deterministic framework, a few studies have been conducted to verify the change in the elastomeric response of isolators caused by the modification of mechanical properties at low temperatures (Deng, Gan, Hayashikawa, & Matsumoto, 2020; Okui, Nakamura, Sato, & Imai, 2019; Warn & Whittaker, 2006). To incorporate the effect of uncertainties and better comprehension of the seismic performance some studies have investigated the cold temperature seismic performance of bridges in a probabilistic framework (A. S. Fosoul & Tait, 2021a; Bandini, Siqueira, Padgett, & Paultre, 2022; Billah & Todorov, 2019; Nassar, Guizani, Nollet, & Tahan, 2019). However, these studies have used either simplistic approaches (e.g. single degree of freedom models, neglecting the cold temperature behavior of all bridge materials such as concrete or steel, etc.) or adoption of discrete temperature scenarios (i.e. summer and winter).

1.4 Research objectives

This thesis utilizes a comprehensive seismic performance of a conventionally designed bridge in Ontario, Canada, in order to shed light on the seismic performance of continuous reinforced concrete bridges located in seismic active zones, supported by relatively weak soil, and exposed to subfreezing temperatures. The scope of the research work has been set to achieve the following objectives:

1. Evaluating the seismic performance of a conventionally designed bridge in Ontario, Canada, as a representative of more than 44% percent of the bridges in this province by developing component- and system-level fragility curves and implementing SU-FREI as a viable seismic retrofit method to mitigate the seismic demand on the bridge and determining the efficiency of this system by quantifying the damage potential of different bridge components.
2. Quantifying the effectiveness of using seismic isolation systems for an existing bridge supported by weak soil.
3. Evaluating the cold temperature seismic behavior of the as-build and retrofitted bridges by performing IDA and fragility analysis in order to determine the probability of damage to different bridge components under a vast range of subfreezing temperatures and earthquake intensities.

1.5 Organization of the Thesis

This thesis is presented as a sandwich thesis through which the research objectives presented above are addressed in one or more of the journal articles included as chapters of the thesis. Chapter 2 to Chapter 4 are prepared to be standalone journal manuscripts, therefore, each chapter contains its own introduction, conclusion and references.

Chapter 2 of this thesis addresses the first research objective. This chapter starts with developing a comprehensive 3D nonlinear finite element model of a conventionally designed multi-span reinforced concrete bridge. An IDA is carried out using 45 synthetic ground motion records specifically developed for eastern Canada. Predefined damage states and acceptance criteria for different bridge components are applied and component-

and system-level fragility curves are developed. To improve the seismic performance of the bridge, a type of isolation system called SU-FREI is designed and implemented in the finite element model to gauge the extent to which the isolation system mitigates the seismic demand on the bridge. An IDA is performed with the same ground motion records and fragility curves are developed.

Chapter 3 of this thesis addresses the second research objective. The effectiveness of seismic isolation systems is a function of the relative stiffness between the superstructure, isolation layer, substructure, and supporting soil. Since the bridge in this study is supported by a set of closely spaced pile groups located on sensitive clay, incorporating the SSI was inevitable. To this end, pile groups (including vertical and battered piles) are added to the finite element bridge model and effects of soil-foundation-pile and pile-soil-pile interactions are accounted for. Component-level fragility curves are developed through utilizing IDA using 45 synthetic ground motion records and damage potential of different bridge components are investigated for the as-built and retrofitted bridge.

Chapter 4 of this thesis addresses the third research objective; In this chapter the low temperature mechanical behavior of constitutive materials of bridge components, namely, concrete, reinforcing steel, rubber, and soil is investigated and appropriate low temperature mechanical models are adopted. The bridge is conditioned on a range of temperatures from room to -37 ºC and different exposure durations from 1 to 28 days. An IDA is conducted on four bridge representations, namely, monolithic fixed-base, isolated fixed-base, monolithic bridge supported by pile groups, and isolated bridge supported by pile groups.

Component-level fragility curves are developed for different bridge components and probability of damage to bridge is investigated.

Chapter 5 concludes the thesis, summarizes the findings of this research, and outlines directions for future research.

References

A. S. Fosoul, S., & Tait, M. (2020). *Seismic fragility assessment of an existing multi-span isolated bridge in Eastern Canada*. Paper presented at the 8th International Conference on Advanced Composite Materials in Bridges and Structures, Sherbrooke, Canada.

A. S. Fosoul, S., & Tait, M. (2021a). *Seismic fragility assessment of isolated bridges in cold regions: A case study for eastern Canada*. Paper presented at the 17th World Conference on earthquake Engineering, Sendai, Japan.

A. S. Fosoul, S., & Tait, M. (2021b). *Seismic performance assessment of an isolated bridge-soil-foundation system*. Paper presented at the 17th World Conference on Earthquake Engineering, Sendai, Japan.

AASHTO. (2012). American Association of State Highway and Transportation Officials. *Washington, DC*.

Abdel-Mohti, A., & Pekcan, G. (2013). Effect of skew angle on seismic vulnerability of RC box-girder highway bridges. *International Journal of Structural Stability and Dynamics, 13*(06), 1350013. doi:10.1142/s0219455413500132

Al-Anany, Y., Van Engelen, N., & Tait, M. (2017). Vertical and Lateral Behavior of Unbonded Fiber-Reinforced Elastomeric Isolators. *Journal of Composites for Construction, 21*(5), 04017019.

Al-Anany, Y. M., Moustafa, M. A., & Tait, M. J. (2018). Modeling and Evaluation of a Seismically Isolated Bridge Using Unbonded Fiber-Reinforced Elastomeric Isolators. *Earthquake Spectra, 34*(1), 145-168. doi:10.1193/072416eqs118m

Al-Anany, Y. M., & Tait, M. J. (2015). A numerical study on the compressive and rotational behavior of fiber reinforced elastomeric isolators (FREI). *Composite Structures, 133*, 1249-1266.

Al-Anany, Y. M., & Tait, M. J. (2017a). Experimental assessment of utilizing fiber reinforced elastomeric isolators as bearings for bridge applications. *Composites Part B: Engineering, 114*, 373-385.

Al-Anany, Y. M., & Tait, M. J. (2017b). Fiber reinforced elastomeric isolators for the seismic isolation of bridges. *Composite Structures, 160*, 300-311.

Alam, M. S., Bhuiyan, M. R., & Billah, A. M. (2012). Seismic fragility assessment of SMA-bar restrained multi-span continuous highway bridge isolated by different laminated rubber bearings in medium to strong seismic risk zones. *Bulletin of Earthquake Engineering, 10*(6), 1885-1909.

Angelilli, C. J. (2007). *Surveillance of the performance of elastomeric bearings on Marylands concrete bridges*: University of Maryland, College Park.

Bandini, P. A. C., Siqueira, G. H., Padgett, J. E., & Paultre, P. (2022). Seismic Performance Assessment of a Retrofitted Bridge with Natural Rubber Isolators in Cold Weather

Environments Using Fragility Surfaces. *Journal of Bridge Engineering, 27*(6), 04022040. doi:doi:10.1061/(ASCE)BE.1943-5592.0001873

Billah, A. H. M. M., & Todorov, B. (2019). Effects of subfreezing temperature on the seismic response of lead rubber bearing isolated bridge. *Soil Dynamics and Earthquake Engineering, 126*, 105814. doi:https://doi.org/10.1016/j.soildyn.2019.105814

Buckle, I., Constantinou, M., Dicleli, M., & Ghasemi, H. (2006). Seismic Isolation of Highway Bridges.

Canadian Highway Bridge Design Code. (2019). Canadian Standard Association.

Carbonari, S., Morici, M., Dezi, F., Gara, F., & Leoni, G. (2017). Soil-structure interaction effects in single bridge piers founded on inclined pile groups. *Soil Dynamics and Earthquake Engineering, 92*, 52-67. doi:https://doi.org/10.1016/j.soildyn.2016.10.005

Cardone, D., & Gesualdi, G. (2012). Experimental evaluation of the mechanical behavior of elastomeric materials for seismic applications at different air temperatures. *International Journal of Mechanical Sciences*, *64*(1), 127-143.

Castaldo, P., & Priore, R. L. (2018). Seismic performance assessment of isolated bridges for different limit states. *Journal of civil structural health monitoring*, *8*(1), 17-32.

Chapman, L., & Putnam, D. (1984). The Physiography of Southern Ontario, Ontario Geological Survey Special. *Queen's Printer, Toronto, Ontario, 270*.

Choi, E., DesRoches, R., & Nielson, B. (2004). Seismic fragility of typical bridges in moderate seismic zones. *Engineering Structures, 26*(2), 187-199.

Dai, W., Rojas, F., Shi, C., & Tan, Y. (2018). Effect of soil structure interaction on the dynamic responses of base isolated bridges and comparison to experimental results. *Soil Dynamics and Earthquake Engineering, 114*, 242-252.

de Raaf, M. G., Tait, M. J., & Toopchi-Nezhad, H. (2011). Stability of fiber-reinforced elastomeric bearings in an unbonded application. *Journal of Composite materials, 45*(18), 1873-1884.

Deng, P., Gan, Z., Hayashikawa, T., & Matsumoto, T. (2020). Seismic response of highway viaducts equipped with lead-rubber bearings under low temperature. *Engineering Structures, 209*, 110008. doi:https://doi.org/10.1016/j.engstruct.2019.110008

Dezfuli, F. H., & Alam, M. S. (2013). Multi-criteria optimization and seismic performance assessment of carbon FRP-based elastomeric isolator. *Engineering Structures, 49*, 525-540.

Dicleli, M., Albhaisi, S., & Mansour, M. (2005). Static soil–structure interaction effects in seismic-isolated bridges. *Practice Periodical on Structural Design and Construction, 10*(1), 22-33.

Dolsek, M. (2009). Incremental dynamic analysis with consideration of modeling uncertainties. *Earthquake Engineering & Structural Dynamics, 38*(6), 805-825.

Elgamal, A., Yan, L., Yang, Z., & Conte, J. P. (2008). Three-dimensional seismic response of Humboldt Bay bridge-foundation-ground system. *Journal of Structural Engineering, 134*(7), 1165-1176.

Filiatrault, A., & Holleran, M. (2001). *Characteristics of reinforced concrete bridge components under seismic strain rates and low temperatures.* Paper presented at the Proc., 18th US–Japan Bridge Engineering Workshop.

Fosoul, S. A. S., & Tait, M. J. Seismic Performance Assessment of An Existing Multi-span Bridge in Eastern Canada Retrofitted with Fiber Reinforced Elastomeric Isolator. *Canadian Journal of Civil Engineering, In press*. doi:10.1139/cjce-2021-0344

Fosoul, S. A. S., & Tait, M. J. (2021). Soil-pile-structure interaction effects on seismic demands and fragility estimates of a typical Ontario highway bridge retrofitted with fiber reinforced elastomeric isolator. *Soil Dynamics and Earthquake Engineering, 151*, 106967. doi:https://doi.org/10.1016/j.soildyn.2021.106967

Foster, A. D. B. (2012). *Base isolation using stable unbonded fibre reinforced elastomeric isolators (SU-FREI).*

Ghobarah, A., & Ali, H. (1988). Seismic performance of highway bridges. *Engineering Structures, 10*(3), 157-166.

González, F., Padrón, L. A., Carbonari, S., Morici, M., Aznárez, J. J., Dezi, F., & Leoni, G. (2019). Seismic response of bridge piers on pile groups for different soil damping models and lumped parameter representations of the foundation. *Earthquake Engineering & Structural Dynamics, 48*(3), 306-327. doi:10.1002/eqe.3137

Hwang, H., Jernigan, J. B., & Lin, Y.-W. (2000). Evaluation of seismic damage to Memphis bridges and highway systems. *Journal of Bridge Engineering, 5*(4), 322-330.

Jangid, R. (2004). Seismic response of isolated bridges. *Journal of Bridge Engineering, 9*(2), 156-166.

Kelly, J., & Calabrese, A. (2012). Mechanics of fiber reinforced bearings. PEER Report 2012/101, Pacific Earthquake Engineering Research Center. *University of California, Berkeley*.

Kelly, J. M. (2002). Seismic isolation systems for developing countries. *Earthquake Spectra, 18*(3), 385-406.

Kelly, J. M., & Konstantinidis, D. (2011). *Mechanics of rubber bearings for seismic and vibration isolation* (Vol. 222): Wiley Online Library.

Kelly, J. M., & Takhirov, S. M. (2001). *Analytical and Experimental Study of Fiber-reinforced Elastometric Isolators*: Pacific Earthquake Engineering Research Center.

Kumar, M., Whittaker, A. S., & Constantinou, M. C. (2014). An advanced numerical model of elastomeric seismic isolation bearings. *Earthquake Engineering & Structural Dynamics, 43*(13), 1955-1974.

Lee, D. J. (1994). *Bridge bearings and expansion joints*: CRC Press.

Lee, G. C., Shih, T. S., & Chang, K. C. (1988). Mechanical Properties of Concrete at Low Temperature. *Journal of Cold Regions Engineering, 2*(1), 13-24. doi:doi:10.1061/(ASCE)0887-381X(1988)2:1(13)

Lupoi, A., Franchin, P., & Pinto, P. E. (2007). *Further probing of the suitability of pushover analysis for the seismic assessment of bridge structures.* Paper presented at the Proceedings of the ECCOMAS thematic conference on computational methods in

structural dynamics and earthquake engineering (COMPDYN), Rethymno, Greece, Paper.

Mackie, K., & Stojadinović, B. (2003). *Seismic demands for performance-based design of bridges*: Pacific Earthquake Engineering Research Center Berkeley.

Mackie, K. R., Lu, J., & Elgamal, A. (2012). Performance-based earthquake assessment of bridge systems including ground-foundation interaction. *Soil Dynamics and Earthquake Engineering, 42*, 184-196. doi:https://doi.org/10.1016/j.soildyn.2012.05.023

Mackie, K. R., & Stojadinović, B. (2005). *Fragility basis for California highway overpass bridge seismic decision making*: Pacific Earthquake Engineering Research Center, College of Engineering, University of California, Berkeley.

Mangalathu, S., & Jeon, J.-S. (2019). Stripe-based fragility analysis of multispan concrete bridge classes using machine learning techniques. *Earthquake Engineering & Structural Dynamics, 48*(11), 1238-1255. doi:10.1002/eqe.3183

Mordini, A., & Strauss, A. (2008). An innovative earthquake isolation system using fibre reinforced rubber bearings. *Engineering Structures, 30*(10), 2739-2751.

Muntasir Billah, A., & Shahria Alam, M. (2015). Seismic fragility assessment of highway bridges: a state-of-the-art review. *Structure and Infrastructure Engineering, 11*(6), 804-832.

Murray, R., & Detenber, J. (1961). First and second order transitions in neoprene. *Rubber chemistry and technology, 34*(2), 668-685.

Mylonakis, G., & Gazetas, G. (2000). Seismic soil-structure interaction: Beneficial or detrimental? *Journal of Earthquake Engineering, 4*(3), 277-301. doi:10.1080/13632460009350372

Nassar, M., Guizani, L., Nollet, M.-J., & Tahan, A. (2019). A probability-based reliability assessment approach of seismic base-isolated bridges in cold regions. *Engineering Structures, 197*, 109353. doi:https://doi.org/10.1016/j.engstruct.2019.109353

Nielson, B. G., & DesRoches, R. (2007a). Analytical seismic fragility curves for typical bridges in the central and southeastern United States. *Earthquake Spectra, 23*(3), 615-633.

Nielson, B. G., & DesRoches, R. (2007b). Seismic fragility methodology for highway bridges using a component level approach. *Earthquake Engineering & Structural Dynamics, 36*(6), 823-839.

Okui, Y., Nakamura, K., Sato, T., & Imai, T. (2019). Seismic response of isolated bridge with high damping rubber bearings. *Steel Construction, 12*(1), 2-9. doi:https://doi.org/10.1002/stco.201800029

Pan, Y., Agrawal, A. K., & Ghosn, M. (2007). Seismic fragility of continuous steel highway bridges in New York State. *Journal of Bridge Engineering, 12*(6), 689-699.

Pauletta, M., Cortesia, A., & Russo, G. (2015). Roll-out instability of small size fiber-reinforced elastomeric isolators in unbonded applications. *Engineering Structures, 102*, 358-368.

Sciascetti, A. (2017). *The Effect of Temperature on Unbonded Fiber-Reinforced Elastomeric Isolators.*

Sciascetti, A., & Tait, M. (2019). Effect of Temperature on the Response of Unbonded Fiber-Reinforced Elastomeric Isolators. *Journal of Structural Engineering, 145*(11), 04019124. doi:doi:10.1061/(ASCE)ST.1943-541X.0002401

Shinozuka, M., Feng, M. Q., Lee, J., & Naganuma, T. (2000). Statistical analysis of fragility curves. *Journal of Engineering Mechanics, 126*(12), 1224-1231.

Siqueira, G. H., Sanda, A. S., Paultre, P., & Padgett, J. E. (2014). Fragility curves for isolated bridges in eastern Canada using experimental results. *Engineering Structures, 74*, 311-324.

Sritharan, S., Suleiman, M. T., & White, D. J. (2007). Effects of seasonal freezing on bridge column–foundation–soil interaction and their implications. *Earthquake Spectra, 23*(1), 199-222.

Stefanidou, S. P., Sextos, A. G., Kotsoglou, A. N., Lesgidis, N., & Kappos, A. J. (2017). Soil-structure interaction effects in analysis of seismic fragility of bridges using an intensity-based ground motion selection procedure. *Engineering Structures, 151*, 366-380.

Stevenson, A. (1986). *Low Temperature Stiffening of Structural Rubber Bearings.* Paper presented at the Proceedings of the International Rubber Conference.

Suleiman, M. T., Sritharan, S., & White, D. J. (2006). Cyclic Lateral Load Response of Bridge Column-Foundation-Soil Systems in Freezing Conditions. *Journal of*

Structural Engineering, 132(11), 1745-1754. doi:doi:10.1061/(ASCE)0733-9445(2006)132:11(1745)

Tavares, D. H., Padgett, J. E., & Paultre, P. (2012). Fragility curves of typical as-built highway bridges in eastern Canada. *Engineering Structures, 40*, 107-118.

Tehrani, P., & Mitchell, D. (2013). Seismic risk assessment of four-span bridges in Montreal designed using the Canadian Bridge design code. *Journal of Bridge Engineering, 19*(8), A4014002.

Toopchi-Nezhad, H., Drysdale, R. G., & Tait, M. J. (2009). Parametric study on the response of stable unbonded-fiber reinforced elastomeric isolators (SU-FREIs). *Journal of Composite materials, 43*(15), 1569-1587.

Toopchi-Nezhad, H., Tait, M. J., & Drysdale, R. G. (2008). Lateral response evaluation of fiber-reinforced neoprene seismic isolators utilized in an unbonded application. *Journal of Structural Engineering, 134*(10), 1627-1637.

Toopchi-Nezhad, H., Tait, M. J., & Drysdale, R. G. (2008). Testing and modeling of square carbon fiber-reinforced elastomeric seismic isolators. *Structural Control and Health Monitoring, 15*(6), 876-900.

Toopchi-Nezhad, H., Tait, M. J., & Drysdale, R. G. (2009). Shake table study on an ordinary low-rise building seismically isolated with SU-FREIs (stable unbonded-fiber reinforced elastomeric isolators). *Earthquake Engineering & Structural Dynamics, 38*(11), 1335-1357.

Ucak, A., & Tsopelas, P. (2008). Effect of soil–structure interaction on seismic isolated bridges. *Journal of Structural Engineering, 134*(7), 1154-1164.

Van Engelen, N. C., Konstantinidis, D., & Tait, M. J. (2016). Structural and nonstructural performance of a seismically isolated building using stable unbonded fiber-reinforced elastomeric isolators. *Earthquake Engineering & Structural Dynamics, 45*(3), 421-439.

Van Engelen, N. C., Tait, M. J., & Konstantinidis, D. (2014). Model of the shear behavior of unbonded fiber-reinforced elastomeric isolators. *Journal of Structural Engineering, 141*(7), 04014169.

Vlassis, A., & Spyrakos, C. (2001). Seismically isolated bridge piers on shallow soil stratum with soil–structure interaction. *Computers & Structures, 79*(32), 2847-2861.

Wang, Z., Padgett, J. E., & Dueñas-Osorio, L. (2012). *Influence of soil structure interaction on the fragility of an isolated bridge-soil-foundation system.* Paper presented at the 15th world conf. earthq. eng., Lisbon, Portugal.

Warn, G. P., & Whittaker, A. S. (2006). Property Modification Factors for Seismically Isolated Bridges. *Journal of Bridge Engineering, 11*(3), 371-377. doi:doi:10.1061/(ASCE)1084-0702(2006)11:3(371)

Wesolowsky, M. J., & Wilson, J. C. (2003). Seismic isolation of cable-stayed bridges for near-field ground motions. *Earthquake Engineering & Structural Dynamics, 32*(13), 2107-2126.

Whiteley, J., Armstrong, B., & Welburn, R. (1982). Reinforcing and prestressing steels for cryogenic applications. *Cryogenic Concrete*, 252-279.

Xiang, N., & Alam, M. S. (2019). Comparative Seismic Fragility Assessment of an Existing Isolated Continuous Bridge Retrofitted with Different Energy Dissipation Devices. *Journal of Bridge Engineering, 24*(8), 04019070.

Xie, Y., Zhang, J., & Huo, Y. (2018). Simplified Drift Demand Prediction of Bridges under Liquefaction-Induced Lateral Spreading. *Journal of Bridge Engineering, 23*(8), 04018053. doi:doi:10.1061/(ASCE)BE.1943-5592.0001266

Yi, J.-H., Kim, S.-H., & Kushiyama, S. (2007). PDF interpolation technique for seismic fragility analysis of bridges. *Engineering Structures, 29*(7), 1312-1322.

Zhang, J., & Huo, Y. (2009). Evaluating effectiveness and optimum design of isolation devices for highway bridges using the fragility function method. *Engineering Structures, 31*(8), 1648-1660.

Zhang, J., Huo, Y., Brandenberg, S. J., & Kashighandi, P. (2008). Effects of structural characterizations on fragility functions of bridges subject to seismic shaking and lateral spreading. *Earthquake Engineering and Engineering Vibration, 7*(4), 369-382. doi:10.1007/s11803-008-1009-2

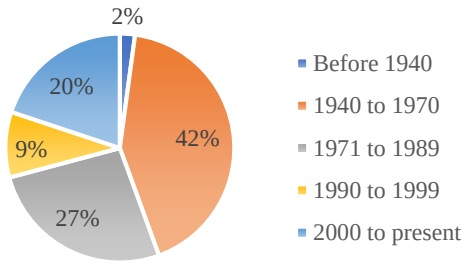

Figure 1.1. Construction year of Ontario bridges

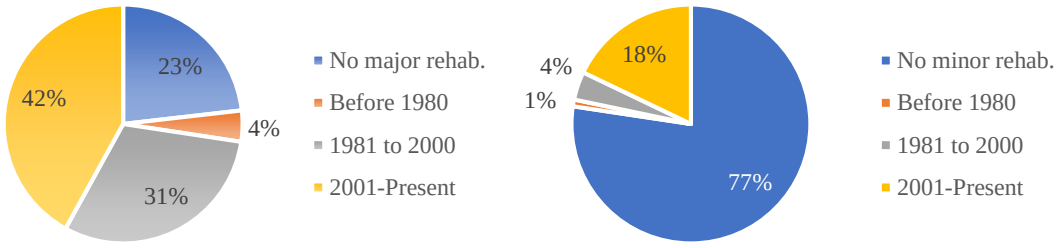

(a) (b)

Figure 1.2. Current condition of Ontario bridges in terms of (a) major and (b) minor rehabilitation

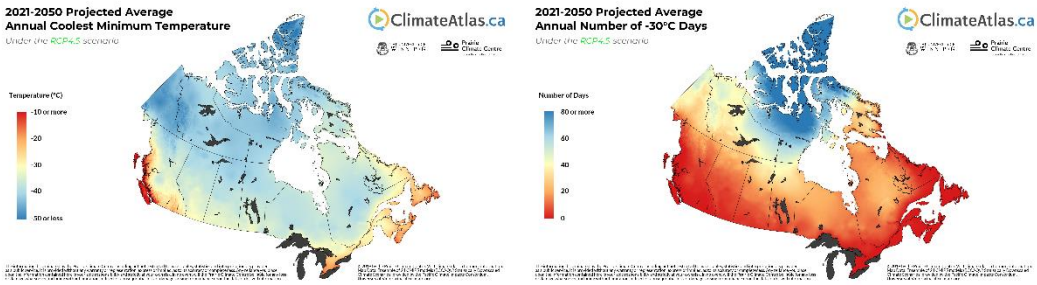

Figure 1.3. Projected annual subfreezing temperature conditions in Canada (reprinted with permission from Prairie Climate Center (Centre, 2019))

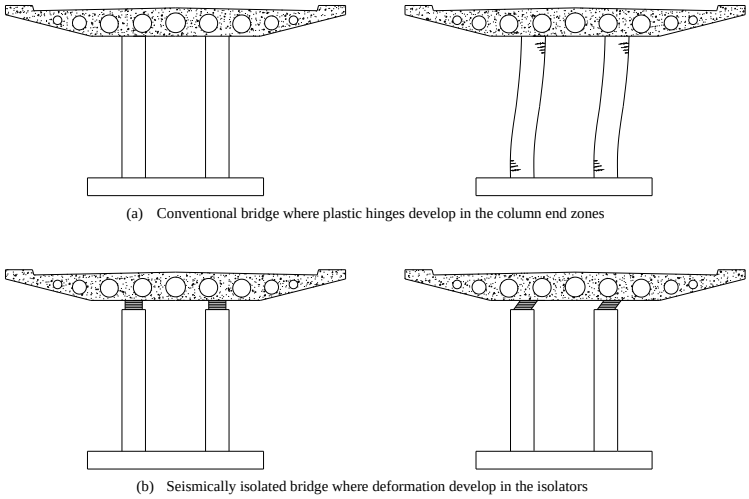

Figure 1.4. Comparison of a monolithic and a seismically isolated bridge

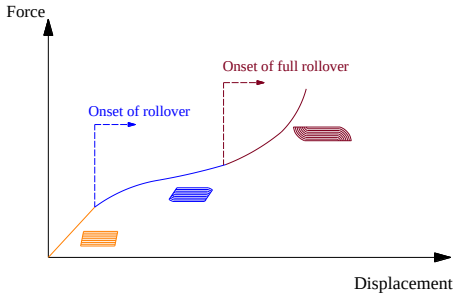

Figure 1.5. Phases of U-FREI load-displacement curve depicting rollover (Sciascetti, 2017)

2 Seismic Performance Assessment of An Existing Multi-Span Bridge in Eastern Canada Retrofitted with Fiber Reinforced Elastomeric Isolator

Abstract

A seismically resilient transportation network entails pre-prioritized retrofit plans for conventionally designed highway bridges. This is particularly important for the province of Ontario in Canada, where more than 44% of the multi-span bridges have been constructed prior to 1970. To support future seismic risk mitigation efforts, this study evaluates the seismic performance of a multi-span continuous reinforced concrete bridge in Ontario, Canada, in its as-built and retrofitted conditions. Seismic retrofit is conducted utilizing novel Fiber Reinforced Elastomeric Isolators (FREI). Analytical fragility curves are developed using Incremental Dynamic Analysis (IDA) on a three-dimensional nonlinear finite element model of the bridge using 45 synthetic ground motion records for eastern Canada. Results indicate that seismic isolation can effectively mitigate the seismic demand on columns and transfer the shear forces to the end abutments resulting in excessive backfill soil deformation. However, this deformation does not necessarily result in bridge failure and traffic disruption.

Keywords: IDA, Fragility analysis, Retrofit, FREI, Seismic isolation

2.1 Introduction

Highway bridges are key components in modern transportation networks in many countries across the world. According to *Statistics Canada* (*Ontario Structure Inspection Manual*, 2018), approximately 43% of the total number of bridges in Canada are located in Ontario and 44% of these have been constructed before 1970. The Canadian Highway Bridge Design Code, CHBDC (*Canadian Highway Bridge Design Code*, 2019), is amended on a routine cycle, and the National Building Code of Canada, NBCC 2015 (*National Building Code of Canada*, 2015), has adopted a uniform hazard spectrum with a 2% probability of exceedance in 50 years (2475 years return period), as opposed to 10% (475 years return period) in the previous code (*National Building Code of Canada*, 1995). Therefore, seismic assessment of existing infrastructures as well as considering rehabilitation systems for retrofitting deficient bridges is needed. Seismic fragility analysis is a valuable tool for the former case where the latter can be achieved through seismic isolation. In regions with a lower degree of seismicity or insufficient bridge damage records, such as eastern Canada, the analytical approach is paramount in developing fragility curves (Mangalathu, Jeon, Padgett, & DesRoches, 2016; Monteiro, Zelaschi, Silva, & Pinho, 2017).

Field reconnaissance reports from previous earthquakes have revealed that seismic isolation is a viable technique to improve the seismic performance of both existing and new highway bridges (Zhang & Huo, 2009). One of the most widely used types of isolation systems are elastomeric isolators which are typically comprised of elastomer layers interleaved with reinforcement layers (e.g. steel shims, fabrics, etc.) by means of vulcanization. Recently, FREI have emerged as a potential low-cost alternative to Steel

Reinforced Elastomeric Isolators (SREI) by replacing the reinforcing steel layers with lighter fiber reinforcement, allowing the FREI to be manufactured in larger sheets and subsequently be cut into isolators of arbitrary size (Kelly, 1999). More recently, bridge design codes (e.g. (AASHTO, 2012; CSA, 2019)) permit the use of fiber fabric as a substitute for steel shims for reinforcing the elastomeric pads. The unbonded application of the FREI (Unbonded FREI, U-FREI), enables the isolator to exhibit a unique three-stage response as shown in Figure 2.1. At lower lateral displacements, U-FREI remains in full contact with the upper and lower supports, exhibiting a linear behavior similar to that of a SREI or bonded FREI. By increasing the lateral displacement, the isolator gradually reduces contact with the supports, as a result of roll over, resulting in a reduction in shear area and consequently lateral stiffness. Under very large lateral displacements, full contact between the originally vertical faces of the U-FREI and supports occurs leading to an increase in the lateral stiffness.

To date, few studies have been conducted to evaluate the seismic performance of a seismically isolated bridge with FREI (Y. M. Al-Anany, Moustafa, & Tait, 2018). Furthermore, these studies investigated generic short-span bridges modeled using linear elastic components and their results may be biased. To the best of the authors' knowledge, no studies have employed a fragility analysis on bridges that have been retrofitted using U-FREI. Therefore, the effectiveness of this type of isolation system on reducing the probability of damage to different bridge components and at different damage states on a retrofitted bridge has not been previously investigated.

A comparative study between the seismic performance of the proposed retrofitted bridge with U-FREI and the existing fixed bridge has been completed in this study. In the current "as-built" condition of the bridge, the deck is supported by pot bearings installed at the interface of the deck with supporting columns and the two seat-type abutments. However, the pot bearings installed on the middle five pairs of columns are of fixed-type and restrain the deck from horizontal displacements. Therefore, it is assumed that the "as-built" bridge consists of a deck which is monolithically connected to the supporting columns. This assumption also maximizes the force demand on the columns. However, a simplified abutment model consists of a rigid element with defined nonlinear longitudinal response is rigidly connected to the superstructure centerline (Aviram, Mackie, & Stojadinović, 2008). The retrofit plan is to isolate the bridge superstructure from all columns and abutments. As the superstructure is expected to experience large lateral displacements, as a consequence of installing U-FREI, the effect of backfill soil is accounted for. Since this study attempts to evaluate the effectiveness of the FREI and incorporating the effects of bridge-soil-pile interaction leads to a significant change in the total stiffness of the bridge system, and consequently, alters the seismic response of the bridge, the foundations are assumed to be fixed and modeling the soil domain is excluded from this study. An IDA with a set of 45 synthetic ground motion records is carried out and the structural responses, such as column drift, FREI deformation, and abutment displacement are monitored. The fragility curves are generated by integrating capacity distributions with correlated component demand distributions for a range of ground motion intensities.

2.2 Prototype bridge and finite element modeling

2.2.1 Bridge description

An existing conventionally designed highway bridge in Ontario, Canada, is selected for this study (Figure 2.2). This bridge is constructed in 1969 and represents the typical traditionally designed bridges in Ontario. As shown in Figure 2.3, the bridge has an overall length of 236.0 m with nine spans supported by eight pairs of reinforced concrete columns. The superstructure consists of a nine-cell continuous cast-in-place reinforced concrete voided slab. It should be noted that post-tensioned cast in place concrete decks constitutes about 20% of the bridges in Ontario. The columns are circular with a diameter of 0.914 m and an average clear height of 6.1 m reinforced with 20 #14 steel rebars producing a longitudinal reinforcement ratio of approximately 4.4% confined with #5 spirals with a 50 mm pitch. A detailed description of the characteristic parameters of the bridge components is provided in Table 2.1.

This bridge is referred to as a “Major-route bridge” according to CHBDC (CSA, 2019). Therefore, the seismic performance categories of the as built and retrofitted bridges are determined to be 3 and 2, respectively. Moreover, this bridge is comprised of nine spans that makes it an irregular bridge according to CHBDC (CSA, 2019). It should be mentioned that CHBDC has determined the target service level and damage level of major-route bridges to be service disruption and extensive, respectively, for a seismic event with 2% probability of exceedance in 50 years.

2.2.2 Finite element modeling of the prototype bridge

Based on the specifications obtained from the examined bridge plans, a three-dimensional finite element model of the prototype bridge is generated in OpenSees (McKenna, 2011). A spine-line model is selected to model the superstructure comprised of a line *elasticBeamColumn* element lumped at the centerline of the deck cross-section.

A *nonlinearBeamColumn* element with spread plasticity is utilized to capture probable nonlinearity of the bridge columns as illustrated in Figure 2.3. The fiber section of the columns was composed of unconfined and confined concrete as well as longitudinal steel bars. The stress-strain constitutive relationships were specified by Mander's model for concrete (Mander, Priestley, & Park, 1988) and the Giuffre-Menegotto-Pinto model with isotropic strain hardening for steel (Filippou, Bertero, & Popov, 1983), respectively.

Nonlinear behavior of the backfill soil in the longitudinal direction was modeled using the *HyperbolicGapMaterial* model in OpenSees developed by Shamsabadi et al. (Shamsabadi, Rollins, & Kapuskar, 2007). Figure 2.3 also demonstrates the connectivity of the deck to the U-FREI using zero-length springs and then U-FREI to the abutment backfill soil using the backfill soil spring. Average initial stiffness and ultimate passive resistance per meter of the back wall width are determined to be 8550 kN/m and 238 kN/m, respectively, with a 50.8 mm wide expansion gap.

2.2.3 Design and modeling of FREI

The FREI have been designed based on the provisions of CSA-S6-19 (CSA, 2019) for dead and total loads of 3285 kN and 4500 kN, respectively, for serviceability limit state and 4130 kN and 6425 kN, respectively, for ultimate limit state. In order for the elastomeric bearings to be considered as seismic isolators, the total shear strain due to compression, shear, and rotation should be less than the code specified value of 5.5 (CSA, 2019). An isolator containing eight layers of a natural rubber layer with a hardness of 55 durometers, Shore A (*Standard Test Method for Rubber Property--Durometer Hardness*, 2005) has been designed to satisfy these requirements. The geometrical properties of the FREI are tabulated in Table 2.1. For this FREI, the shape factor, S, defined as the ratio of loaded plan area of the isolator to the unloaded perimeter area of a single elastomer layer is 4.9, which falls within the common range of typical bridge elastomeric bearings (Stanton, 2008). The aspect ratio, defined as the ratio of the total length/width of the isolator to the total height of the bearing, is 3.12 that ensures lateral stability (i.e. maintaining a positive lateral tangential stiffness) of FREI (Foster, 2012). The vertical stiffness of each individual FREI is determined to be 274×10^6 N/m using the following relation

$$K_v=\frac{E_c\times A}{t_r} \tag{2.1}$$

where A is the cross-sectional area of the isolator and the compression modulus of the FREI, E_c, is determined to be 102 MPa using the following expression (Kelly & Van Engelen, 2015)

$$E_c=96\times G\times S^2\times\left(2+\frac{a}{b}\right)^2\times\left[\sum_n\left[\frac{1}{\left(\alpha_1^2+\beta_1^2\right)\times\left(2+\frac{a}{b}\right)^2+n^2\times\pi^2}\times\frac{1}{n^2\times\pi^2}\times\left(1-\frac{\tanh\left(\lambda_1(n)\right)}{\lambda_1(n)}\right)\right]\right] \quad (2.2)$$

$$\alpha_1=\sqrt{\frac{24\times G\times S^2\times t}{E_f\times t_f}} \quad (2.3)$$

$$\beta_1=\sqrt{\frac{12\times G\times S^2}{K_{bulk}}} \quad (2.4)$$

$$\lambda_1(n)=\frac{\sqrt{\left(\alpha_1^2+\beta_1^2\right)\times\left(2+\frac{a}{b}\right)^2+n^2\times\pi^2}}{\frac{a}{b}} \qquad n = 1, 3, ..., 9999 \quad (2.5)$$

where a, b, t, and t_f are introduced in Table 2.1. The Bulk modulus of the elastomer, K_{bulk}, the shear modulus of the elastomer, G, and the effective elastic modulus of the reinforcement, E_f, are determined to be 1090 MPa, 0.81 MPa, and 230 GPa, respectively.

The horizontal stiffness of the isolators is determined to be 2.18×10^6 N/m based on the following expression

$$K_h=\frac{G\times A}{t_r} \quad (2.6)$$

In order to capture the FREI softening and stiffening regimes, a non-iterative rate-independent Takeda-Elastic model is used in this study. The characteristic parameters of this model can be calibrated using the effective lateral stiffness and damping obtained from an experimental test, excluding the need to fit the entire hysteresis loops. The model contains a Takeda-based bilinear plastic model (Takeda, Sozen, & Nielsen, 1970) in parallel with a nonlinear elastic spring (see Figure 2.3). In order to validate the implemented Takeda-Elastic model in this study, the hysteretic behavior of the isolator is

compared with the experimental data obtained from a study by Sciascetti (Sciascetti, 2017). It is shown in Figure 2.4 that the Takeda-Elastic model can simulate the hysteretic behavior of the SU-FREI by capturing the softening and stiffening of the SU-FREI along with the peak displacements.

The Stable Unbonded-FREI (SU-FREI) element is implemented in OpenSees by defining a zero-length element at the interface of the superstructure and supporting piers and abutments. This element provides the horizontal stiffness in both directions using two parallel uniaxial materials, namely, *ElasticMultilinear* and *Hysteretic* with characteristic values tabulated in Table 2.1. As shown in Figure 2.3 (c), the *Hysteretic* spring represents a bilinear Takeda model with three characteristic parameters including initial stiffness, k_1, post yield stiffness, k_2, and a yield displacement of u_y. The induced shear force in this Takeda-based bilinear model can be expressed using the following relations:

$$\begin{aligned} F_{TB} &= k_1 u && u < u_y \\ F_{TB} &= k_1 u_y + k_2(u - u_y) && u \geq u_y \end{aligned} \tag{2.7}$$

where u is the FREI displacement amplitude at each time instant.

The *ElasticMultilinear* spring represents a Nonlinear Elastic Spring (NES) which is developed using a fifth-order polynomial. The force of the nonlinear spring, F_{NES}, at displacement u can be expressed as

$$F_{NES}=a_1 u+a_2 u^3+a_3 u^5 \tag{2.8}$$

where a_i are the polynomial parameters (Osgooei, Tait, & Konstantinidis, 2017). The effectives stiffness of the SU-FREI provided with these two parallel springs can be

determined by dividing the summation of the developed forces in the two springs by the displacement amplitude, u, as follows

$$\begin{aligned} k_{eff} &= k_1 + a_1 + a_2 u^2 + a_3 u^4 && u < u_y \\ k_{eff} &= (k_1 - k_2)\frac{u_y}{u} + k_2 + a_1 + a_2 u^2 + a_3 u^4 && u \geq u_y \end{aligned} \tag{2.9}$$

Since the NES does not introduce any damping to the system, the only source of energy dissipation is the Takeda-based bilinear spring. Therefore, the effective damping ratio of the isolation system can be determined using the following relation

$$\beta_{eff} = \frac{(3k_1 u_y + k_2 u - k_2 u_y)(k_1 - k_2)(u - u_y)}{2\pi k_{eff} k_1 u^2} \tag{2.10}$$

The six characteristic model parameters, namely, k_1, k_2, u_y, a_1, a_2, and a_3 are determined by minimizing the error between the values of the predicted effective stiffness (Equation (2.9)) and effective damping ratio (Equation (2.10)) obtained from experimental test results at the displacement amplitudes considered in test. These characteristic parameters are adopted and scaled from a set of experimental tests conducted on a set of quarter scale FREI by Sciascetti and Tait (Sciascetti, 2017) where the damping ratio is determined to be in the range of 8-11% depending on the exerted shear force. As shown in Figure 2.4 and demonstrated in Equation (2.10), the energy dissipation is a function of the displacement amplitude where at relatively small amplitudes (i.e. 0.25-0.5 t_r), damping is within 9.5 to 10.7% and in larger amplitudes (i.e. larger than 0.75 t_r), damping decreases to about 8%. This energy dissipation capacity is embedded in the simulated FREI springs and the potential energy of the structure will be dissipated in accordance with the lateral displacements of the installed FREIs.

2.3 IDA-based seismic risk assessment

The conventional IDA technique entails a series of nonlinear dynamic time-history analyses of a finite element model of the bridge for a set of monotonically increasing ground motion records. Several studies have shown that spectral acceleration at the fundamental period of the structure, $S_a(T_1)$ is a suitable Intensity Measure, IM, in terms of efficiency, sufficiency, effectiveness, and robustness (Chomchuen & Boonyapinyo, 2017; Muntasir Billah & Shahria Alam, 2015; Ramanathan, Padgett, & DesRoches, 2015). For example, Ramanathan et al. (Ramanathan et al., 2015) showed that S_a (T = 1 sec.) is an optimal IM for concrete box-girder bridges. As the fundamental period of the isolated bridge in this study is 1.0 sec., spectral acceleration at 1.0 sec. (S_a (T_1 = 1 sec.)) is selected as the IM. It should be noted that the fundamental period of the monolithic bridge is 0.4 sec.

Analytical fragility function represents the probability of exceeding a certain state of damage, referred to as limit/damage states, conditioned on a specific intensity of seismic excitation as follows

$$\text{Fragility} = P\,[LS \mid IM = y] \tag{2.11}$$

where y is the realized condition of the ground motion IM. Given the lognormal distribution of both structural demand and capacity, the bridge component fragility can be described by the following equation

$$P[LS|IM]=\Phi\left[\frac{\ln\left(\frac{S_D}{S_C}\right)}{\sqrt{\beta_{D|IM}^2+\beta_C^2}}\right] \tag{2.12}$$

where Φ is the standard normal cumulative distribution, S_D is the median and $\beta_{D|IM}$ is the logarithmic standard deviation for the demand, and S_C is the median and β_C is the logarithmic standard deviation for the capacity. While determining the damage potential of bridge components by developing component-level fragility curves is insightful, the overall bridge safety is typically evaluated using system-level fragility curves. These fragility curves are derived by calculating the upper and lower first-order bounds of fragility (Xiang & Alam, 2019). The system-level fragility curves for a serial system, in which failure of any components results in the overall system failure, can be achieved by combining the fragilities of every single bridge component and implementing them in the following expression:

$$\max_{i=1:n}\left[P\left(F_{component_i}\right)\right] \le P\left(F_{system}\right) \le 1 - \prod_{i=1}^{n}\left[1 - P\left(F_{component_i}\right)\right] \tag{2.13}$$

where $P(F_{component,i})$ and $P(F_{system})$ are defined as probabilities of damage for component i of the bridge and the entire bridge system, respectively. In this expression, the left-hand side of the inequality represents the lower bound of the fragility assuming that the demands placed on the bridge components are completely correlated (unconservative), whereas the right-hand side represents the upper bound of fragility assuming zero correlation between the component demands (conservative). In this study, the serial connection of the bridge piers, isolators, and the deck permit using Equation (2.13) for computing the bounds of

fragility. As such, the overall bridge system is deemed to achieve a particular damage state if at least one bridge component reaches or exceeds that damage. Therefore, only the upper bound values are presented in order to illustrate a conservative estimation of the system-level fragility.

2.3.1 Characterization of damage states

Performance levels or damage/limit states are associated with qualitative descriptions or functional interpretations of the damage in the bridge, such as slight, moderate, extensive, and collapse as presented in the Federal Emergency Management Agency loss assessment package HAZUS-MH (FEMA, 2003). Multiple failure modes, including columns, abutment soil, and unseating at the abutments are considered in this study. The median values of the damage states, S_c, along with their corresponding logarithmic standard deviations, β_c, are adopted from the relevant previous studies and are presented in Table 2.2.

In this study, the quantitative measure of the damage state for the columns is considered as maximum drift ratio according to a study by Dutta and Mander (Dutta & Mander, 1998) in which the damage states are presented as seismically and non-seismically designed columns. As the columns in this study meet the seismic design provisions of CSA S6-19 (CSA, 2019), drift limits of seismically designed columns are adopted. Moreover, these damage states are in accordance with those proposed by Perdomo and Monteiro (Perdomo & Monteiro, 2020) based on a simplified damage state model developed for circular reinforce concrete bridge columns. It should be pointed out that these drift limits are typical values used to assess the seismic performance of bridges in analytical studies (M.

Shinozuka, S. Banerjee, & S.-H. Kim, 2007; M. Shinozuka, S. Banerjee, & S. H. Kim, 2007; Waller, 2011). The damage states used for the abutments in active, passive, and transverse actions are adopted from a study by Nielson (Nielson, 2005) where the prescriptive available damage states are combined and updated with survey-based results by means of a Bayesian updating approach. Unseating of the deck is also considered as an extreme case of the bridge collapse. It is important to highlight that SU-FREI have been observed not to exhibit damage under large shear strains up to and exceeding 250% in numerous experimental studies on the vertical, lateral, and rotational behavior of isolators as well as stability and lateral offset (Y. Al-Anany, Van Engelen, & Tait, 2017).

2.3.2 Seismic hazard and selection of ground motions

A seismic hazard deaggregation was carried out for the bridge site in order to characterize the distribution of contributions by magnitude and distance. Seismic hazard, mean magnitude (M_w), and mean distance are obtained as 0.125g, 6.9, and 63 km, respectively, for the period of 1.0 sec. (fundamental period of the isolated bridge) and a 2% in 50 years probability of exceedance. The average shear wave velocity for the upper 30 m of the subsurface stratigraphy measured for a nearby site was approximately 127 m/s. Therefore, it is considered that a soil type E corresponding to soft soil is applicable for the bridge site.

Since a sufficient number of ground motion records are not available for the location of the bridge, synthetic acceleration time histories were used (Siqueira, Sanda, Paultre, & Padgett, 2014; D. Tavares, Suescun, Paultre, & Padgett, 2013; D. H. Tavares, Padgett, & Paultre, 2012). Records were developed by Atkinson (Atkinson, 2009) for eastern Canada using the stochastic finite-fault method in conformance with the *National Building Code of*

Canada Uniform Hazard Spectra (UHS) for a various range of site soil classes. Simulated ground motions are provided for two magnitudes (i.e. M = 6 and 7) with two fault distance ranges (i.e. near-field and far-field) and four site soil classes (i.e. A, C, D, and E). Therefore, a set of synthetic ground motions containing 45 far-field records for the given magnitude, soil to site distance (obtained from the deaggregation analysis) and soil type were selected (Atkinson, 2009). The records were used as individual horizontal components both in longitudinal and transverse directions. The effects of vertical acceleration and spatially variable ground motions are beyond the scope of this study. The synthetic ground motion records have been scaled so that their mean response spectrum match the spectral acceleration of 1.0 sec. of the design spectrum developed for site class E in NBCC 2015 (*National Building Code of Canada*, 2015). This scaling aims to guarantee that the scaling procedure in the IDA will be started from the same base point for all ground motion records.

2.4 Seismic performance evaluation

To investigate the seismic performance of the archetype bridge prior to and post-retrofit, IDA is carried out on the established bridge model independently in the longitudinal and transverse directions of the bridge axis. Therefore, the bridge must be able to equally withstand the input excitations from all possible directions (Aviram et al., 2008). Three EDPs are selected and monitored during the IDA, namely, peak drift ratio, peak backfill soil deformation in active action and peak backfill soil deformation in passive actions.

2.4.1 Pre-retrofit component vulnerability

Summarized IDA curves along with the corresponding fragilities and component responses of the monolithic bridge are shown in Figure 2.5. IDA results of the monolithic bridge reveal that given the design level spectral acceleration at the period of 1 sec. in a 2% in 50-year probability of exceedance, no damage occurs to the columns due to excessive drift. This acceptable behavior of columns can be attributed to the relatively large reinforcement ratio and small pitch of spirals. It can be observed that the median of peak drift ratio of the bridge in the transverse direction is slightly smaller than that in the longitudinal direction for all the prescribed DS except the slight DS.

In this bridge, abutments are considered to be the most vulnerable components in both orthogonal directions. In the slight limit state, the first three dominant vulnerable component types, which have the lowest median of damage and highest probability of exceeding the DS, are abutment deformation in active action, transverse action, and passive action followed by column drift in longitudinal and transverse directions, respectively. This is a recurring theme for the other three DS. Table 2.3 presents the component fragility curve parameters where S_D is the median of damage at each DS, $\beta_{D|IM}$ is the dispersion due to Record To Record (RTR) variability, β_{TOT} is the total dispersion of demand, which is defined as the square root of the sum of squares of $\beta_{D|IM}$ and β_C, Damage Margin Ratio (DMR) is the ratio of median damage capacity at each DS to MCE demand (S_a = 0.24g) and P [DS|$S_{a2/50}$] is the probability of exceeding a prescribed DS at the MCE hazard level (seismic event with 2% probability of exceedance in 50 years).

2.4.2 Post-retrofit component vulnerability

Seismic performance of the isolated bridge in longitudinal and transverse directions are demonstrated in Figure 2.5. As shown in this figure, isolating the superstructure improved the behavior of columns by introducing the FREI and preventing the columns from carrying large inertial forces of the deck. However, the abutment back wall is considered to be the most fragile component in both orthogonal directions. As shown in Table 2.3, the probability of slight damage to the abutments in active, transverse, and passive actions is 100%, 94%, and 80%, respectively, where the probability of damage to columns is negligible. This negative performance of the abutment back wall can be explained by the excessive horizontal displacements of the deck due to the presence of FREIs.

Unlike the monolithic bridge where the middle columns experience smaller drift ratios with respect to the columns next to abutments, the middle columns of the isolated bridge undergo larger drift ratios with respect to those of the columns adjacent to the end abutments. This can be attributed to the relative stiffness of the FREI and the supporting column. As shown in Figure 2.3, the column heights increase from the sides to the middle of the bridge resulting in smaller lateral stiffness of the columns.

Provided that the elastomer is incompressible and that the length of the surface that has lost contact with the upper and lower supports is equal to the lateral displacement, full rollover strain can be approximated using the following relation (Kelly & Konstantinidis, 2007)

$$\gamma_f = \frac{5}{3}\frac{h}{t_r} \tag{2.14}$$

According to the FREI specifications provided in Table 2.1, full rollover shear strain of the used isolators is 1.69, which approximately corresponds to the spectral intensity of 1.69 g as shown in Figure 2.6. Figure 2.6 (a) demonstrates the hysteretic loops of the FREI at different earthquake intensities from 0.125g up to 1.69g where the onset of full rollover is anticipated. Figure 2.6 (b) demonstrates the peak shear strain of the installed FREIs. It is shown that the peak shear strain of all isolators decreased by increasing the intensity level beyond 1.69g. Moreover, FREIs on abutments and adjacent columns experience larger shear strains which can be attributed to the contribution of the abutment mass in the lateral displacements and larger relative stiffness of piers 1 and 8 to the stiffness of isolators due to smaller heights. Residual deformation of the U-FREI due to sliding is not of a concern for this bridge because 1) the two end abutments prevent the superstructure from experiencing large lateral displacements, therefore isolator displacement in the stiffening regime is limited where sliding is more probable to occur, and 2) according to a study by Russo and Pauletta (Russo, Pauletta, & Cortesia, 2013), the sliding instability typically occurs at lower values of compressive stress (<0.5 MPa), which is much lower than considered in this study.

2.5 Comparative results and discussion

Figure 2.7 presents a comparison between summarized IDA curves along with their corresponding fragility curves of the as-built and isolated bridge for the longitudinal and transverse direction of the bridge. This figure highlights the efficiency of the unbonded

FREI to mitigate the seismic demand on the columns and their ability to transfer the lateral forces to the end abutments. This mechanism is perceived to be desirable because even severe damage to the abutments does not lead to a global collapse of the bridge and traffic closure (Padgett & DesRoches, 2007). Table 2.4 has summarized the fragility components of the bridge along with the extent to which the isolation system has impacted the performance of the bridge components. It is shown that utilizing U-FREI has increased the median of damage and DMR of the column drifts by 160%, 88%, 63%, and 44% at slight, moderate, extensive, and collapse damage states. On the other hand, seismic isolation had an adverse impact on the abutments and has decreased their median of damage and DMR by 76-64%. The efficient behavior of FREIs at smaller damage states is due to the softening regime at relatively small displacements. By increasing the earthquake intensity level and its corresponding displacement demand, U-FREI enter their stiffening regime, which results in a larger contribution of columns and reduced demand on abutments. In the transverse direction, unbonded FREI increased the median of damage to columns by 89%, 58%, 33%, and 24% for the four prescribed DS (see Table 2.4). In return, the median abutment deformation has decreased by 80-54%. It should be pointed out that isolating the superstructure does not impact the dispersion of the structural response by a regular trend. The upper bound of system-level fragility curves of the bridge is calculated using Equation (13). As shown in Figure 2.8 and Table 2.5, seismic isolation has decreased the median of damage for the first three DS by 76-65%. This behavior is due to the vulnerability of the abutment of this bridge to lateral displacements. However, the median of collapse has increased the median of collapse by 39% and 18% in longitudinal and transverse directions,

respectively. These trends reveal that seismic isolation is effective in reducing the probability of collapse of the bridge whereas the probability of damage (mostly to abutments) can be increased. Please note that the system fragility curves of the monolithic and isolated bridges are demonstrated using solid and dashed lines, respectively.

Deck and column response histories of the as-built and retrofitted bridge in longitudinal and transverse directions are compared and presented in Figure 2.9 and Figure 2.10. These comparisons are made at the MCE design level and represent the bridge behavior for a seismic event with a 2% in 50 years probability of exceedance. As shown in Figure 2.9 and Figure 2.10 and summarized in Table 2.6, using unbonded FREI as a retrofit measure significantly reduces the absolute deck acceleration by 40% and 30% in the two orthogonal directions of the bridge. This reduction is achieved through decoupling the superstructure from the ground motion and allowing the deck to have larger lateral displacements. Thereby, deck displacement of the isolated bridge is increased by a factor of 1.6 and 1.9 in longitudinal and transverse directions, respectively. However, seismic isolation is shown to have a negligible effect on changing the velocity of the deck. Figure 2.10 illustrates the effectiveness of utilizing unbonded FREI on mitigating the base shear and base moment of columns. While the bridge undergoes larger base shear and moments in the transverse direction, the isolation system has reduced the demand by almost the same amount of 85%. This is the same trend for the peak base moment of columns where using FREI has reduced the peak moment of column bases by 78%.

2.6 Conclusion

This paper presents the seismic vulnerability assessment of a multi-span continuous concrete bridge retrofitted with FREI. Results of the current as-built condition of the bridge indicate that the most vulnerable bridge components are backfill soil deformation in active, transverse, and passive actions, respectively, following by the column drifts in longitudinal and transverse directions. As mentioned previously, seismic isolation alters the load-carrying mechanism by mitigating the seismic demand of columns and transferring the lateral forces to abutments. Therefore, isolation using FREI resulted in a low probability of damage to columns in both longitudinal and transverse directions for all damage states whereas the probability of damage to abutments increased. The effectiveness of using FREI is demonstrated to be a function of damage state where the largest impact is on slight DS and the smallest is on collapse DS. The isolated bridge exhibited a larger increase in the median damage capacity of column drift in the longitudinal direction relative to transverse direction. On the contrary, backfill soil deformation in active, passive, and transverse directions were found to have a decrease in their median damage capacity. Overall, isolation using FREI is demonstrated to be an effective approach for mitigating the column demands and reducing the acceleration of the superstructure.

2.7 Acknowledgments

The authors would like to express their gratitude for the support provided of the Ministry of Transportation Ontario (MTO) through the Highway Infrastructure Innovation Funding Program (HIIFP) and Natural Sciences and Engineering Research Council of Canada (NSERC).

2.8 Contributor's statement

S. A.: Data curation, Formal Analysis, Methodology, Software, Writing – original draft, Writing – review and editing

M. T.: Conceptualization, Funding acquisition, Methodology, Supervision, Writing – review and editing

2.9 Funding statement

This research was supported by the Ministry of Transportation Ontario (MTO).

2.10 Data Availability Statement

All data, models, and code generated or used during the study appear in the submitted article.

References

AASHTO. (2012). American Association of State Highway and Transportation Officials. *Washington, DC*.

Al-Anany, Y., Van Engelen, N., & Tait, M. (2017). Vertical and Lateral Behavior of Unbonded Fiber-Reinforced Elastomeric Isolators. *Journal of Composites for Construction, 21*(5), 04017019.

Al-Anany, Y. M., Moustafa, M. A., & Tait, M. J. (2018). Modeling and Evaluation of a Seismically Isolated Bridge Using Unbonded Fiber-Reinforced Elastomeric Isolators. *Earthquake Spectra, 34*(1), 145-168. doi:10.1193/072416eqs118m

Atkinson, G. M. (2009). Earthquake time histories compatible with the 2005 National building code of Canada uniform hazard spectrum. *Canadian Journal of Civil Engineering, 36*(6), 991-1000.

Aviram, A., Mackie, K. R., & Stojadinović, B. (2008). *Guidelines for nonlinear analysis of bridge structures in California*: Pacific Earthquake Engineering Research Center.

Canadian Highway Bridge Design Code. (2019). Canadian Standard Association.

Chomchuen, P., & Boonyapinyo, V. (2017). Incremental dynamic analysis with multi-modes for seismic performance evaluation of RC bridges. *Engineering Structures, 132*, 29-43. doi:https://doi.org/10.1016/j.engstruct.2016.11.026

CSA. (2019). S6-19 Canadian highway bridge design code *Section 11: Joints and Bearings*. Toronto, Ontario.

Dutta, A., & Mander, J. (1998). *Seismic fragility analysis of highway bridges.* Paper presented at the Proceedings of the INCEDE-MCEER center-to-center project workshop on earthquake engineering Frontiers in transportation systems.

FEMA. (2003). Multi-hazard loss estimation methodology, earthquake model *Washington, DC, USA: Federal Emergency Management Agency*.

Filippou, F. C., Bertero, V. V., & Popov, E. P. (1983). Effects of bond deterioration on hysteretic behavior of reinforced concrete joints.

Foster, A. D. B. (2012). *Base isolation using stable unbonded fibre reinforced elastomeric isolators (SU-FREI).*

Kelly, J. M. (1999). Analysis of fiber-reinforced elastomeric isolators. *Journal of Seismology and Earthquake Engineering, 2*(1), 19-34.

Kelly, J. M., & Konstantinidis, D. (2007). *Low-cost seismic isolators for housing in highly-seismic developing countries.* Paper presented at the 10th world conference on seismic isolation, energy dissipation and active vibrations control of structures, Istanbul, Turkey.

Kelly, J. M., & Van Engelen, N. C. (2015). *Single series solution for the rectangular fiber-reinforced elastomeric isolator compression modulus* (PEER 2015/03). Retrieved from Pacific Earthquake Engineering Research (PEER) Center, University of California, Berkeley:

Mander, J. B., Priestley, M. J., & Park, R. (1988). Theoretical stress-strain model for confined concrete. *Journal of Structural Engineering, 114*(8), 1804-1826.

Mangalathu, S., Jeon, J.-S., Padgett, J. E., & DesRoches, R. (2016). ANCOVA-based grouping of bridge classes for seismic fragility assessment. *Engineering Structures, 123*, 379-394.

McKenna, F. (2011). OpenSees: a framework for earthquake engineering simulation. *Computing in Science & Engineering, 13*(4), 58-66.

Monteiro, R., Zelaschi, C., Silva, A., & Pinho, R. (2017). Derivation of fragility functions for seismic assessment of RC bridge portfolios using different intensity measures. *Journal of Earthquake Engineering*, 1-17.

Muntasir Billah, A., & Shahria Alam, M. (2015). Seismic fragility assessment of highway bridges: a state-of-the-art review. *Structure and Infrastructure Engineering, 11*(6), 804-832.

National Building Code of Canada. (1995). National Research Council of Canada.

National Building Code of Canada. (2015). National Research Council of Canada.

Nielson, B. G. (2005). *Analytical fragility curves for highway bridges in moderate seismic zones*. Georgia Institute of Technology.

Ontario Structure Inspection Manual. (2018). Ministry of Transportation Ontario.

Osgooei, P. M., Tait, M. J., & Konstantinidis, D. (2017). Non-iterative computational model for fiber-reinforced elastomeric isolators. *Engineering Structures, 137*, 245-255.

Padgett, J. E., & DesRoches, R. (2007). Bridge functionality relationships for improved seismic risk assessment of transportation networks. *Earthquake Spectra, 23*(1), 115-130.

Perdomo, C., & Monteiro, R. (2020). Simplified damage models for circular section reinforced concrete bridge columns. *Engineering Structures, 217*, 110794.

Ramanathan, K., Padgett, J. E., & DesRoches, R. (2015). Temporal evolution of seismic fragility curves for concrete box-girder bridges in California. *Engineering Structures, 97*, 29-46. doi:https://doi.org/10.1016/j.engstruct.2015.03.069

Russo, G., Pauletta, M., & Cortesia, A. (2013). A study on experimental shear behavior of fiber-reinforced elastomeric isolators with various fiber layouts, elastomers and aging conditions. *Engineering Structures, 52*, 422-433.

Sciascetti, A. (2017). *The Effect of Temperature on Unbonded Fiber-Reinforced Elastomeric Isolators.*

Shamsabadi, A., Rollins, K. M., & Kapuskar, M. (2007). Nonlinear soil–abutment–bridge structure interaction for seismic performance-based design. *Journal of geotechnical and geoenvironmental engineering, 133*(6), 707-720.

Shinozuka, M., Banerjee, S., & Kim, S.-H. (2007). *Statistical and mechanistic fragility analysis of concrete bridges*. Retrieved from

Shinozuka, M., Banerjee, S., & Kim, S. H. (2007). *Fragility considerations in highway bridge design*. Retrieved from

Siqueira, G. H., Sanda, A. S., Paultre, P., & Padgett, J. E. (2014). Fragility curves for isolated bridges in eastern Canada using experimental results. *Engineering Structures, 74*, 311-324.

Standard Test Method for Rubber Property--Durometer Hardness. (2005). American Society for Testing Materials.

Stanton, J. F. (2008). *Rotation limits for elastomeric bearings* (Vol. 596): Transportation Research Board.

Takeda, T., Sozen, M. A., & Nielsen, N. N. (1970). Reinforced concrete response to simulated earthquakes. *Journal of the Structural Division, 96*(12), 2557-2573.

Tavares, D., Suescun, J., Paultre, P., & Padgett, J. (2013). Seismic fragility of a highway bridge in Quebec. *Journal of Bridge Engineering, 18*(11), 1131-1139.

Tavares, D. H., Padgett, J. E., & Paultre, P. (2012). Fragility curves of typical as-built highway bridges in eastern Canada. *Engineering Structures, 40*, 107-118.

Waller, C. L. (2011). *A methodology for probabilistic performance-based seismic risk assessment of bridge inventories.* Carleton University.

Xiang, N., & Alam, M. S. (2019). Comparative Seismic Fragility Assessment of an Existing Isolated Continuous Bridge Retrofitted with Different Energy Dissipation Devices. *Journal of Bridge Engineering, 24*(8), 04019070. doi:doi:10.1061/(ASCE)BE.1943-5592.0001425

Zhang, J., & Huo, Y. (2009). Evaluating effectiveness and optimum design of isolation devices for highway bridges using the fragility function method. *Engineering Structures, 31*(8), 1648-1660.

Table 2.1. Mechanical properties of the bridge components

Component	Material model	Details
Deck	3D nonlinear beam-column element	Total length = 236 m
		Thickness = 0.91 m
		Concrete compressive strength, f_{ck} = 35 MPa
		Mass density, ρ = 2400 kg/m^3
		Young's modulus, E = 2.8×10^7 kPa
		Poisson's ratio, μ = 0.2
		Cross sectional area, A = 6 m^2
		Moment of inertia along the y-direction, I_y = 51 m^4
		Moment of inertia along the z-direction, I_z = 0.4 m^4
		Torsional moment of inertia, J = 1.362 m^4
Pier	3D fiber-section forced-based beam-column element with nonlinear fiber materials	Diameter = 0.91 m
		Cover = 76.2 mm
		Yield strength of steel, f_y = 2.75×10^5 kPa
		Young's modulus, E_s = 2×10^8 kPa
		Strain hardening ratio, b = 0.01
FREI	Takeda-Elastic model	Width, a = 850 mm
		Length, 2b = 850 mm
		Rubber thickness (cover layers) = 5 mm
		Rubber thickness (inner layers) = 43.16 mm
		Reinforcement fiber thickness = 0.51 mm
		Total rubber thickness, t_r = 269 mm
		Total fiber thickness, t_f = 3.57 mm
		Total height of bearing, h = 272.5 mm
		Bilinear Takeda
		K_1 (N/m) = 6727 N/m
		K_2 (N/m) = 557 N/m
		u_y (m) = 0.0087 m
		Nonlinear Elastic Spring
		a_1 (N/m) = 2043.4 N/m
		a_3 (N/m^3) = -4.71×10^{-3} N/m^3
		a_5 (N/m^5) = 1.61×10^{-8} N/m^5

Table 2.2. Quantitative description of damage states

Failure mode	Structural response	Slight		Moderate		Extensive		Collapse		Reference
		S_c	β_c	S_c	β_c	S_c	β_c	S_c	β_c	
Column failure	Drift (%)	1	0.25	2.5	0.25	5	0.46	7.5	0.46	(Dutta & Mander, 1998)
Abutment soil failure in passive action	Abutment soil deformation (mm)	37	0.46	146	0.46	N/A*	0	N/A*	0	(Nielson, 2005)
Abutment soil failure in active action	Abutment soil deformation (mm)	9.8	0.7	37.9	0.9	77.2	0.85	N/A*	0	(Nielson, 2005)
Abutment soil failure in transverse action	Abutment soil deformation (mm)	9.8	0.7	37.9	0.9	77.2	0.85	N/A*	0	(Nielson, 2005)
Unseating of the deck at abutment	Displacement of the deck relative to the abutment (m)	N/A	N/A	N/A	N/A	N/A	N/A	1.37	0	

* Padgett and DesRoches determined that severe damage to abutments does not essentially result in a global collapse (Padgett & DesRoches, 2007)

Table 2.3. Fragility parameters of the bridge components

		Monolithic					Isolated				
		Longitudinal			Transverse		Longitudinal			Transverse	
		Peak drift	Peak active backfill soil defo.	Peak passive backfill soil defo.	Peak drift	Peak abutment defo.	Peak drift	Peak active backfill soil defo.	Peak passive backfill soil defo.	Peak drift	Peak abutment defo.
Slight	S_D (g)	0.58	0.13	0.45	0.64	0.15	1.51	0.03	0.11	1.21	0.03
	$\beta_{D\|IM}$	0.24	0.39	0.38	0.35	0.35	0.32	0.00	0.33	0.33	0.66
	β_{TOT}	0.34	0.80	0.60	0.43	0.78	0.41	0.70	0.56	0.41	0.96
	DMR	2.42	0.54	1.88	2.67	0.63	6.29	0.13	0.46	5.05	0.13
	$P[DS\|IM_{2/50}]$	2.49	77.90	14.50	1.10	73	0.00	100	80	0.0	94
Moderate	S_D (g)	1.25	0.46	1.41	1.20	0.53	2.35	0.11	0.51	1.89	1.05
	$\beta_{D\|IM}$	0.31	0.38	0.29	0.29	0.35	0.32	0.33	0.31	0.32	0.34
	β_{TOT}	0.40	0.98	0.54	0.38	0.96	0.40	0.96	0.56	0.41	0.96
	DMR	5.21	1.92	5.88	5.00	2.23	9.79	0.46	2.13	7.89	4.38
	$P[DS\|IM_{2/50}]$	0.0	25	0.0	0.0	20	0.0	70	7.50	0.0	57.50
Extensive	S_D (g)	2.07	0.88	-	1.94	0.89	3.38	0.31	-	2.59	0.41
	$\beta_{D\|IM}$	0.25	0.34	-	0.24	0.32	0.30	0.27	-	0.32	0.32
	β_{TOT}	0.53	0.92	-	0.52	0.91	0.55	0.89	-	0.56	0.91
	DMR	8.63	3.67	-	15.5	7.08	14.08	1.29	-	20.7	11
	$P[DS\|IM_{2/50}]$	0.0	7.75	-	0.0	7.50	0.0	40	-	0.0	31
Collapse	S_D (g)	2.68	-	-	2.52	-	3.85	-	-	3.14	-
	$\beta_{D\|IM}$	0.24	-	-	0.27	-	0.27	-	-	0.27	-
	β_{TOT}	0.52	-	-	0.53	-	0.53	-	-	0.53	-
	DMR	11.17	-	-	20.2	-	16.04	-	-	25.1	-
	$P[DS\|IM_{2/50}]$	0.0	-	-	0.0	-	0.0	-	-	0.0	-

Table 2.4. Discrepancy in the fragility parameters of bridge components

		Longitudinal									Transverse					
		Peak column drift			Peak backfill soil deformation: active action			Peak backfill soil deformation: passive action			Peak column drift			Peak abutment deformation		
		Monolithic	Isolated	Discrepancy (%)	Monolithic	Isolated	Discrepancy (%)	Monolithic	Isolated	Discrepancy (%)	Monolithic	Isolated	Discrepancy (%)	Monolithic	Isolated	Discrepancy (%)
Slight	S_D (g)	0.58	1.51	160.34	0.13	0.03	-76.92	0.45	0.11	-75.56	0.64	1.21	89.41	0.15	0.03	-80.00
	$\beta_{D\|IM}$	0.24	0.32	37.36	0.39	0.01	-97.40	0.38	0.33	-13.43	0.35	0.33	-6.39	0.35	0.66	85.85
	β_{TOT}	0.34	0.41	19.08	0.80	0.70	-12.39	0.60	0.56	-5.18	0.43	0.41	-4.17	0.78	0.96	22.41
	DMR	2.42	6.29	160.34	0.54	0.13	-76.92	1.88	0.46	-75.56	2.67	5.05	89.41	0.63	0.13	-80.00
Moderate	S_D (g)	1.25	2.35	88.00	0.46	0.11	-76.09	1.41	0.51	-63.83	1.20	1.89	57.83	0.53	0.20	-62.55
	$\beta_{D\|IM}$	0.31	0.32	1.51	0.38	0.33	-14.54	0.29	0.31	7.18	0.29	0.32	13.06	0.35	0.34	-1.70
	β_{TOT}	0.40	0.40	0.92	0.98	0.96	-2.08	0.54	0.56	2.10	0.38	0.41	7.62	0.96	0.96	-0.22
	DMR	5.21	9.79	88.00	1.92	0.46	-76.09	5.88	2.13	-63.83	5.00	7.89	57.83	2.23	0.83	-62.55
Extensive	S_D (g)	2.07	3.38	63.29	0.88	0.31	-64.77	-	-	-	1.94	2.59	33.46	0.89	0.41	-53.67
	$\beta_{D\|IM}$	0.25	0.30	19.99	0.34	0.27	-20.21	-	-	-	0.24	0.32	32.55	0.32	0.32	0.56
	β_{TOT}	0.53	0.55	5.00	0.92	0.89	-2.52	-	-	-	0.52	0.56	7.88	0.91	0.91	0.07
	DMR	8.63	14.08	63.29	3.67	1.29	-64.77	-	-	-	8.08	10.79	33.46	3.69	1.71	-53.67
Collapse	S_D (g)	2.68	3.85	43.66	-	-	-	-	-	-	2.52	3.14	24.41	-	-	-
	$\beta_{D\|IM}$	0.24	0.27	9.92	-	-	-	-	-	-	0.27	0.27	-0.11	-	-	-
	β_{TOT}	0.52	0.53	2.27	-	-	-	-	-	-	0.53	0.53	-0.03	-	-	-
	DMR	11.17	16.04	43.66	-	-	-	-	-	-	10.52	13.08	24.41	-	-	-

Table 2.5. System-level fragility parameters of the bridge

		Longitudinal			Transverse		
		Monolithic	Isolated	Discrepancy (%)	Monolithic	Isolated	Discrepancy (%)
Slight	S_D (g)	0.13	0.03	-76.47	0.15	0.06	-60.00
	DMR	1.02	0.24	-76.47	1.20	0.48	-60.00
	$P[DS\|S_{a2/50}]$	81.50	100.00	22.70	73.10	93.40	27.77
Moderate	S_D (g)	0.45	0.15	-66.67	0.53	0.20	-61.90
	DMR	3.60	1.20	-66.67	4.20	1.60	-61.90
	$P[DS\|S_{a2/50}]$	25.40	71.00	179.53	20.50	57.70	181.46
Extensive	S_D (g)	0.84	0.30	-64.88	0.83	0.38	-54.22
	DMR	6.72	2.36	-64.88	6.64	3.04	-54.22
	$P[DS\|S_{a2/50}]$	7.75	41.00	429.03	7.50	30.50	306.67
Collapse	S_D (g)	2.68	3.73	39.06	2.53	2.97	17.62
	DMR	21.46	29.85	39.06	20.20	23.76	17.62
	$P[DS\|S_{a2/50}]$	0.00	0.00	-	0.00	0.00	-

Table 2.6. Peak response history of bridge components

	Longitudinal			Transverse		
	Monolithic	Isolated	Discrepancy (%)	Monolithic	Isolated	Discrepancy (%)
Deck						
Peak displacement [m]	0.029	0.093	220.34	0.025	0.075	197.22
Peak velocity [m/s]	0.367	0.446	21.72	0.343	0.445	30.01
Peak abs. acceleration [g]	0.590	0.458	-22.44	0.618	0.403	-34.75
Column						
Peak base shear [kN]	1146.3	277.7	-75.8	1354.5	262.2	-80.6
Peak base moment [kN.m]	3312	1028.2	-69	3501.3	1009.7	-71.2

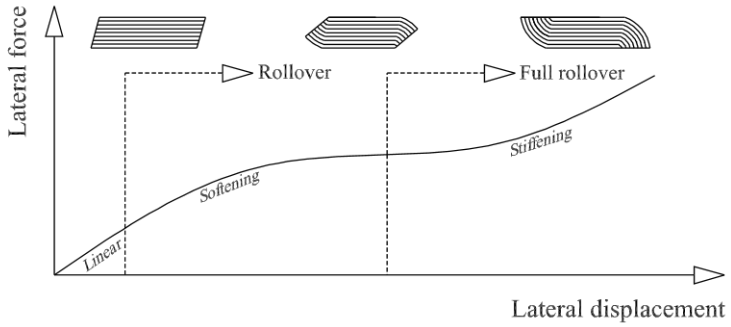

Figure 2.1. Softening and stiffening regimes of unbonded FREI

Figure 2.2. The overpass over the highway

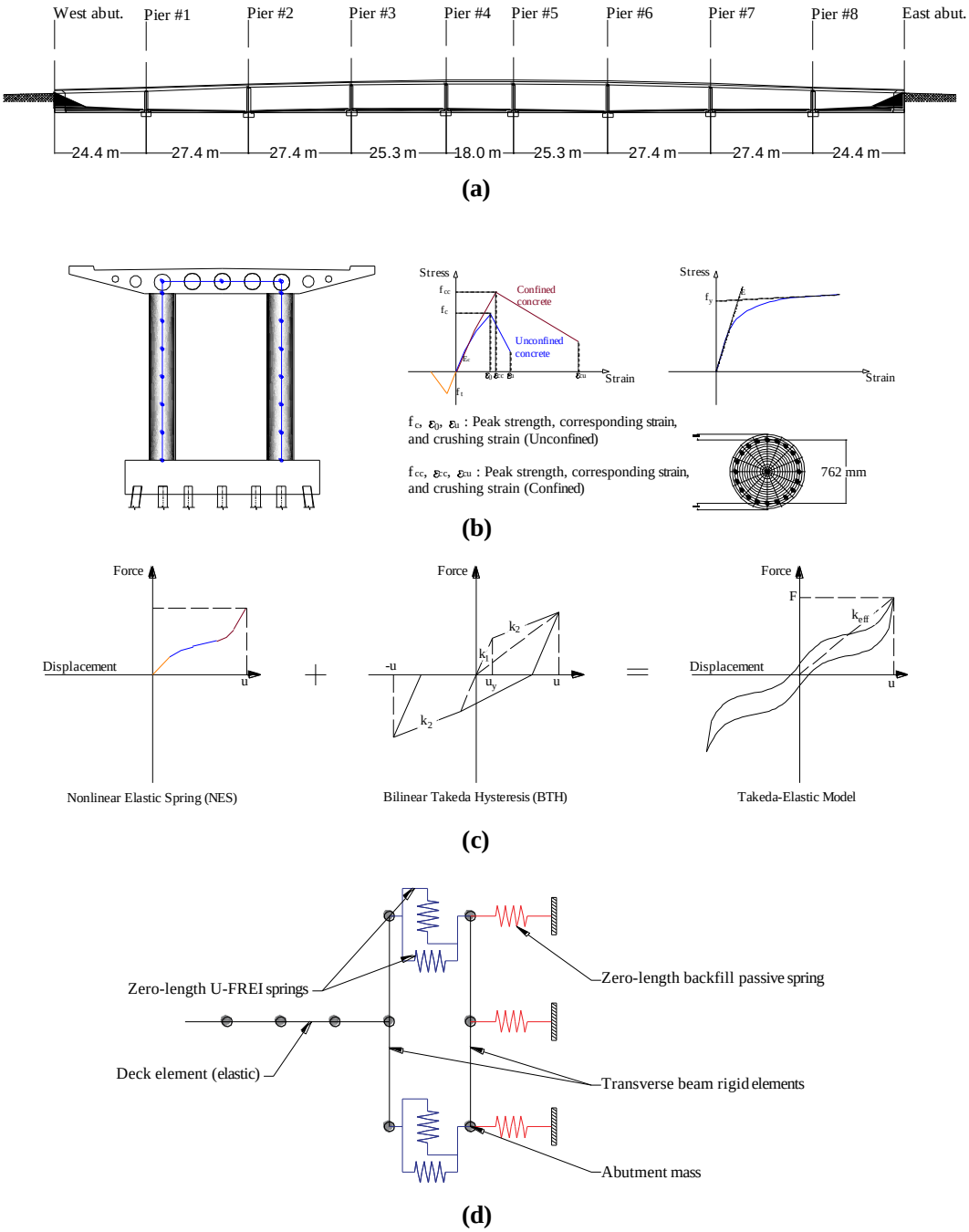

Figure 2.3. (a) Bridge model overview, (b) Characteristic parameters of fiber section of column, (c) Schematic definition of the Pivot-Elastic model (Osgooei et al. 2017), and (d) Connectivity of abutment to deck and backfill soil

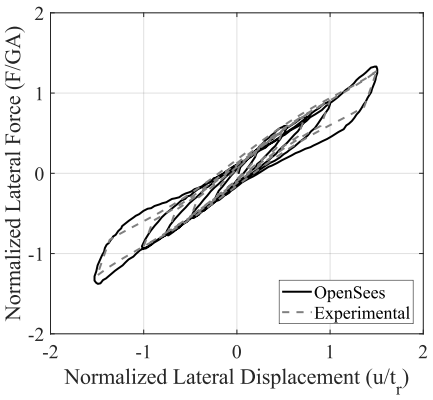

Figure 2.4. Comparison of the Takeda-Elastic model with the experimental data (Sciascetti, 2017)

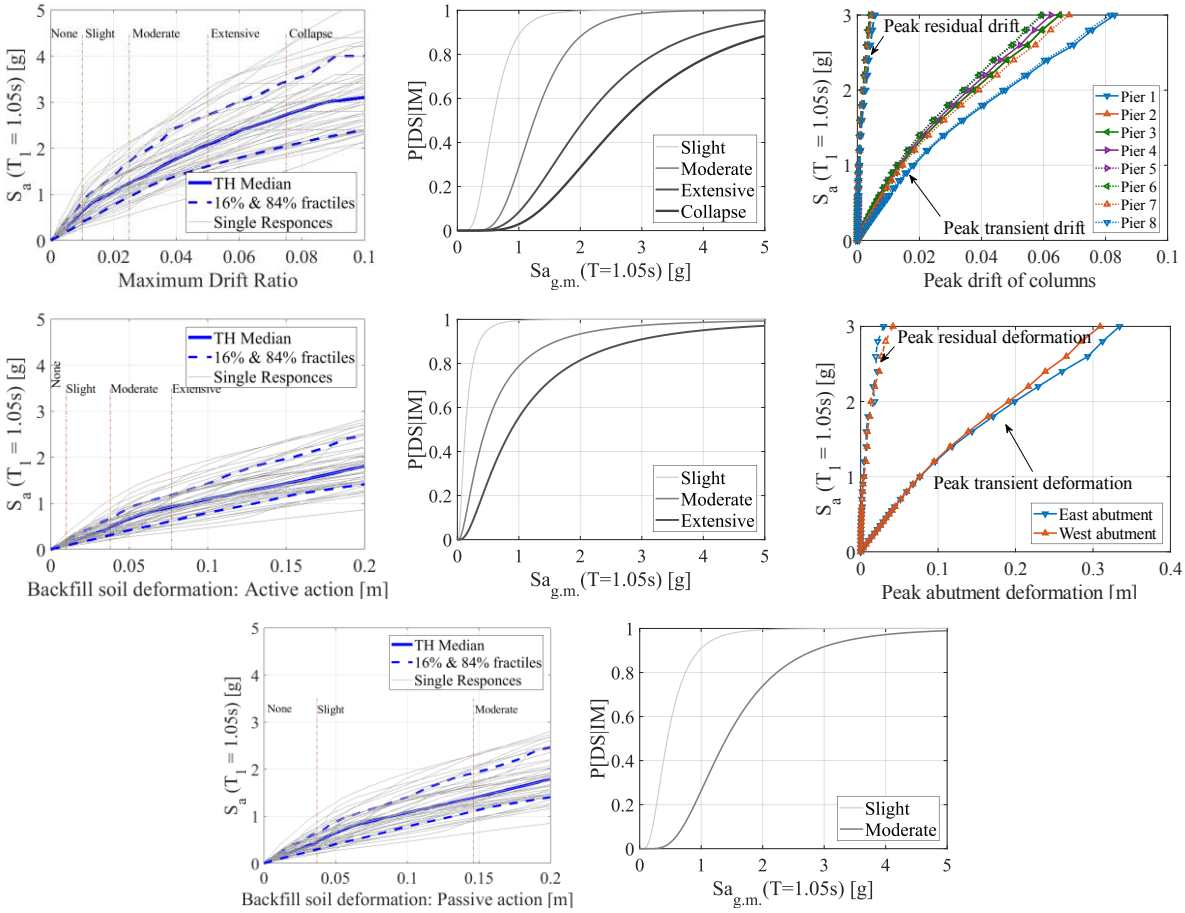

(a) Longitudinal direction of the monolithic bridge

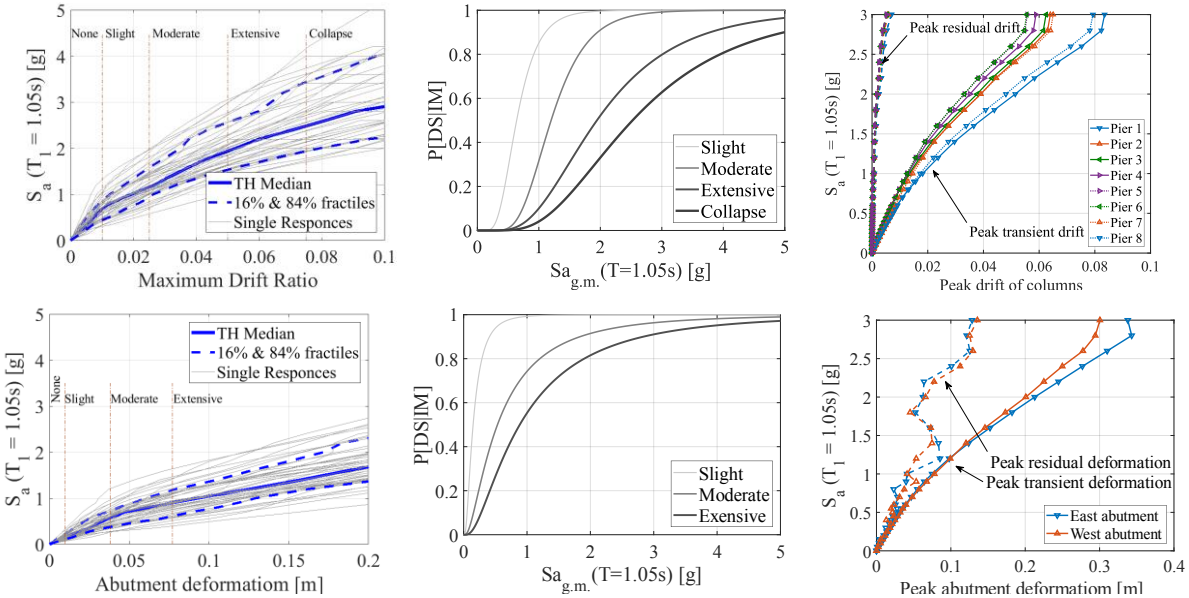

(b) Transverse direction of the monolithic bridge

Figure 2.5. Performance levels and fragility curves of the bridge

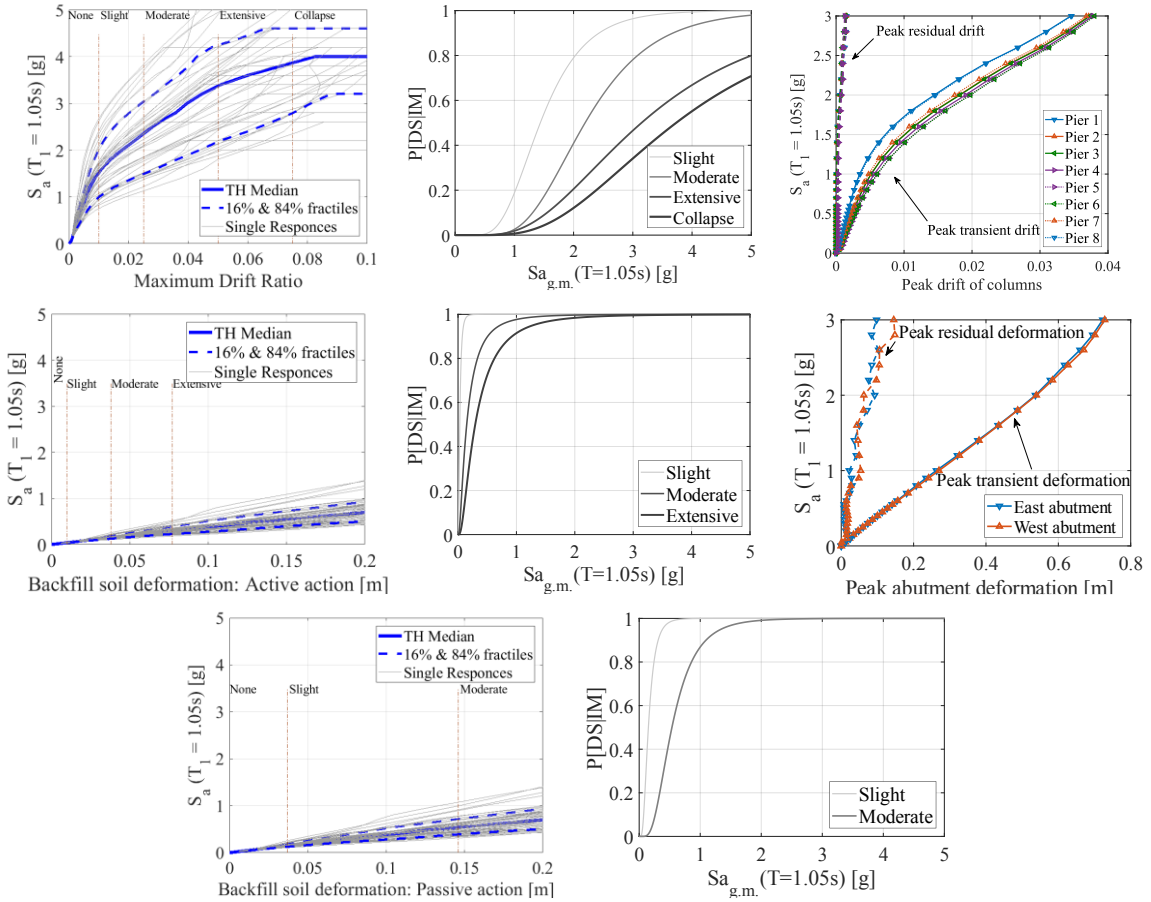

(c) Longitudinal direction of the isolated bridge

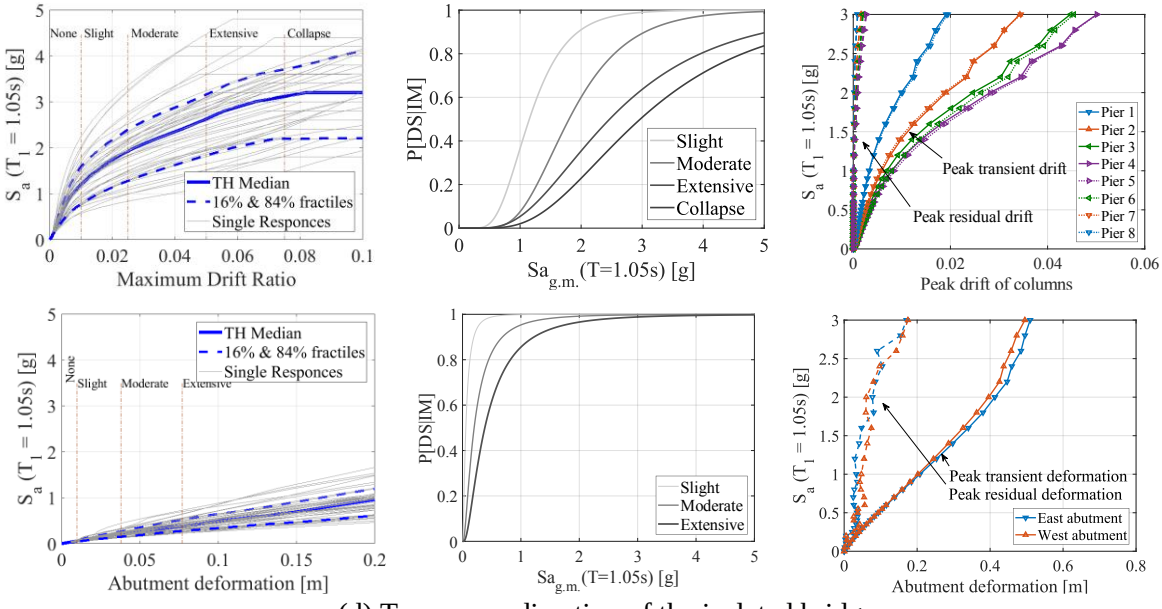

(d) Transverse direction of the isolated bridge

Figure 2.5. Performance levels and fragility curves of the bridge (cont.)

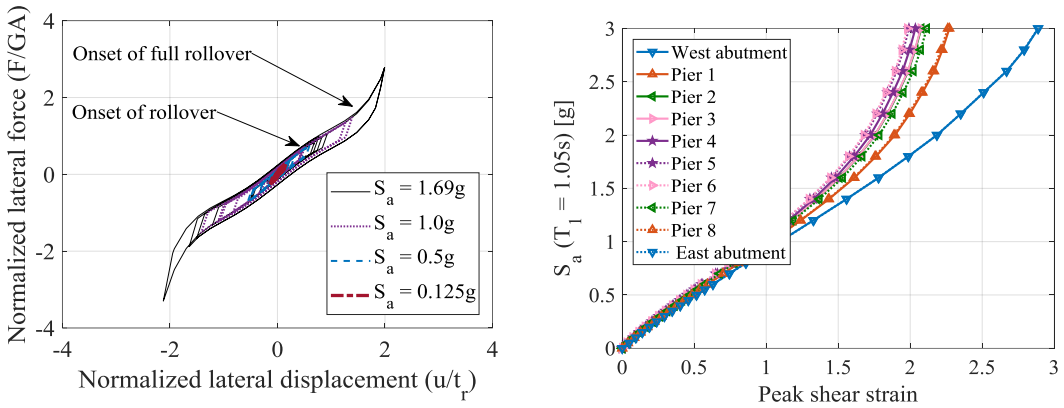

Figure 2.6. Hysteretic behavior and peak shear strains of FREI

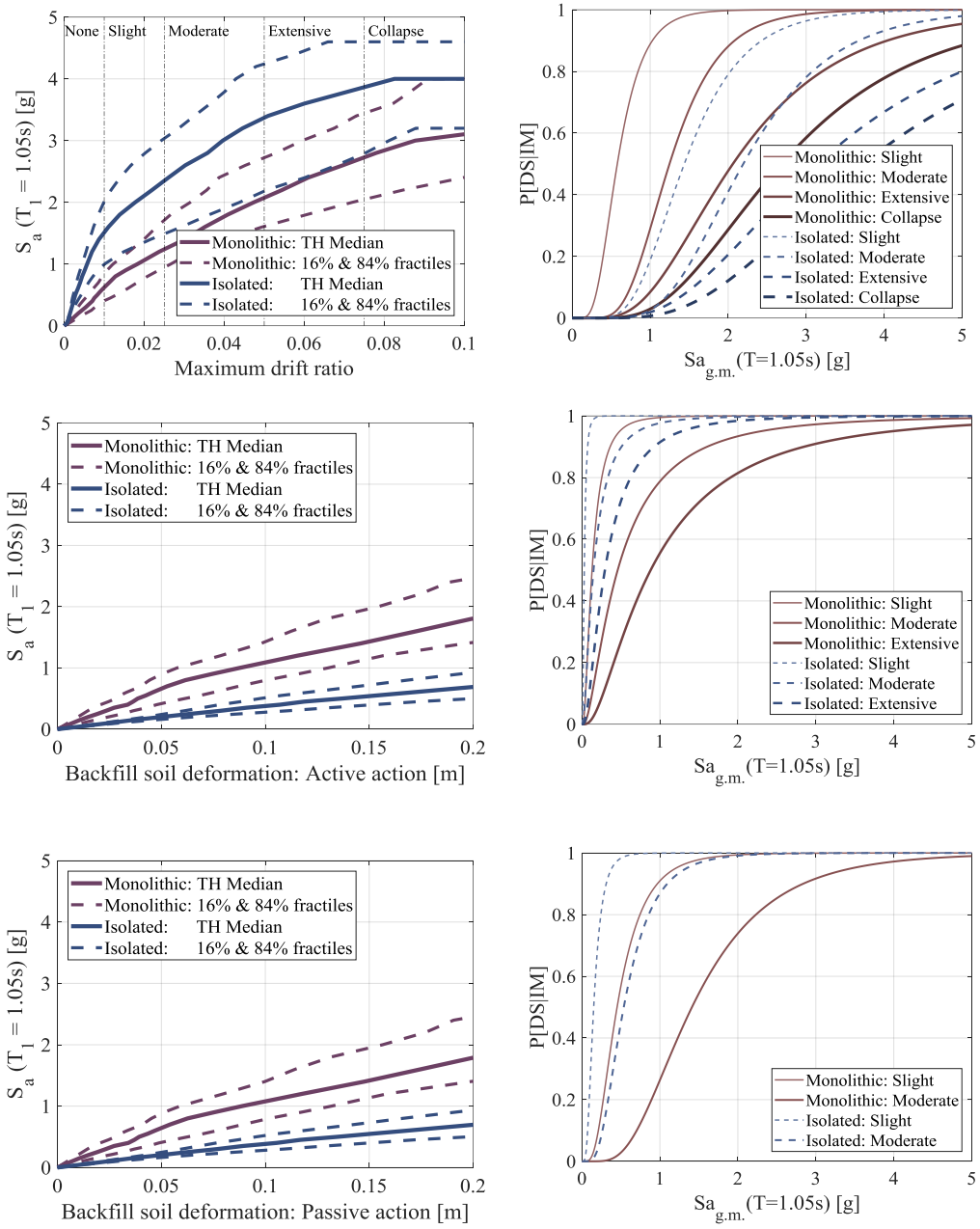

(a) Longitudinal direction

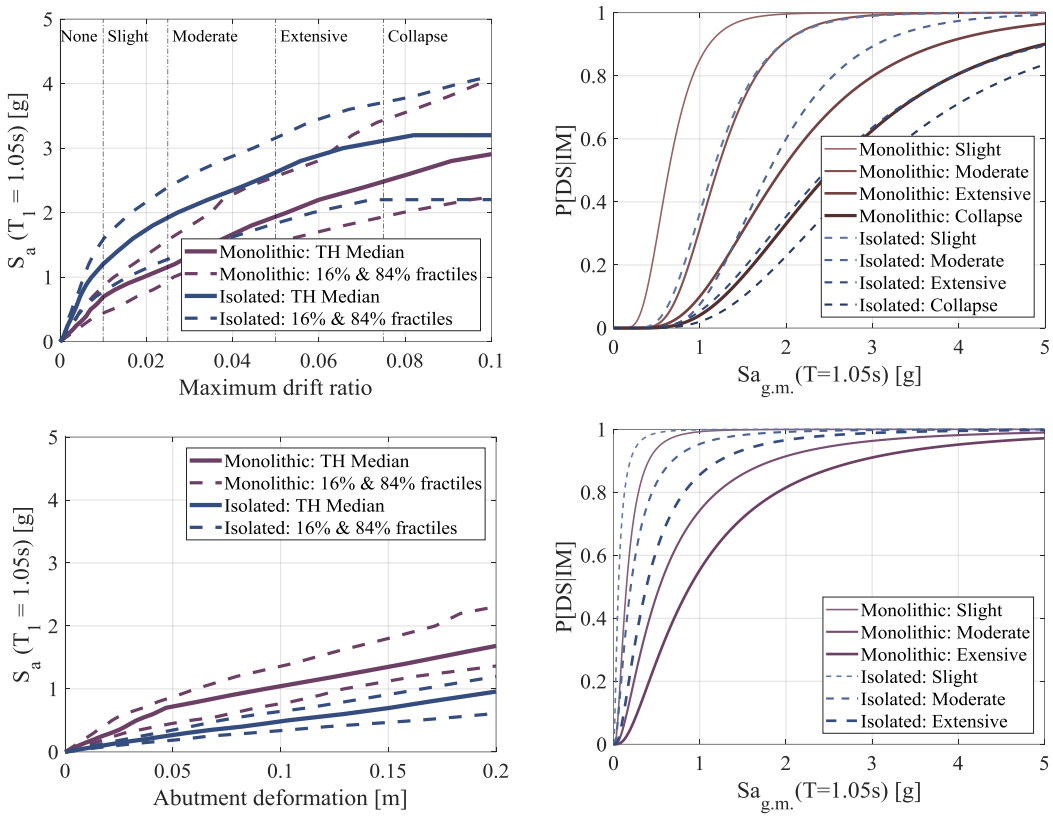

(b) Transverse direction

Figure 2.7. Summarized IDA curves and seismic fragility curves of the bridge

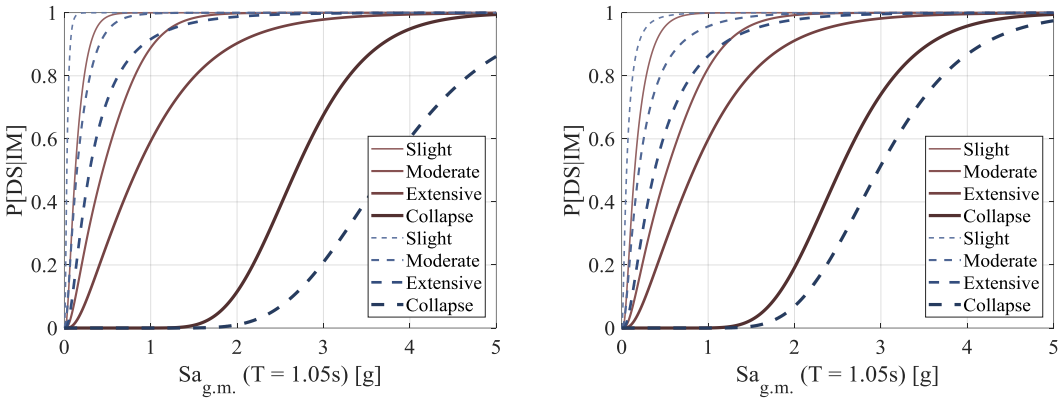

Figure 2.8. System fragility curves of the bridge in (a) Longitudinal and (b) transverse directions

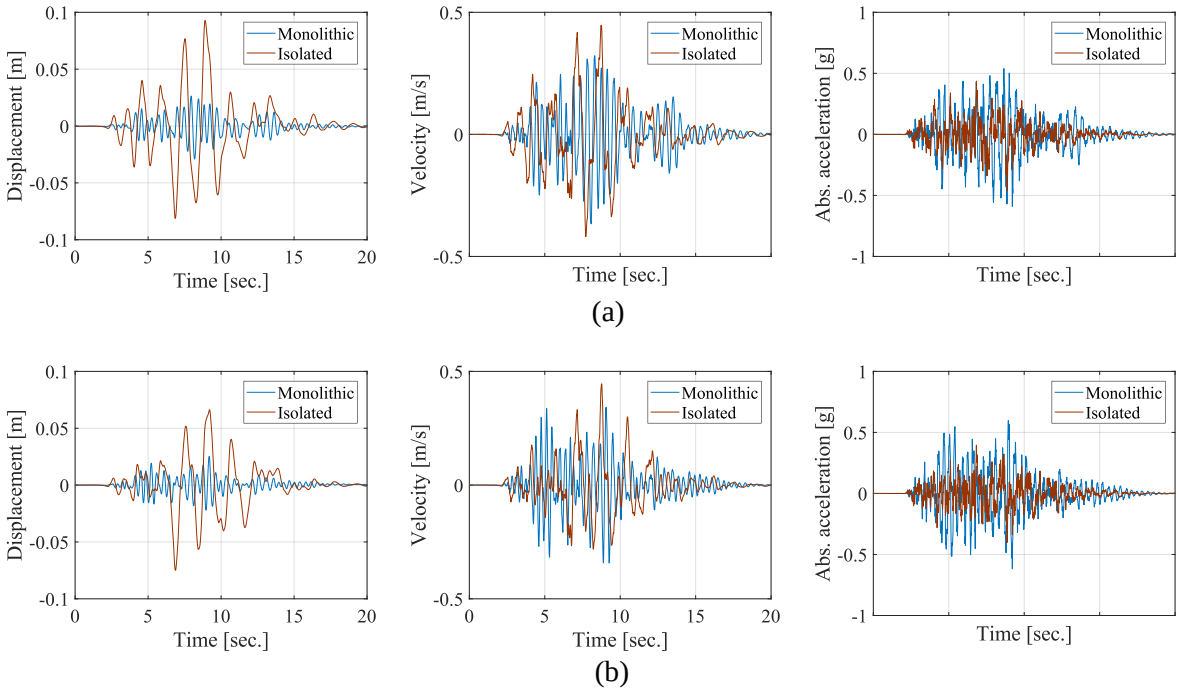

Figure 2.9. Deck response histories prior and after rehabilitation in (a) longitudinal direction, and (b) transverse direction

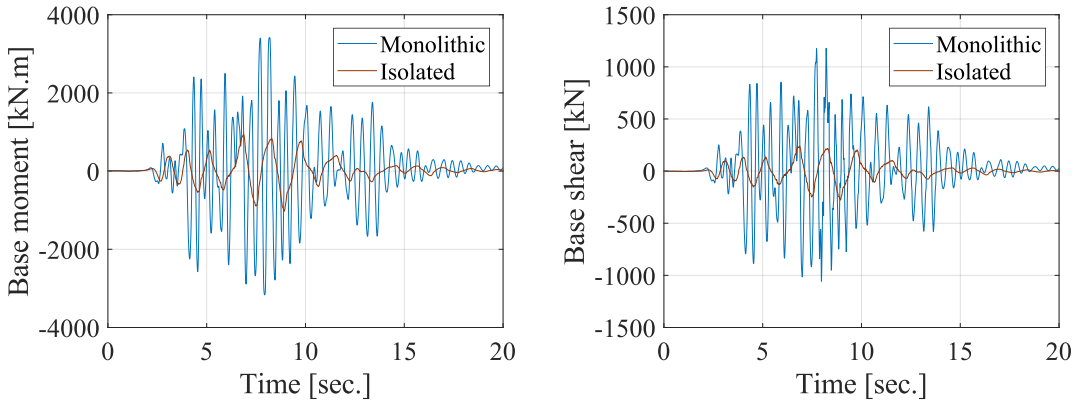

(a)

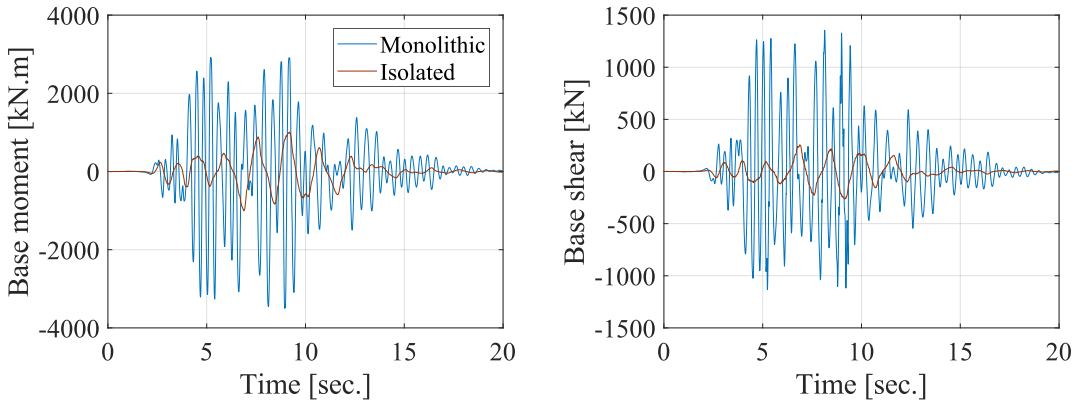

(b)

Figure 2.10. Column response histories prior and after rehabilitation in (a) longitudinal direction, and (b) transverse direction

3 Soil-Pile-Structure Interaction Effects on Seismic Demands and Fragility Estimates of a Typical Ontario Highway Bridge Retrofitted with Fiber Reinforced Elastomeric Isolator

Abstract

This study investigates the seismic performance of a seismically isolated soil-pile-structure system incorporating the effects of isolation system, soil layers of low stiffness and strength, pile inclination, pile-soil-pile interactions, and bridge-embankment interaction. A coupled three-dimensional nonlinear finite element model of an existing bridge in Ottawa, Ontario is developed as a representative of the 44% of the total bridges in Ontario that have been built prior to 1970. A seismic retrofit technique which involves isolating the bridge superstructure utilizing a novel type of elastomeric isolator called Fiber Reinforced Elastomeric Isolator (FREI) is adopted. Two bridge conditions, namely, monolithic (pre-retrofit) and isolated (retrofitted) are considered to investigate the effect of Soil-Structure-Interaction (SSI) on the seismic performance of the bridge prior to and after the retrofit in its longitudinal and transverse directions, independently. Analytical fragility curves are developed for the bridge components based on the outputs of an Incremental Dynamic Analysis (IDA) using 45 synthetic ground motion records. It is shown that seismic isolation can effectively reduce the superstructure acceleration by allowing the deck to experience large lateral displacement. Therefore, the transferred shear forces to the columns and their supporting piles are decreased significantly. While seismic isolation of the bridge is found to be beneficial for bridge components, it has a detrimental effect on the extensive and collapse damage states of abutment piles in the longitudinal direction. This conclusion is limited to the conventional abutment models

where the abutment backwall damage has not been taken into account. Using more complex physics-based abutment spring systems may reveal that using the seismic isolation systems can mitigate the probability of extensive damage and collapse to abutment piles by allowing the abutment to serve as a fuse and dissipate the imposed energy by its fracture mechanism.

Keywords: Soil-Structure-Interaction, Fiber Reinforced Elastomeric Isolator, Incremental Dynamic Analysis, Analytical fragility curve, Beam on Nonlinear Winkler Foundation

3.1 Introduction

Robust seismic risk assessment of urban infrastructures requires a versatile representation of the structural system along with its comprising components and their corresponding interactions. Highway bridges, one of the most vital but fragile elements of transportation networks, are composed of various structural components such as deck, piers, abutments, backfill soil, and foundations. The diversity of the bridge constitutive components accentuates the need for considering a vast range of interactions including deck-abutment, abutment-embankment (Kotsoglou & Pantazopoulou, 2007; Zhang & Makris, 2002) and soil-foundation-pier (Elgamal, Yan, Yang, & Conte, 2008; Mylonakis, Nikolaou, & Gazetas, 2006) where the Soil-Structure Interaction (SSI) is deemed to represent the most prominent factor in modifying the dynamic response and seismic performance of bridges (Mylonakis & Gazetas, 2000). Owing to the multi-parametric problem nature of the soil domain, however, the impact (either favorable or unfavorable) of SSI on the seismic response of bridges is scarce and findings in this domain are conflicting (Stefanidou, Sextos, Kotsoglou, Lesgidis, & Kappos, 2017). Until recently, the consensus amongst researchers was that SSI effects are beneficial to the seismic response of bridges through providing a natural isolation layer beneath the bridge with additional flexibility

and damping (Ucak & Tsopelas, 2008). Mylonakis and Gazetas explored the performance of a simplified bridge-foundation system under a set of actual ground motion records on soft soil and concluded that the elongated period and increased damping of the system has an adverse effect on the imposed seismic demands (Mylonakis & Gazetas, 2000). In another study, Jeremic et al. conducted a comprehensive finite element analysis on the seismic performance of the I-880 viaduct in California and concluded that depending on the characteristics of the input excitation, SSI can be both beneficial and detrimental (Jeremić, Kunnath, & Xiong, 2004). Several other studies have been carried out on the effect of SSI on the seismic response of bridges and shown that SSI has a conspicuous effect on the bridges having relatively light superstructures and heavy substructures regardless of the soil stiffness (Stefanidou et al., 2017).

The influence of SSI on the seismic performance of the bridge system is a function of the adopted modeling approach of the underlying soil domain. These approaches can be categorized as (a) linear or nonlinear lumped springs at the column bases representing the dynamic characteristics of the of bridge foundations and the supporting soil deposit (Xiang & Alam, 2019; Yang, Werner, & DesRoches, 2015); (b) coupled comprehensive 3D representation of the entire soil-foundation-bridge system (Elgamal et al., 2008; Rahmani, Taiebat, Liam Finn, & Ventura, 2016); and (c) employing the concept of Beam on a Nonlinear Winkler Foundation (BNWF) using a set of distributed dynamic soil springs (p-y, t-z, and q-z) to account for the nonlinear interaction along the length of the piles (Noori, Memarpour, Yakhchalian, & Soltanieh, 2019; Xie & DesRoches, 2019). While the inherent nonlinearity and frequency-dependency nature of the soil is prohibitive in using lumped springs, and computational burden and cost of analyzing an integrated finite element model of the entire soil-bridge system are cumbersome, BNWF is discerned to be the most

easy-to-manipulate yet accurate approach for simulating the soil domain (Xie & DesRoches, 2019).

Numerous studies have investigated the influence of SSI on the seismic performance of conventionally designed bridges (Carbonari, Morici, Dezi, Gara, & Leoni, 2017; González et al., 2019; Mallick & Raychowdhury, 2015). However, there are few publications available in the literature on the extent to which the SSI affects the structural response of seismically isolated bridges (Ucak & Tsopelas, 2008). This lack of inclusion of SSI presumably stems from the premise that SSI effects behave like an additional isolation layer, thereby increasing the period shift that the isolation system had initially introduced to the system resulting in a reduction in the seismic demand. It is illustrated schematically in Figure 3.1 where the fundamental period of the isolated structure has been shifted away because of the presence of the isolation system followed by another shift due to SSI effects. Owing to the relatively high degree of nonlinearity of isolated systems and their corresponding excessive computational costs, most studies are inclined toward using simplifying techniques such as using two-degree of freedom linear elastic models for the bridge (Vlassis & Spyrakos, 2001), linear elastic behavior for the isolation system (Tongaonkar & Jangid, 2003), lumped springs in lieu of soil domain (Dicleli, Albhaisi, & Mansour, 2005), and closed-form solutions to simulate the SSI effect (Ucak & Tsopelas, 2008). However, the degree to which these simplifications distort the seismic response of structures and the interplay between the inherent nonlinearity in the soil domain with the highly nonlinear behavior of the isolation layer should be scrutinized.

The dynamic response of a coupled seismically isolated bridge-soil-foundation system is complex, particularly for soft soils with relatively large degrees of nonlinearity. Moreover, the efficiency of

the isolation system itself is highly dependent on the frequency characteristics of the structure, as well as the frequency content and amplitude of the earthquake excitation (Wang, Padgett, & Dueñas-Osorio, 2012). Hence, investigating the seismic performance of bridges in component and system-level under different earthquake intensities is not insightful by employing deterministic approaches (Zhang & Huo, 2009). Seismic fragility analysis is a paramount approach for evaluating the seismic performance of bridges in a probabilistic framework, based on the probability of a bridge system or component reaching or exceeding distinct prescribed damage states under a vast range of earthquake intensities. While the well-accepted fragility function method has often been utilized to evaluate the vulnerability of highway bridges (Mangalathu & Jeon, 2019; Martínez, Hube, & Rollins, 2017; Xie, Zhang, DesRoches, & Padgett, 2019), a limited number of studies are focused on the fragility analysis of bridges incorporating the effect of SSI (Aygün, Dueñas-Osorio, Padgett, & DesRoches, 2010; Kwon & Elnashai, 2010; Xie & DesRoches, 2019) and little attention is placed on exploring the fragility of an integrated seismically isolated bridges-soil-foundation system (Dai, Rojas, Shi, & Tan, 2018).

The primary goal behind the present study is to interrogate the prevailing perception that incorporating the SSI effects mitigate the probability of damage to bridge system and its comprising components subjected to seismic excitations. To this end, the 7th line overcrossing bridge, a conventionally designed bridge in Ottawa, is adopted as a testbed for this study. The seismic performance of this bridge is investigated in its as-built and retrofitted condition to characterize the extent to which the SSI effects alter the seismic behavior of a monolithic bridge and its isolated counterpart. The rehabilitation of the bridge is carried out using a novel type of elastomeric isolators called Fiber Reinforced Elastomeric Isolator (FREI). FREI has superior characteristics with respect to an equivalent steel-reinforced elastomeric isolator such as lighter

weight, low manufacturing cost, and ability to be installed unbonded (Kelly, 1999). Efficiency and sufficiency of FREI to mitigate the seismic demand of structures have been explored extensively under various loading types, namely, vertical, lateral, rotational, and their combination (Y. Al-Anany, Van Engelen, & Tait, 2017; Y. M. Al-Anany & Tait, 2015, 2017). Thereby, modern bridge design codes (e.g. CSA-S6-19 and AASHTO 2012) permit the use of fiber fabrics instead of steel shims as the reinforcing layer (AASHTO, 2012; *Canadian Highway Bridge Design Code*, 2019). Recently, Al-Anany et al. (Y. M. Al-Anany, Moustafa, & Tait, 2016) and Sciascetti (Sciascetti, 2017) have conducted studies on the seismic performance of a generic three-span bridge isolated with FREI to a limited extent, the effect of SSI in their studies is neglected.

This study aims to investigate the effect of SSI on the seismic performance of seismically isolated bridges using FREI through a detailed SSI modeling approach (p-y spring) and the lumped springs for abutment-embankment interaction. A probabilistic framework is then set up by conducting an Incremental Dynamic Analysis (IDA) to provide a basis for constructing the seismic fragility curves of the bridge components.

3.2 Prototype bridge and finite element modeling

3.2.1 Bridge description

The province of Ontario owns around one-third of the total number of bridges across Canada (*Inventory of publicly owned bridge and tunnel assets,* 2016). While a large number of these bridges are not designed in accordance with the modern ductile seismic provisions, 60% and 77% of these bridges have not experienced any major and minor rehabilitation, respectively, in the last 20 years (*Inventory of publicly owned bridge and tunnel assets,* 2016). On the other hand, the region's seismic hazard was modified from 475 to 2475 years return period earthquakes in the

2005 edition of the National Building Code of Canada (NBCC) (*National Building Code of Canada*, 2015). Therefore, the 7th line overpass in Ottawa, Ontario, is selected as the testbed for this study as a representative to 44% of the Ontario bridges that have been constructed prior to 1970. As shown in Figure 3.2, the bridge is 236 *m* long, supported by eight pair of intermediate columns, two seat-type abutments, and about 56.4 *m* of sensitive clay underneath. This section of the bridge lies on the boundary of the minor physiographic regions known as Ottawa valley clay plain and the Russell and Prescott sand plain and is characterized by relatively thick deposits of sensitive marine clay, silt, and silty clay that were deposited within the Champlain sea basin (Chapman & Putnam, 1984). The bridge is symmetric and does not have skewness in the abutments. The superstructure is composed of 11.0 *m* wide 9-cell post-tensioned cast in place voided slab supported by eight pairs of circular reinforced concrete columns reinforced with 20 longitudinal steel rebars producing a 4.4% longitudinal reinforcement ratio and spiral confinement with a 0.051 *m* pitch. The diameter of the columns is 0.91 *m* with a center-to-center distance of 4.3 *m* and an average height of 6.1 *m* where middle columns are longer than the columns adjacent to abutments. Piers and abutments are supported by rigid pile caps lied on a group of driven friction H-shaped steel sections. The dimension of pile caps is 7.0×2.75×1.2 *m* under piers and 11.0×5.1×0.75 *m* under abutments. Pile sections are comprised of HP 12×74 steel profiles. Pier pile groups are composed of 20 piles including four vertical piles in the middle and 16 perimeter battered piles (6 longitudinally and 10 transversely battered) whereas abutment pile groups are constituted of 23 piles including 13 vertical and 10 longitudinally battered piles, as illustrated in Figure 3.3. All supporting piles under piers and abutments are 56.4 *m* long. It should be pointed out that the available geotechnical test results of the bridge site revealed that the average shear wave velocity in the upper 30 *m* of the subsurface stratigraphy is approximately 127 *m/s* that

corresponds to soft soil categorized as site class E. In the case of the seismically isolated bridge, FREIs are installed in the transition zone between the superstructure and the supporting columns or abutments in order to decouple the deck from the ground motions. The structural and mechanical details of all bridge components are tabulated in Table 3.1.

3.2.2 Finite element modeling of the prototype bridge

A three-dimensional nonlinear finite element of the bridge-pile-soil system is developed in OpenSees (McKenna, 2011). In addition to the as-built condition of the existing bridge, a seismically isolated counterpart of the bridge using FREI is developed to investigate the effect of SSI on both monolithic and isolated bridges. The analytical model of the bridge is developed using the original construction drawings and calibrated with previously performed experiments. A detailed explanation of the superstructure, supporting piers, isolation system, pile groups and soil domain, and abutments are provided, accordingly.

3.2.2.1 Superstructure

Various modeling approaches have been developed for simulating the bridge superstructures such as the spine-line model and grillage model where former strikes a good balance between computational efficiency and accuracy whereas latter is useful for simulating skewed bridges (Aviram, Mackie, & Stojadinović, 2008; Kaviani, Zareian, & Taciroglu, 2014). Since the skewness of abutments is not of a concern in this study, a three-dimensional spine-line model is adopted with line elements located at the centroid of the cross-section following the bridge alignment. The superstructure is modeled using elastic beam-column elements because the deck is not expected to contribute to the lateral resistance of the bridge against earthquakes and flexural yielding during seismic response is not anticipated. Following the recommendation of discretizing the

superstructure, cap beam, and column bents to at least five elements of equal length (Aviram et al., 2008), the deck is discretized into 10 elements per span with translational and rotational masses lumped at the nodal points.

3.2.2.2 Piers

Bridge columns are anticipated to experience damage or collapse under severe ground motions, and thus nonlinear beam-column elements with spread plasticity are used to represent columns. The clear height of columns to be taken from the level of pile cap to the bottom surface of the deck is discretized into eight elements along with a rigid element on top of the column with a length equal to the difference between the column top to the centroid of the deck cross-section. The fiber section of columns is comprised of unconfined and confined concrete as well as longitudinal reinforcement fibers. As shown in Figure 3.4 the stress-strain constitutive relationship for concrete and steel rebars are considered to be representing by a Mander's model (Mander, Priestley, & Park, 1988) and Giuffre-Menegotto-Pinto model with isotropic hardening (Filippou, Bertero, & Popov, 1983), respectively.

3.2.2.3 Seismic isolation system

The retrofit measure adopted in this study is isolating the superstructure utilizing a novel type of elastomeric isolator, which is FREI. Unbonded application of FREIs (a.k.a. U-FREI) provides a unique lateral behavior in which the isolator experiences a softening at relatively small displacements followed by a stiffening at larger lateral amplitudes. At lower lateral amplitudes, U-FREI top and bottom faces are still in full contact with upper and lower supports, and thus, the isolator behaves linearly like a bonded isolator. By increasing the amplitude of the lateral displacement top and bottom surfaces of the FREI lose their contact with supports resulting in a

reduction in the shear area and stiffness. At large displacements, initially vertical sides of FREI reach a full contact to upper and lower supports (full rollover) that results in an increase in the shear area and stiffness, consequently. The three-stage lateral behavior of the U-FREI is illustrated in Figure 3.5. Several models have been developed to accurately simulate this unique nonlinear behavior of U-FREI (Foster, 2012; Toopchi-Nezhad, Tait, & Drysdale, 2009). While most of these models are iterative and amplitude-dependent, Osgooei et al. (Osgooei, Tait, & Konstantinidis, 2017) developed a non-iterative rate-independent Takeda-Elastic model (Figure 3.5) that is comprised of a nonlinear elastic spring in parallel with a Takeda-based bilinear plastic model (Takeda, Sozen, & Nielsen, 1970). The combination of these two models provides the required values of effective stiffness and damping ratio of the isolation system at a given displacement amplitude (Moghimi Osgooei, 2014). While the summation of the shear forces in the system provides the required effective stiffness obtained from an experimental test on the FREI, the bilinear plastic model provides the required damping and the nonlinear elastic spring guarantees the unique softening and stiffening behavior of the FREI. The induced shear force of the bilinear Takeda-Elastic model can be expressed using the following relations:

$$\begin{aligned} F_{TB} &= k_1 u && u < u_y \\ F_{TB} &= k_1 u_y + k_2 \left(u - u_y\right) && u \geq u_y \end{aligned} \tag{3.1}$$

where k_1 and k_2 are initial and post-yield stiffness, respectively, and u_y is the yield displacement. The nonlinear elastic spring is represented using a fifth-order polynomial with the force-displacement relation as follows:

$$F_{NES} = a_1 u + a_2 u^3 + a_3 u^5 \tag{3.2}$$

where the a_i are the polynomial constants (Moghimi Osgooei, 2014). Accordingly, effective stiffness of the U-FREI can be determined by dividing the summation of developed forces in the two parallel springs to the displacement amplitude using the following equations:

$$\begin{aligned} K_{eff} &= k_1 + a_1 + a_2 u^2 + a_3 u^4 && u < u_y \\ K_{eff} &= (k_1 - k_2)\frac{u_y}{u} + k_2 + a_1 + a_2 u^2 + a_3 u^4 && u \geq u_y \end{aligned} \tag{3.3}$$

In the Takeda-Elastic model, the only source of energy dissipation is the Takeda-based bilinear plastic model. Therefore, the effective damping ratio of the system at displacement amplitudes larger than the yield displacement can be determined by

$$\beta_{eff} = \frac{1}{4\pi}\left[\frac{\left(k_1 u_y + k_2\left(u - u_y\right)\right)\times 2\left(u - \frac{k_1 u_u + k_2\left(u - u_y\right)}{k_1}\right)}{k_{eff}\times u^2}\right] \tag{3.4}$$

The aforementioned model parameters (i.e. k_1, k_2, u_y, a_1, a_2, and a_3) are determined by employing a minimization technique (e.g. least square method) to minimize the error the effective stiffness and damping obtained from Equations 3 and 4 with those determined experimentally (Moghimi Osgooei, 2014). In this study, the model parameters are calibrated using the experimental test data conducted on a quarter-scale FREI by Sciascetti (Sciascetti, 2017). For the case study herein, a FREI is designed based on the provisions of CSA-S6-19 (*Canadian Highway Bridge Design Code*, 2019) such that the vertical normal stress and lateral shear strain of the isolator do not exceed the code specified values. The mechanical specifications of the designed isolator are demonstrated in Table 3.1. To implement the Takeda-Elastic model in OpenSees, two parallel zero-length elements represented by *Hysteretic* and *ElasticMultiLinear* materials are employed using the fitted data presented in Table 3.2.

3.2.2.4 Pile groups and soil domain

Each bridge pier and abutment are supported on a group of 20 and 23 piles, respectively. The diameter of each pile is 3.1 m and the spacing between any two piles is almost three times the diameter of the pile, which makes it a closely spaced pile group. Similar to column sections, piles are modeled using beam-column elements with spread plasticity which is characterized by a Giuffre-Menegotto-Pinto with isotropic hardening constitutive model for steel material that is known as *steel02* material. The BNWF approach after Boulanger et al. (Boulanger, Curras, Kutter, Wilson, & Abghari, 1999) is employed to simulate the pile-soil interaction due to horizontally applied dynamic and vertically applied static loads. The soil-pile interface is composed of three nodes (i.e. pile node, dummy node, and soil node), one contact element, and an equal DOF constraint where the pile nodes and dummy nodes are defined with three dimensions and six-degrees-of-freedom (3 translational, and 3 rotational) and three dimensions and three degrees-of-freedom, respectively. Two series of laterally oriented p-y spring elements in two mutually perpendicular horizontal directions (i.e. longitudinal and transverse directions) are attached to each soil node to simulate the lateral resistance of the soil-pile interface. The frictional resistance along the length of each pile and the tip resistance at the tip of the pile are represented by a series of vertically oriented t-z spring elements to accommodate the rocking motion of the pile group and q-z spring elements, respectively. The connectivity of nodes at the soil-pile interface is illustrated in Figure 3.6. The constitutive behavior of p-y, t-z, and q-z spring elements are defined using *Pysimple1*, *Tzsimple1*, and *Qzsimple1* uniaxial materials, respectively. The soil properties are taken from an available geotechnical report exhibiting that the underneath soil is a single layer of sensitive clay. These properties along with the API provisions (API, 2007) for laterally and axially

loaded piles are used to determine the backbone curve parameters for p-y, t-z, and q-z springs exhibited in Figure 3.7.

Pile groups often tend to exhibit less lateral resistance than the sum of the lateral resistance of the individual piles due to soil-pile-soil interaction. The reduction in the pile group lateral capacity is a result of the edging and shadowing effect where the shear zone in front of each pile overlaps with those of other closely spaced piles in other rows and columns. The most widespread approach for incorporating the group effect is modifying the p-y backbone curves through reducing the soil resistance by a constant factor, P_m. Various recommendations for determining P_m of uniformly-spaced rectangular pile groups are available in the seismic design codes (AASHTO, 2012; *Canadian Highway Bridge Design Code*, 2019; FEMA:P-751, 2012). These recommendations are primarily based on experimental tests conducted by different researchers on a specific geometry of pile groups with certain regularly-spaced rows in group. However, the pile groups in this study are neither rectangular nor regularly-spaced. Therefore, another approach developed by Van Impe and Reese (Van Impe & Reese, 2010) is adopted. This approach is capable of considering the number of piles with arbitrary spacing in addition to spacing/diameter of the piles in the group. As such, a reduction factor for every individual pile is calculated considering the shadowing effect of all surrounding piles including leading, trailing, side-by-side, and skewed piles for every loading direction. The multiplication of the reduction factors of each pile in a row results in the row reduction factor, and P_m is the average of the reduction factors for all rows. Thereby, P_m for abutment pile groups is determined to be 0.81 and 0.84 for longitudinal and transverse directions, respectively, whereas it is 0.66 and 0.63 for pier pile groups in the two mentioned orthogonal directions.

The effect of batter on the behavior of laterally loaded piles is taken into account by using a modifying constant as a function of the batter angle and loading direction (Van Impe & Reese, 2010). This parameter is used to modify the value of p_{ult} and the p-y curves, accordingly. Depending on the batter angle of the battered piles shown in Figure 3.3 and the loading direction, the modifying constant for the abutment pile group is determined to be 0.75 (1.32) for out-batter (in-batter) loading directions, respectively, whereas they are 0.81 (1.24) for the pier pile groups. Due to cyclic nature of the earthquake excitation, an average value of the mentioned constants is considered.

3.2.2.5 Abutments, pounding, and backfill soil

Abutments can be represented using a roller model, simplified model, and spring model, according to their required degree of complexity and efficiency (Aviram et al., 2008). In this study, a complex spring model developed by Mackie and Stojadinovic (Mackie & Stojadinovic, 2006) is adopted that includes the participating mass corresponding to the concrete abutment and mobilized backfill soil. Prior to gap closure, the superstructure forces are transmitted to the abutment and subsequently the pile groups and backfill soil through the FREI. Afterwards, the superstructure collides with the abutment back wall and mobilizes the passive backfill pressure. A system of zero-length spring elements representing pounding and backfill soil is used in a series configuration with the zero-length FREI spring. Pounding between deck and abutment is accounted for using a bilinear contact element proposed by Muthukumar and DesRoches (Muthukumar & DesRoches, 2006) and implemented in OpenSees by *ImpactMaterial*. For embankment-abutment interaction, a zero-length element representing a simplified model for backfill stiffness developed by Shamsabadi et al. (Shamsabadi, Rollins, & Kapuskar, 2007) is adopted and implemented in OpenSees using a *HyperbolicGap* material. The nonlinear behavior of the impact and the backfill

soil elements are illustrated in Figure 3.8. It should be pointed out that the bridge does not have a shear key acting in the transverse direction.

3.3 Seismic fragility methodology using IDA

IDA-based seismic fragility analysis is based on four successive steps; (1) seismic hazard assessment and ground motion selection, (2) performing IDA, (3) assigning damage limit states, and (4) developing fragility curves for bridge system and its constitutive components, each of which are explained accordingly.

3.3.1 Seismic hazard assessment and ground motions selection

The primary step in performing seismic fragility analysis of structural systems is selecting an appropriate suite of ground motion records whose response spectra match a site-specific target response spectrum. The updated Maximum Considered Earthquake (MCE) level response spectra in the NBCC (*National Building Code of Canada*, 2015) from 10% to 2% probability of exceedance in 50 years necessitates the reevaluation of the seismic performance of conventionally designed bridges. Hence, a deaggregation analysis is conducted for the bridge site location (Latitude 45.36 N, and Longitude -75.52 W) to determine the contribution of events to seismic hazard. Seismic hazard, mean magnitude (M_w), and mean distance for the fundamental period of the bridge (T_1 = 1.0 sec.), 2% in 50 years probability of exceedance, and soil class C are determined to be 0.125g, 6.9, and 63 km respectively. However, the available geotechnical report for a nearby site revealed that the average shear wave velocity for the upper 30 m of the subsurface stratigraphy is approximately 127 m/s that corresponds to soft soil or soil class E. It is explicitly mentioned in the report that the soil is not susceptible to liquefaction. Therefore, a target response spectra corresponding to the results obtained from deaggregation analysis and updated using

NBCC (*National Building Code of Canada*, 2015) for soil class E is adopted in which the spectral acceleration for the fundamental period of the bridge is 0.24g.

Owing to the low seismicity and number of occurred earthquake events in eastern Canada, a sufficient number of ground motion records are not available for the bridge site. However, Atkinson (Atkinson, 2009) has developed different suites of synthetic accelerograms for various range of soil classes in eastern Canada in accordance with the NBCC uniform hazard spectra. Therefore, a suite of 45 synthetic far-field accelerograms for the prescribed magnitude and soil type is adopted. The selected records are applied as individual components for both longitudinal and transverse directions and vertical acceleration and spatially variable ground motions are disregarded. Figure 3.9 demonstrated the response spectra of selected ground motion records.

3.3.2 IDA

Once the finite element model and the ground motion records have been chosen, IDA is carried out. IDA entails a series of successive nonlinear time history analyses of the analytical model under a set of monotonically increasing ground motion records in order to predict the entire range of nonlinear response of bridge components from a linear elastic range up to dynamic instability. In this context, the scalar that reflects the ground motion intensity is called Intensity Measure (IM), the quantity that represents the seismic structural response is called Engineering Demand Parameter (EDP), and the maximum response of the structure which reflects the damage level of bridge components are referred to as Damage Measure (DM). In this study, spectral acceleration at the fundamental period of the bridge, S_a (T_1) is adopted as IM and pile cap displacements under piers and abutments, column drift, and backfill soil deformation in active and passive actions are considered as the monitored EDP.

3.3.3 Characterization of damage limit states

Characterizing the damage limit states is a crucial step in the fragility assessment of structural systems. Once the IDA is performed, limit states are applied to the IDA curves in order to determine the mean and standard deviation of bridge component response at each limit state. Damage limit states of individual bridge components are typically defined with discrete levels of qualitative descriptions and their corresponding quantitative values. Four limit states (i.e. slight, moderate, extensive, and collapse) are used in this study according to the recommendation of HAZUS-MH (FEMA, 2003). Table 3.3 demonstrates the qualitative description of the adopted damage states and Table 3.4 presents the quantitative representation of these limit states in terms of a median value for damage, S_c, and its corresponding logarithmic standard deviation, β_c. Multiple EDPs such as column drift, pile cap displacement for piers and abutments, and backfill soil deformation in active and passive actions in both longitudinal and transverse directions are considered in this study.

Maximum drift ratio is adopted for evaluating the DM in bridge columns. Since the columns of the 7th line bridge meet the seismic design provision of CSA-S06 (*Canadian Highway Bridge Design Code*, 2019), quantitative damage states corresponding to seismically designed columns presented in a study by Dutta and Mander (Dutta & Mander, 1998) is adopted for both longitudinal and transverse directions. Abutment backfill soil deformation in active, passive, and transverse directions are adopted from a study by Nielson (Nielson, 2005) in which the available damage states are combined with survey-based results and updated by means of a Bayesian updating approach. Padgett and DesRoches (Padgett & DesRoches, 2007) have shown that substantial damage to the bridge abutments does not necessarily result in a bridge closure. Pile cap displacements for piers and abutments are adopted from a study by Aygun et al. (Aygün et al.,

2010) for both longitudinal and transverse directions. Deck unseating is another limit state corresponding to excessive deck displacement particularly for the case of the isolated bridge. It should be noted that FREI does not experience any type of damage under large shear strains up to 250% according to the conducted experimental tests by researchers (Y. Al-Anany et al., 2017; Losanno, Sierra, Spizzuoco, Marulanda, & Thomson, 2019; Russo, Pauletta, & Cortesia, 2013).

3.3.4 Seismic fragility curves

The final step in conducting a seismic fragility analysis of a structural system is developing analytical fragility curves. Seismic fragility describes the conditional probability of a structural system or its comprising components reaching or exceeding a certain damage level damage state for a given IM, which is often expressed as

$$F = P(\text{damage state} \mid IM = y) \tag{3.5}$$

where y is a given intensity of IM. Assuming a lognormal distribution for the damage states and the seismic demand, the component level fragility curves can be developed using the following equation

$$P[LS \mid IM] = \Phi\left[\frac{\ln\left(\frac{S_D}{S_C}\right)}{\sqrt{\beta_{D|IM}^2 + \beta_C^2}}\right] \tag{3.6}$$

where Φ is the standard normal cumulative function. S_D and $\beta_{D|IM}$ are the median and logarithmic standard deviation of seismic demand, respectively, where S_C and β_C are the median and logarithmic standard deviation of the component capacity, respectively.

3.4 Seismic fragility assessment of the soil-pile-bridge system

In this section, results of IDA, component-level fragilities, and bridge response histories are presented. First, the seismic performance of the current as-built condition of the bridge founded on the pile groups (i.e. monolithic bridge) is investigated. Then, the isolated bridge case is scrutinized and finally a comparison is made between the two cases in order to study the SSI effect on different bridge types. Additionally, the seismic response of the fixed-base bridge is compared with that of the bridge founded on pile groups.

IDA is performed on the bridge model in the longitudinal and transverse directions of the bridge, independently, because of the complicated nature of the wave propagation, lack of available bidirectional tests on the FREI, and lack of experimental models incorporating the coupled behavior of different bridge components. Fragility curves are developed based on the IDA results where the peak transient and residual response of columns, deck, abutments, and pile groups are highlighted.

3.4.1 Case I: Monolithic bridge with SSI

3.4.1.1 Seismic IDA and fragility curves

In order to evaluate damage potential of the bridge at different limit states by the concept of IDA, the bridge was subjected to a set of monotonically increasing ground motion records in longitudinal and transverse directions, independently. The summarized IDA curves using the DM|IM approach including the median, 16% and 84% percentiles for each bridge component at the two aforementioned orthogonal directions of the bridge are demonstrated in Figure 3.10 and Figure 3.11. The Record-To-Record (RTR) variability in the seismic response of the bridge components can be clearly observed when the component response enters a nonlinear phase and

becomes larger by increasing the IM. It is shown that the RTR variability is larger in column drifts and pier pile cap displacements with respect to abutment pile cap displacements and abutment deformations. Comparison of these two figures also reveals the vulnerability of the abutments and their supporting pile group system. As tabulated in Table 3.5, backfill soil deformation in active action, abutment pile cap displacement and backfill soil deformation in passive action are the first three fragile components in the longitudinal direction where the tensile capacity of abutments is only provided by the nominal contribution of the supporting pile group whereas the compressive resistance of the abutment backfill soil adds to the pile group contribution in passive action. As shown in Table 3.6, abutments are more vulnerable in the transverse direction of the bridge, which can be attributed to the lack of transversely battered piles in the abutment pile groups.

Seismic fragility curves of the bridge components in terms of the prescribed damage limit states are developed using Equations 5 and 6 and illustrated in Figure 3.12 and Figure 3.13. In the longitudinal direction, median damage capacity of the abutment pile cap displacement ranges within 0.17g-0.54g where this range is 0.12g-0.66g for the backfill soil deformation in active action and 0.37g-1.16g for the backfill soil deformation in passive action. On the contrary, the median damage capacity of the pier pile cap displacement and peak column drift ranges between 0.72g-2.64g and 0.61g-2.69g making these two components reliable. Table 3.7 presents the component fragility curve parameters of the bridge in the two orthogonal directions. S_D is the median of damage at each LS, $\beta_{(D|IM)}$ represents the RTR variability of the component response, $\beta_{(TOT)}$ is the total dispersion of demand defined as the square root of sum of squares of $\beta_{(D|IM)}$ and β_C and Damage Margin Ratio (DMR) is defined as quantity that measure the ratio of damage median capacity to the MCE hazard level of the bridge site (S_a = 0.24g). Since the columns and their supporting pile groups have a relatively large DMR ranging between 3 to 11, and probabilities

of damage as small as 1.5%, it can be concluded that piers are not prone to severe damage. On the other hand, a 6.3% probability of collapse of the abutment pile caps makes them the most critical component in the longitudinal direction. It should be pointed out that although the probability of damage to abutment backfill soil is in part significant, it will not necessarily lead to bridge closure. As there is no abutment backfill to contribute in the lateral resistance of the bridge in the transverse direction, lateral load resistance involves pier more than longitudinal direction. Therefore, the probability of damage to pier pile caps and columns have been increased whereas abutment pile caps tend to have smaller damage probabilities.

3.4.1.2 Individual component responses

Minimization of the residual deformations of the bridge components after seismic events guarantees the plausibility of the bridge to be kept functional and open to traffic. However, the experimental data on residual damage measures is very limited. Therefore, four tentative damage states based on the experimental investigations of O'Brien et al. (O'Brien, Saiidi, & Sadrossadat-Zadeh, 2007) are adopted to quantify the residual drift damage level where residual column drift less than 0.25%, 0.25%-0.75%, 0.75%-1.00% and larger than 1.00% corresponds to slight, moderate, extensive and collapse damage states, respectively. The individual transient and residual responses of column drifts and pile cap displacements are presented in Figure 3.14 and Figure 3.15 for longitudinal and transverse directions, respectively. It is shown that end piers adjacent to abutments and their supporting pile groups experience larger relative deformations with respect to intermediate piers and pile groups. These larger deformations at end piers can be attributed to the shorter height of columns and their corresponding larger lateral stiffness. As demonstrated in Table 3.8, residual column drifts at the MCE hazard level is less than 0.25% in both bridge directions

which implies that the bridge piers remain fully operational after a design earthquake. Moreover, pier and abutment residual pile cap displacements under design earthquake is negligible.

The seismic performance of the pile groups in the two orthogonal bridge directions is investigated by developing the maximum lateral pile displacement and mobilized soil reaction profiles of the pile groups. As an example, Figure 3.16 and Figure 3.17 demonstrate the maximum positive and negative pile group response of the west abutment and its adjacent pier as representatives of abutment and pier pile groups. As shown in Figure 3.16-a, the abutment experiences about 63% larger lateral displacements in negative direction than the positive direction. This asymmetric response is due to the effect of battered piles in the tow of the pile cap that provides larger soil resistance when the lateral load induces tensile forces in the piles which is demonstrated in Figure 3.16-b. However, piles in the pier pile groups are distributed symmetric so that their lateral deformation and mobilized soil reaction is symmetric in positive and negative directions, as shown in Figure 3.16-c and d. Moreover, transversely battered piles have a major contribution to the lateral resistance of pier pile groups by providing a maximum of 30 kN of resistance per each pile. Figure 3.17 illustrates that the lateral pile displacement and soil reaction of pier and abutment pile groups are almost symmetric due to symmetric configuration of the piles with respect to the bridge deck in the transverse direction.

3.4.2 Case II: Isolated bridge with SSI

3.4.2.1 Seismic IDA and fragility curves

Seismic performance of the retrofitted bridge using U-FREI is investigated in order to scrutinize the effect of seismic isolation on the seismic behavior of bridge components in the presence of SSI effects. The summarized IDA curves of the bridge components in longitudinal and transverse

directions are demonstrated in Figure 3.18 and Figure 3.19, respectively. In the retrofitted bridge, the most fragile component is the abutments pile cap displacement with a median collapse capacity of 0.5g and 0.55g in longitudinal and transverse directions, respectively. The median damage capacity of the bridge components and their associated 16% and 84% percentiles are presented in Table 3.9 and Table 3.10. Seismic fragility curves of the bridge components are illustrated in Figure 3.20 and Figure 3.21 for the two excitation directions and the fragility parameters are summarized in Table 3.11. In the MCE level, no damage has been observed in columns and pier pile caps as the isolation layer has decoupled the superstructure from the earthquake excitation that results in a reduction in the transferred shear forces to columns and their supporting piles. However, there is still a 7.4% and 3.6% probability of collapse due to excessive abutment pile cap displacements. It should be pointed out that the fragilities presented for the U-FREI do not represent any kind of damage since the previous experiments have revealed that the U-FREI can experience shear strains in excess of 250% without exhibiting damage.

3.4.2.2 Individual component responses

The individual response of pile caps and column drifts are illustrated in Figure 3.22 and Figure 3.23 for the longitudinal and transverse directions of the bridge. Similar to the monolithic bridge, piers adjacent to the end abutments have experienced larger pile cap displacements whereas the middle piers have demonstrated the least. On the contrary, middle columns have experienced larger drifts with respect to end piers. This can be explained by the relative stiffness of the isolator, column, and the supporting soil layer. When the isolation system diminishes the transferred shear forces, shorter columns with larger relative stiffness with respect to their supporting soil layer tend to have smaller drift ratios in comparison with long columns with smaller bending stiffness. These figures also demonstrate that isolators installed on the end abutments experience larger shear

strains particularly in strong earthquake excitations. It is shown in Table 3.12 that the isolated bridge is not susceptible to any kind of severe damage at the MCE hazard level as the transient and residual deformations are almost negligible for the potentially critical bridge components.

As shown in Figure 3.24 and Figure 3.25, supporting piles of the isolated bridge exhibited similar behavior to that of monolithic bridge. However, seismic isolation has resulted in more than 100% decrease in the peak lateral pile displacement and mobilized soil reaction of the pier pile groups of the isolated bridge and also shifted up the depth of the maximum soil reaction from about 2 to 3 *m* in monolithic bridge to 1 *m* in the isolated bridge. Figure 3.25 also represents the same trend for the transverse direction of the bridges.

3.5 Comparative results and discussion

A comparison of the seismic fragility curves of the monolithic and isolated bridge cases is demonstrated in Figure 3.26 and Figure 3.27 in order to highlight the effect of seismic isolation on the seismic performance of a soil-pile-structure system. It is shown that seismic isolation has a significant effect in slight damage states and its effectiveness diminishes by moving from slight DS to collapse. The median damage capacity of columns in the longitudinal direction has been increased in the range of 184% to 38% for the four prescribed limit states whereas this range is 239% to 81% for the transverse direction. This range is 216% to 34% and 203% to 24% for the longitudinal and transverse pier pile cap displacements which shows that isolation system has effectively preserved the columns and their supporting pile groups from slight damages to collapse. The median damage capacity of the backfill soil deformation of the isolated bridge in passive action have been increased by 20% and 4% for the slight and moderate damage states whereas in active action it has been increased by 8% for slight DS but decreased by 12% and 23% for moderate

and extensive damage states, respectively. In longitudinal direction, the median of damage to abutment pile cap displacements have been increased by 18% and 5% for slight and moderate limit state whereas it has been decreased by 2% and 5% for extensive and collapse limit states. However, it has been increased for all limit states by 12% to 4% in transverse direction. The increase in the median of extensive damage and collapse of abutment piles in the longitudinal direction can be attributed to large displacements of the superstructure. There have been several studies on the seismic performance of isolated bridges and the recurring theme is that decoupling the superstructure results in excessively large displacements (Li & Conte, 2016; Raheem, 2009; Siqueira, Sanda, Paultre, & Padgett, 2014; Xiang & Alam, 2019). In relatively small earthquake intensities, the lateral displacement of the superstructure does not exceed the gap between the deck and abutment. As the input excitation amplifies, the deck embarks on colliding the abutment and triggers the pounding spring modeled at the interface of the deck and the abutment. This results in abrupt increase in the transmitted shear force and acceleration in the abutment and supporting piles. It should be pointed out that the dispersion of the bridge component response has been increased in the isolated bridge except for the abutment pile cap displacement and backfill soil deformation in active action which demonstrates that the seismic isolation of the bridge using U-FREI generally results in introducing larger extents of uncertainty to the entire system. Peak response of bridge components for the monolithic and isolated bridges are compared in Table 3.13 and Table 3.14 for longitudinal and transverse directions, respectively.

A comparison between the response histories of the critical bridge components at the MCE level is demonstrated in Figure 3.28 and Figure 3.29. In longitudinal direction, seismic isolation has increased the peak deck displacement and velocity by 242% and 86%, respectively. Although the deck acceleration is anticipated to be reduced in the isolated bridge, at some instances it has

reached a value of about 1g. These few spikes in the deck acceleration time history are due to the pounding between the deck and abutment where the excessive deck displacement has triggered the pounding and the backfill soil as shown in Figure 3.30. As shown in Table 3.15, seismic isolation results in about 71% and 58% decrease in the peak column base shear and base moment of columns.

3.6 Conclusion

This study focuses on the seismic risk assessment of a conventionally designed bridge system in Ottawa, Ontario, retrofitted with U-FREI. A nonlinear 3D model of the bridge including superstructure, substructure, abutment-embankment interaction and the nonlinear soil-pile-structure interaction is built in OpenSees. Fragility curves are developed for four damage states based on an IDA with a set of 45 synthetic ground motion records. A comparison between the seismic performance of the monolithic and seismically isolated bridge revealed that:

1. Abutment pile groups are the most critical bridge components of the monolithic bridge in longitudinal and transverse directions. The probability of damage to column due to excessive drift and their supporting piles due to excessive displacement is larger in the transverse direction with respect to the longitudinal direction. However, these probabilities are found to be negligible and does not jeopardize the functionality of the bridge.
2. Like the monolithic bridge, the abutment pile cap displacement has the highest probability of damage in both orthogonal directions. While the probability of damage to abutments due to excessive deformations in both directions are significant, columns and pier piles are totally in a safe damage margin with zero probability of damage at all damage states.

3. Seismic isolation has increased the median damage capacity of the columns, pier pile cap displacements, and backfill soil deformation in passive action in longitudinal direction. However, median damage capacity of abutment pile cap is increased for slight and moderate damage states but decreased for extensive and collapse damage states. In a similar manner, median damage capacity of backfill soil deformation is active action is increased for slight damage state but decreased for moderate and extensive damage states. In the transverse direction, all bridge components follow the same trend as longitudinal direction except for abutment pile cap displacement where the median of damage is increased at all damage states after seismic isolation.
4. It is shown that seismic isolation of the bridges located on soft soil is beneficial for the piers and their supporting pile groups whereas it can be detrimental to the abutment due to excessive deck displacement and the pounding effect between the deck and abutment that might induce larger demand on abutment and result in greater deck accelerations.

The findings observed from this study are based on a case study of a multi-span continuous reinforced concrete bridge in eastern Canada. To better study the detrimental effect of the isolation system on the abutment foundation, a more complex and physics-based spring system (Zheng et al., 2021) will be considered in future studies to better capture the dynamic interactions of abutment-embankment and abutment-foundation.

3.7 Acknowledgments

The authors would like to express their gratitude for the financial support provided by the Ministry of Transportation Ontario (MTO) through the Highway Infrastructure Innovation Funding Program (HIIFP) and Natural Sciences and Engineering Research Council (NSERC).

References

AASHTO. (2012). American Association of State Highway and Transportation Officials. *Washington, DC*.

Al-Anany, Y., Van Engelen, N., & Tait, M. (2017). Vertical and Lateral Behavior of Unbonded Fiber-Reinforced Elastomeric Isolators. *Journal of Composites for Construction, 21*(5), 04017019.

Al-Anany, Y. M., Moustafa, M. A., & Tait, M. J. (2016). Modeling and Evaluation of a Seismically Isolated Bridge Using Unbonded Fiber Reinforced Elastomeric Isolators. *Earthquake Spectra*.

Al-Anany, Y. M., & Tait, M. J. (2015). A numerical study on the compressive and rotational behavior of fiber reinforced elastomeric isolators (FREI). *Composite Structures, 133*, 1249-1266.

Al-Anany, Y. M., & Tait, M. J. (2017). Fiber reinforced elastomeric isolators for the seismic isolation of bridges. *Composite Structures, 160*, 300-311.

API. (2007). American petroleum institute recommended practice for planning, designing and constructing fixed offshore platforms—working stress design. *American Petroleum Institute, Washington Google Scholar*.

Atkinson, G. M. (2009). Earthquake time histories compatible with the 2005 National building code of Canada uniform hazard spectrum. *Canadian Journal of Civil Engineering, 36*(6), 991-1000.

Aviram, A., Mackie, K. R., & Stojadinović, B. (2008). *Guidelines for nonlinear analysis of bridge structures in California*: Pacific Earthquake Engineering Research Center.

Aygün, B., Dueñas-Osorio, L., Padgett, J. E., & DesRoches, R. (2010). Efficient longitudinal seismic fragility assessment of a multispan continuous steel bridge on liquefiable soils. *Journal of Bridge Engineering, 16*(1), 93-107.

Boulanger, R. W., Curras, C. J., Kutter, B. L., Wilson, D. W., & Abghari, A. (1999). Seismic soil-pile-structure interaction experiments and analyses. *Journal of geotechnical and geoenvironmental engineering, 125*(9), 750-759.

Canadian Highway Bridge Design Code. (2019). Canadian Standard Association.

Carbonari, S., Morici, M., Dezi, F., Gara, F., & Leoni, G. (2017). Soil-structure interaction effects in single bridge piers founded on inclined pile groups. *Soil Dynamics and Earthquake Engineering, 92*, 52-67. doi:https://doi.org/10.1016/j.soildyn.2016.10.005

Chapman, L., & Putnam, D. (1984). The Physiography of Southern Ontario, Ontario Geological Survey Special. *Queen's Printer, Toronto, Ontario, 270*.

Dai, W., Rojas, F., Shi, C., & Tan, Y. (2018). Effect of soil structure interaction on the dynamic responses of base isolated bridges and comparison to experimental results. *Soil Dynamics and Earthquake Engineering, 114*, 242-252.

Dicleli, M., Albhaisi, S., & Mansour, M. (2005). Static soil–structure interaction effects in seismic-isolated bridges. *Practice Periodical on Structural Design and Construction, 10*(1), 22-33.

Dutta, A., & Mander, J. (1998). *Seismic fragility analysis of highway bridges.* Paper presented at the Proceedings of the INCEDE-MCEER center-to-center project workshop on earthquake engineering Frontiers in transportation systems.

Elgamal, A., Yan, L., Yang, Z., & Conte, J. P. (2008). Three-dimensional seismic response of Humboldt Bay bridge-foundation-ground system. *Journal of Structural Engineering, 134*(7), 1165-1176.

FEMA. (2003). Multi-hazard loss estimation methodology, earthquake model *Washington, DC, USA: Federal Emergency Management Agency*.

FEMA:P-751. (2012). NEHRP Recommended Seismic Provisions: Design Examples: FEMA P-751: Washington, DC.

Filippou, F. C., Bertero, V. V., & Popov, E. P. (1983). Effects of bond deterioration on hysteretic behavior of reinforced concrete joints.

Foster, A. D. B. (2012). *Base isolation using stable unbonded fibre reinforced elastomeric isolators (SU-FREI).*

González, F., Padrón, L. A., Carbonari, S., Morici, M., Aznárez, J. J., Dezi, F., & Leoni, G. (2019). Seismic response of bridge piers on pile groups for different soil damping models and lumped parameter representations of the foundation. *Earthquake Engineering & Structural Dynamics, 48*(3), 306-327. doi:10.1002/eqe.3137

Inventory of publicly owned bridge and tunnel assets. (2016). Infrastructure Canada.

Jeremić, B., Kunnath, S., & Xiong, F. (2004). Influence of soil–foundation–structure interaction on seismic response of the I-880 viaduct. *Engineering Structures, 26*(3), 391-402. doi:https://doi.org/10.1016/j.engstruct.2003.10.011

Kaviani, P., Zareian, F., & Taciroglu, E. (2014). *Performance-based seismic assessment of skewed bridges*: Pacific Earthquake Engineering Research Center.

Kelly, J. M. (1999). Analysis of fiber-reinforced elastomeric isolators. *Journal of Seismology and Earthquake Engineering, 2*(1), 19-34.

Kotsoglou, A., & Pantazopoulou, S. (2007). Bridge–embankment interaction under transverse ground excitation. *Earthquake Engineering & Structural Dynamics, 36*(12), 1719-1740. doi:doi:10.1002/eqe.715

Kwon, O.-S., & Elnashai, A. S. (2010). Fragility analysis of a highway over-crossing bridge with consideration of soil–structure interactions. *Structure and Infrastructure Engineering, 6*(1-2), 159-178. doi:10.1080/15732470802663870

Li, Y., & Conte, J. P. (2016). Effects of seismic isolation on the seismic response of a California high-speed rail prototype bridge with soil-structure and track-structure interactions. *Earthquake Engineering & Structural Dynamics, 45*(15), 2415-2434.

Losanno, D., Sierra, I. E. M., Spizzuoco, M., Marulanda, J., & Thomson, P. (2019). Experimental assessment and analytical modeling of novel fiber-reinforced isolators in unbounded configuration. *Composite Structures, 212*, 66-82.

Mackie, K., & Stojadinovic, B. (2006). *Seismic vulnerability of typical multiple-span California highway bridges.* Paper presented at the Fifth National Seismic Conference on Bridges & Highways Multidisciplinary Center for Earthquake Engineering ResearchCalifornia Department of Transportation Federal Highway Administration Transportation Research Board.

Mallick, M., & Raychowdhury, P. (2015). Seismic analysis of highway skew bridges with nonlinear soil–pile interaction. *Transportation Geotechnics, 3*, 36-47. doi:https://doi.org/10.1016/j.trgeo.2015.03.002

Mander, J. B., Priestley, M. J., & Park, R. (1988). Theoretical stress-strain model for confined concrete. *Journal of Structural Engineering, 114*(8), 1804-1826.

Mangalathu, S., & Jeon, J.-S. (2019). Stripe-based fragility analysis of multispan concrete bridge classes using machine learning techniques. *Earthquake Engineering & Structural Dynamics, 48*(11), 1238-1255. doi:10.1002/eqe.3183

Martínez, A., Hube, M. A., & Rollins, K. M. (2017). Analytical fragility curves for non-skewed highway bridges in Chile. *Engineering Structures, 141*, 530-542. doi:https://doi.org/10.1016/j.engstruct.2017.03.041

McKenna, F. (2011). OpenSees: a framework for earthquake engineering simulation. *Computing in Science & Engineering*, *13*(4), 58-66.

Moghimi Osgooei, P. (2014). *Advanced Numerical Modeling of Fiber-Reinforced Elastomeric Isolators (FREIs).*

Muthukumar, S., & DesRoches, R. (2006). A Hertz contact model with non-linear damping for pounding simulation. *Earthquake Engineering & Structural Dynamics*, *35*(7), 811-828.

Mylonakis, G., & Gazetas, G. (2000). Seismic soil-structure interaction: Beneficial or detrimental? *Journal of Earthquake Engineering*, *4*(3), 277-301. doi:10.1080/13632460009350372

Mylonakis, G., Nikolaou, S., & Gazetas, G. (2006). Footings under seismic loading: Analysis and design issues with emphasis on bridge foundations. *Soil Dynamics and Earthquake Engineering*, *26*(9), 824-853.

National Building Code of Canada. (2015). National Research Council of Canada.

Nielson, B. G. (2005). *Analytical fragility curves for highway bridges in moderate seismic zones.* Georgia Institute of Technology.

Noori, H. R., Memarpour, M. M., Yakhchalian, M., & Soltanieh, S. (2019). Effects of ground motion directionality on seismic behavior of skewed bridges considering SSI. *Soil Dynamics and Earthquake Engineering, 127*, 105820. doi:https://doi.org/10.1016/j.soildyn.2019.105820

O'Brien, M., Saiidi, M. S., & Sadrossadat-Zadeh, M. (2007). A study of concrete bridge columns using innovative materials subjected to cyclic loading.

Osgooei, P. M., Tait, M. J., & Konstantinidis, D. (2017). Non-iterative computational model for fiber-reinforced elastomeric isolators. *Engineering Structures, 137*, 245-255.

Padgett, J. E., & DesRoches, R. (2007). Bridge functionality relationships for improved seismic risk assessment of transportation networks. *Earthquake Spectra, 23*(1), 115-130.

Raheem, S. E. A. (2009). Pounding mitigation and unseating prevention at expansion joints of isolated multi-span bridges. *Engineering Structures, 31*(10), 2345-2356.

Rahmani, A., Taiebat, M., Liam Finn, W. D., & Ventura, C. E. (2016). Evaluation of substructuring method for seismic soil-structure interaction analysis of bridges. *Soil Dynamics and Earthquake Engineering, 90*, 112-127. doi:https://doi.org/10.1016/j.soildyn.2016.08.013

Russo, G., Pauletta, M., & Cortesia, A. (2013). A study on experimental shear behavior of fiber-reinforced elastomeric isolators with various fiber layouts, elastomers and aging conditions. *Engineering Structures, 52*, 422-433.

Sciascetti, A. (2017). *The Effect of Temperature on Unbonded Fiber-Reinforced Elastomeric Isolators.*

Shamsabadi, A., Rollins, K. M., & Kapuskar, M. (2007). Nonlinear soil–abutment–bridge structure interaction for seismic performance-based design. *Journal of geotechnical and geoenvironmental engineering, 133*(6), 707-720.

Siqueira, G. H., Sanda, A. S., Paultre, P., & Padgett, J. E. (2014). Fragility curves for isolated bridges in eastern Canada using experimental results. *Engineering Structures, 74*, 311-324.

Stefanidou, S. P., Sextos, A. G., Kotsoglou, A. N., Lesgidis, N., & Kappos, A. J. (2017). Soil-structure interaction effects in analysis of seismic fragility of bridges using an intensity-based ground motion selection procedure. *Engineering Structures, 151*, 366-380.

Takeda, T., Sozen, M. A., & Nielsen, N. N. (1970). Reinforced concrete response to simulated earthquakes. *Journal of the Structural Division, 96*(12), 2557-2573.

Tongaonkar, N., & Jangid, R. (2003). Seismic response of isolated bridges with soil–structure interaction. *Soil Dynamics and Earthquake Engineering, 23*(4), 287-302.

Toopchi-Nezhad, H., Tait, M. J., & Drysdale, R. G. (2009). Simplified analysis of a low-rise building seismically isolated with stable unbonded fiber reinforced elastomeric isolators. *Canadian Journal of Civil Engineering, 36*(7), 1182-1194.

Ucak, A., & Tsopelas, P. (2008). Effect of soil–structure interaction on seismic isolated bridges. *Journal of Structural Engineering, 134*(7), 1154-1164.

Van Impe, W. F., & Reese, L. C. (2010). *Single piles and pile groups under lateral loading*: CRC press.

Vlassis, A., & Spyrakos, C. (2001). Seismically isolated bridge piers on shallow soil stratum with soil–structure interaction. *Computers & Structures, 79*(32), 2847-2861.

Wang, Z., Padgett, J. E., & Dueñas-Osorio, L. (2012). *Influence of soil structure interaction on the fragility of an isolated bridge-soil-foundation system.* Paper presented at the 15th world conf. earthq. eng., Lisbon, Portugal.

Xiang, N., & Alam, M. S. (2019). Comparative Seismic Fragility Assessment of an Existing Isolated Continuous Bridge Retrofitted with Different Energy Dissipation Devices. *Journal of Bridge Engineering, 24*(8), 04019070.

Xie, Y., & DesRoches, R. (2019). Sensitivity of seismic demands and fragility estimates of a typical California highway bridge to uncertainties in its soil-structure interaction modeling. *Engineering Structures, 189*, 605-617. doi:https://doi.org/10.1016/j.engstruct.2019.03.115

Xie, Y., Zhang, J., DesRoches, R., & Padgett, J. E. (2019). Seismic fragilities of single-column highway bridges with rocking column-footing. *Earthquake Engineering & Structural Dynamics, 48*(7), 843-864.

Yang, C.-S. W., Werner, S. D., & DesRoches, R. (2015). Seismic fragility analysis of skewed bridges in the central southeastern United States. *Engineering Structures, 83*, 116-128. doi:https://doi.org/10.1016/j.engstruct.2014.10.025

Zhang, J., & Huo, Y. (2009). Evaluating effectiveness and optimum design of isolation devices for highway bridges using the fragility function method. *Engineering Structures, 31*(8), 1648-1660.

Zhang, J., & Makris, N. (2002). Kinematic response functions and dynamic stiffnesses of bridge embankments. *Earthquake Engineering & Structural Dynamics, 31*(11), 1933-1966.

Zheng, Q., Yang, C. S. W., Xie, Y., Padgett, J., DesRoches, R., & Roblee, C. (2021). Influence of abutment straight backwall fracture on the seismic response of bridges. *Earthquake Engineering & Structural Dynamics, 50*(7), 1824-1844.

Table 3.1. Mechanical and geometrical properties of bridge components

Component	Material model	Details
Deck	3D nonlinear beam-column element	Total length = 236 m Maximum thickness = 0.91 m Concrete compressive strength, f_{ck} = 35 MPa Mass density, ρ = 2400 kg/m^3 Cross sectional area, A = 6 m^2 Moment of inertia along the y-axis, I_y = 51 m^4 Moment of inertia along the z-axis, I_z = 0.4 m^4
Isolator	A non-iterative rate-independent *Takeda-Elastic* model	Width, a = 850 mm Length, 2b = 850 mm Rubber thickness (cover layer) = 5 mm Rubber thickness (intermediate layer) = 43.16 mm Reinforcement fiber thickness = 0.51 mm Total rubber thickness, t_r = 269 mm Total fiber thickness, t_f = 3.57 mm Total height of bearing, h = 272.5 mm
Pier	3D fiber-section forced-based beam-column element with nonlinear fiber materials	Diameter = 0.91 m Cover = 76.2 mm Yield strength, $f_y = 2.75\times10^5$ kPa Young's modulus, $E_s = 2\times10^8$ kPa Strain hardening ratio, b = 0.01
Piles	3D fiber-section forced-based beam-column element with nonlinear fiber materials	Modulus of elasticity, $E_p = 2\times10^8$ kPa Cross-sectional area, A = 0.0141 m^2 Depth, d = 0.308 m Width, w = 0.31 m Moment of inertia along the x-axis, $I_x = 23.7\times10^7$ mm^4 Moment of inertia along the y-axis, $I_y = 7.74\times10^7$ mm^4
Pile-soil interface	BNWF nonlinear springs	Undrained cohesion (top) = 30 kN/m^2 Undrained cohesion (bottom) = 80 kN/m^2 Unit weight, γ = 15.2 kN/m^3 Uniaxial Pysimple1, Tzsimple1, and Qzsimple1.

Table 3.2. Characteristic parameters of the Pivot-Elastic model

Parameter	Value
Bilinear Takeda	
K_1 (N/m)	6727
K_2 (N/m)	557
u_y (m)	0.0087
Nonlinear Elastic Spring	
a_1 (N/m)	2043.4
a_3 (N/m^3)	-4.71×10^{-3}
a_5 (N/m^5)	1.61×10^{-8}

Table 3.3. Qualitative description of damage states

Damage state	Description of the damage state
None	No damage to the bridge
Minor/Slight	Minor cracking or spalling of concrete in the abutments, hinges, columns (superficial damage), or minor cracking to the deck
Moderate	Any column experiencing moderate cracking (shear cracks) and spalling (column structurally still sound), moderate movement of the abutment (<50 mm), keeper bar failure without unseating,
Major/Extensive	Any column degrading without collapse (column structurally unsafe), significant residual displacement at connections, vertical offset of the abutment
Complete/Collapse	Any column collapsing which may result in immediate deck collapse or tilting of the substructure due to foundation failure

Table 3.4. Quantitative description of damage states

Failure mode	Corresponding bridge component	Slight		Moderate		Extensive		Collapse		Reference
		S_c	β_c	S_c	β_c	S_c	β_c	S_c	β_c	
Column failure	Drift (%)	1	0.25	2.5	0.25	5	0.46	7.5	0.5	(Dutta & Mander, 1998)
Abutment soil failure in passive action	Abutment soil deformation (mm)	37	0.46	146	0.46	N/A*	0	N/A*	0	(Nielson, 2005)
Abutment soil failure in active action	Abutment soil deformation (mm)	9.8	0.7	37.9	0.9	77.2	0.85	N/A*	0	(Nielson, 2005)
Abutment soil failure in transverse action	Abutment soil deformation (mm)	9.8	0.7	37.9	0.9	77.2	0.85	N/A*	0	(Nielson, 2005)
Pile foundation failure at abutments	Pile cap displacement (mm)	20	0.4	38	0.4	60	0.4	80	0.4	(Aygün, Dueñas-Osorio, Padgett, & DesRoches, 2010)
Pile foundation failure at piers	Pile cap displacement (mm)	28	0.4	42	0.4	86	0.4	115	0.4	(Aygün et al., 2010)
Unseating of the deck at abutment	Displacement of the deck relative to the abutment (m)	N/A	N/A	N/A	N/A	N/A	N/A	1.37	0	-

* Padgett and DesRoches determined that severe damage to abutments does not essentially result in a global collapse (Padgett & DesRoches, 2007)

Table 3.5. Summarized IDA parameters of the monolithic bridge in longitudinal direction

	DM|IM percentiles (g)														
	Column drift			Abutment pile cap displacement			Pier pile cap displacement			Backfill soil deformation: Active action			Backfill soil deformation: Passive action		
DS	50 %	84 %	16 %	50 %	84 %	16 %	50 %	84 %	16 %	50 %	84 %	16 %	50 %	84 %	16 %
Slight	0.61	0.44	0.81	0.16	0.10	0.22	0.69	0.52	0.94	0.11	0.07	0.16	0.33	0.23	0.50
Moderate	1.23	0.97	1.60	0.28	0.19	0.43	1.12	0.90	1.45	0.35	0.24	0.52	1.11	0.88	1.46
Extensive	2.03	1.54	2.51	0.40	0.30	0.58	2.10	1.63	2.80	0.65	0.48	0.86	-	-	-
Collapse	2.63	2.02	3.33	0.52	0.39	0.71	2.60	2.00	3.31	-	-	-	-	-	-

Table 3.6. Summarized IDA parameters of the monolithic bridge in transverse direction

	DM|IM percentiles (g)											
	Column drift			Abutment pile cap displacement			Pier pile cap displacement			Abutment deformation		
DS	50%	84%	16%	50%	84%	16%	50%	84%	16%	50%	84%	16%
Slight	0.38	0.27	0.49	0.21	0.13	0.26	0.58	0.45	0.77	0.10	0.07	0.14
Moderate	0.74	0.62	0.92	0.32	0.23	0.42	0.95	0.76	1.24	0.32	0.23	0.42
Extensive	1.25	0.99	1.66	0.45	0.32	0.54	2.02	1.56	2.80	0.54	0.41	0.66
Collapse	1.77	1.32	2.23	0.54	0.43	0.68	2.46	1.86	3.22	-	-	-

Table 3.7. Fragility parameters of the monolithic bridge

		Longitudinal					Transverse			
		Peak column drift	Abutment pile cap displacement	Pier pile cap displacement	Peak backfill soil deformation: .	Peak backfill soil deformation: passive action	Peak column drift	Abutment pile cap displacement	Pier pile cap displacement	Peak abutment deformation
Slight	S_D (g)	0.61	0.17	0.72	0.12	0.37	0.39	0.21	0.62	0.11
	$\beta_{D\|IM}$	0.17	0.07	0.21	0.04	0.13	0.12	0.09	0.18	0.04
	β_{TOT}	0.30	0.41	0.45	0.70	0.48	0.28	0.41	0.44	0.70
	DMR	2.55	0.69	3.02	0.50	1.53	1.63	0.89	2.57	0.48
	$P[DS\|S_{a2/50}]$	0.77	79.00	1.56	82.50	26.83	12.81	63.27	3.50	83.95
Moderate	S_D (g)	1.27	0.29	1.16	0.37	1.16	0.76	0.33	0.98	0.33
	$\beta_{D\|IM}$	0.31	0.12	0.31	0.13	0.29	0.17	0.10	0.25	0.10
	β_{TOT}	0.39	0.42	0.50	0.91	0.54	0.30	0.41	0.47	0.91
	DMR	5.28	1.23	4.82	1.56	4.83	3.19	1.36	4.07	1.36
	$P[DS\|S_{a2/50}]$	0.00	41.10	0.08	34.58	0.16	0.06	30.00	0.20	39.12
Extensive	S_D (g)	2.05	0.43	2.20	0.66	-	1.34	0.44	2.09	0.54
	$\beta_{D\|IM}$	0.47	0.15	0.55	0.18	-	0.34	0.12	0.57	0.14
	β_{TOT}	0.66	0.43	0.68	0.87	-	0.57	0.42	0.70	0.86
	DMR	8.55	1.79	9.16	2.77	-	5.58	1.85	8.71	2.25
	$P[DS\|S_{a2/50}]$	0.00	16.11	0.00	13.76	-	0.00	11.63	0.00	18.77
Collapse	S_D (g)	2.69	0.54	2.64	-	-	1.83	0.56	2.56	-
	$\beta_{D\|IM}$	0.62	0.16	0.62	-	-	0.50	0.14	0.69	-
	β_{TOT}	0.77	0.43	0.74	-	-	0.68	0.42	0.80	-
	DMR	11.20	2.24	11.02	-	-	7.63	2.32	10.66	-
	$P[DS\|S_{a2/50}]$	0.00	6.26	0.00	-	-	0.00	4.15	0.00	-

Table 3.8. Peak transient and residual response of critical monolithic bridge components at MCE level

	Pier 1	Pier 2	Pier 3	Pier 4	Pier 5	Pier 6	Pier 7	Pier 8	West abutment	East abutment
Longitudinal										
Peak transient drift (%)	0.32	0.27	0.28	0.28	0.28	0.27	0.28	0.30	-	-
Peak residual drift (%)	0.01	0.01	0.01	0.02	0.02	0.01	0.01	0.01	-	-
Peak transient pier pile cap disp. (m)	0.01	0.01	0.01	0.01	0.00	0.01	0.01	0.01	-	-
Peak residual pier pile cap disp. (m)	0.00	0.00	0.00	0.00	0.00	0.00	0.00	0.00	-	-
Peak transient abut. pile cap disp. (m)	-	-	-	-	-	-	-	-	0.03	0.03
Peak residual abut. pile cap disp. (m)	-	-	-	-	-	-	-	-	0.01	0.01
Transverse										
Peak transient drift (%)	0.52	0.30	0.33	0.40	0.43	0.44	0.48	0.46	-	-
Peak residual drift (%)	0.02	0.01	0.01	0.01	0.01	0.01	0.01	0.02	-	-
Peak transient pier pile cap disp. (m)	0.01	0.01	0.01	0.01	0.01	0.01	0.01	0.01	-	-
Peak residual pier pile cap disp. (m)	0.00	0.00	0.00	0.00	0.00	0.00	0.00	0.00	-	-
Peak transient abut. pile cap disp. (m)	-	-	-	-	-	-	-	-	0.03	0.03
Peak residual abut. pile cap disp. (m)	-	-	-	-	-	-	-	-	0.00	0.00

Table 3.9. Summarized IDA parameters of the isolated bridge in longitudinal direction

	DM|IM percentiles (g)														
	Column drift			Abutment pile cap displacement			Pier pile cap displacement			Backfill soil deformation: Active action			Backfill soil deformation: Passive action		
DS	50%	84%	16%	50%	84%	16%	50%	84%	16%	50%	84%	16%	50%	84%	16%
Slight	1.73	1.12	2.22	0.19	0.13	0.26	2.24	1.54	2.92	0.13	0.09	0.18	0.43	0.29	0.60
Moderate	2.55	1.75	3.21	0.30	0.22	0.40	2.64	1.84	3.43	0.33	0.24	0.43	1.13	0.89	1.53
Extensive	3.23	2.27	4.10	0.41	0.30	0.55	3.27	2.46	4.07	0.51	0.37	0.65	-	-	-
Collapse	3.73	2.68	4.58	0.50	0.35	0.66	3.60	2.63	4.25	-	-	-	-	-	-

Table 3.10. Summarized IDA parameters of the monolithic bridge in transverse direction

	DM|IM percentiles (g)											
	Column drift			Abutment pile cap displacement			Pier pile cap displacement			Abutment deformation		
DS	50%	84%	16%	50%	84%	16%	50%	84%	16%	50%	84%	16%
Slight	1.31	0.81	1.78	2.22	0.16	0.30	1.80	1.26	2.37	0.12	0.08	0.16
Moderate	2.14	1.47	2.93	0.35	0.24	0.46	2.26	1.57	2.92	0.35	0.24	0.46
Extensive	2.90	2.13	3.91	0.46	0.35	0.61	2.90	2.20	3.93	0.54	0.44	0.71
Collapse	3.20	2.50	4.00	0.55	0.44	0.72	3.10	2.40	4.00	-	-	-

Table 3.11. Fragility parameters of the isolated bridge

		Longitudinal					Transverse			
		Peak column drift	Abutment pile cap displacement	Pier pile cap displacement	Peak backfill soil deformation: . .	Peak backfill soil deformation: passive action	Peak column drift	Abutment pile cap displacement	Pier pile cap displacement	Peak abutment deformation
Slight	S_D (g)	1.73	0.20	2.29	0.13	0.44	1.32	0.24	1.88	0.12
	$\beta_{D\|IM}$	0.52	0.07	0.65	0.05	0.14	0.49	0.09	0.57	0.04
	β_{TOT}	0.57	0.41	0.77	0.70	0.48	0.55	0.41	0.69	0.70
	DMR	7.19	0.83	9.54	0.56	1.82	5.49	0.99	7.85	0.50
	$P[DS\|S_{a2/50}]$	0.00	67.90	0.00	79.11	17.60	0.00	56.00	0.00	82.87
Moderate	S_D (g)	2.57	0.31	2.69	0.33	1.21	2.18	0.35	2.29	0.35
	$\beta_{D\|IM}$	0.75	0.10	0.76	0.09	0.35	0.74	0.10	0.67	0.10
	β_{TOT}	0.79	0.41	0.86	0.90	0.58	0.78	0.41	0.78	0.91
	DMR	10.70	1.31	11.21	1.39	5.03	9.10	1.47	9.54	1.46
	$P[DS\|S_{a2/50}]$	0.00	32.52	0.00	37.74	1.80	0.00	24.80	0.00	36.20
Extensive	S_D (g)	3.28	0.42	3.32	0.51	-	3.02	0.47	3.03	0.56
	$\beta_{D\|IM}$	0.87	0.13	0.80	0.13	-	0.91	0.12	0.86	0.14
	β_{TOT}	0.98	0.42	0.89	0.86	-	1.02	0.42	0.95	0.86
	DMR	13.66	1.75	13.85	2.13	-	12.58	1.95	12.62	2.35
	$P[DS\|S_{a2/50}]$	0.00	15.35	0.00	21.00	-	0.00	9.50	0.00	17.40
Collapse	S_D (g)	3.70	0.51	3.53	-	-	3.32	0.58	3.18	-
	$\beta_{D\|IM}$	0.83	0.14	0.78	-	-	0.82	0.14	0.87	-
	β_{TOT}	0.95	0.42	0.88	-	-	0.94	0.42	0.95	-
	DMR	15.42	2.13	14.72	-	-	13.83	2.41	13.26	-
	$P[DS\|S_{a2/50}]$	0.00	7.37	0.00	-	-	0.00	3.59	0.00	-

Table 3.12. Peak transient and residual response of critical isolated bridge components at MCE level

	Pier 1	Pier 2	Pier 3	Pier 4	Pier 5	Pier 6	Pier 7	Pier 8	West abutment	East abutment
Longitudinal										
Peak transient drift (%)	0.11	0.15	0.15	0.18	0.19	0.17	0.14	0.11	-	-
Peak residual drift (%)	0.00	0.00	0.00	0.00	0.00	0.00	0.00	0.00	-	-
Peak transient pier pile cap disp. (m)	0.00	0.00	0.00	0.00	0.00	0.00	0.00	0.00	-	-
Peak residual pier pile cap disp. (m)	0.00	0.00	0.00	0.00	0.00	0.00	0.00	0.00	-	-
Peak transient abut. pile cap disp. (m)	-	-	-	-	-	-	-	-	0.02	0.02
Peak residual abut. pile cap disp. (m)	-	-	-	-	-	-	-	-	0.00	0.00
Transverse										
Peak transient drift (%)	0.10	0.15	0.16	0.18	0.19	0.19	0.14	0.10	-	-
Peak residual drift (%)	0.00	0.00	0.00	0.00	0.00	0.00	0.00	0.00	-	-
Peak transient pier pile cap disp. (m)	0.00	0.00	0.00	0.00	0.00	0.00	0.00	0.00	-	-
Peak residual pier pile cap disp. (m)	0.00	0.00	0.00	0.00	0.00	0.00	0.00	0.00	-	-
Peak transient abut. pile cap disp. (m)	-	-	-	-	-	-	-	-	0.02	0.02
Peak residual abut. pile cap disp. (m)	-	-	-	-	-	-	-	-	0.00	0.00

Table 3.13. Comparison of fragility parameters of bridge components in longitudinal direction

	Peak column drift			Peak abutment pile cap displacement			Peak pier pile cap displacement			Peak backfill soil deformation: active action			Peak backfill soil deformation: passive action		
	Monolithic	Isolated	Discrepancy (%)	Monolithic	Isolated	Discrepancy (%)	Monolithic	Isolated	Discrepancy (%)	Monolithic	Isolated	Discrepancy (%)	Monolithic	Isolated	Discrepancy (%)
Slight															
S_D (g)	0.61	1.73	183.61	0.17	0.20	17.65	0.72	2.29	216.39	0.12	0.13	8.15	0.37	0.44	19.63
$\beta_{D\|IM}$	0.17	0.52	205.88	0.07	0.07	0.00	0.21	0.65	210.71	0.04	0.05	14.16	0.13	0.14	4.48
β_{TOT}	0.30	0.57	90.00	0.41	0.41	0.00	0.45	0.77	70.58	0.70	0.70	-0.20	0.48	0.48	0.18
DMR	2.55	7.19	181.96	0.69	0.83	20.29	3.02	9.54	216.33	0.50	0.56	11.81	1.53	1.82	18.76
Moderate															
S_D (g)	1.27	2.57	102.36	0.29	0.31	5.30	1.16	2.69	132.66	0.37	0.33	-11.86	1.16	1.21	4.46
$\beta_{D\|IM}$	0.31	0.75	141.94	0.12	0.10	-14.31	0.31	0.76	147.40	0.13	0.09	-32.53	0.29	0.35	20.52
β_{TOT}	0.39	0.79	102.56	0.42	0.41	-1.60	0.50	0.86	70.52	0.91	0.90	-1.08	0.54	0.58	6.62
DMR	5.28	10.70	102.65	1.23	1.31	6.79	4.82	11.21	132.69	1.56	1.39	-10.90	4.83	5.03	4.22
Extensive															
S_D (g)	2.05	3.28	60.00	0.43	0.42	-2.33	2.20	3.32	51.06	0.66	0.51	-23.15	-	-	-
$\beta_{D\|IM}$	0.47	0.87	85.11	0.15	0.13	-10.65	0.55	0.80	46.17	0.18	0.13	-29.35	-	-	-
β_{TOT}	0.66	0.98	48.48	0.43	0.42	-1.33	0.68	0.89	31.29	0.87	0.86	-1.11	-	-	-
DMR	8.55	13.66	59.77	1.79	1.75	-2.33	9.16	13.85	51.24	2.77	2.13	-22.97	-	-	-
Collapse															
S_D (g)	2.69	3.70	37.55	0.54	0.51	-4.97	2.64	3.53	33.52	-	-	-	-	-	-
$\beta_{D\|IM}$	0.62	0.83	33.87	0.16	0.14	-10.14	0.62	0.78	25.87	-	-	-	-	-	-
β_{TOT}	0.77	0.95	23.38	0.43	0.42	-2.16	0.74	0.88	19.31	-	-	-	-	-	-
DMR	11.20	15.42	37.68	2.24	2.13	-4.75	11.02	14.72	33.63	-	-	-	-	-	-

Table 3.14. Comparison of fragility parameters of bridge components in transverse direction

	Peak column drift			Peak abutment pile cap displacement			Peak pier pile cap displacement			Peak abutment deformation		
	Monolithic	Isolated	Discrepancy (%)	Monolithic	Isolated	Discrepancy (%)	Monolithic	Isolated	Discrepancy (%)	Monolithic	Isolated	Discrepancy (%)
Slight												
S_D (g)	0.39	1.32	238.29	0.21	0.24	11.94	0.62	1.88	203.23	0.11	0.12	9.09
$\beta_{D\|IM}$	0.12	0.49	323.51	0.09	0.09	0.00	0.18	0.57	216.67	0.04	0.04	0.00
β_{TOT}	0.28	0.55	99.66	0.41	0.41	0.00	0.44	0.69	56.82	0.70	0.70	0.00
DMR	1.63	5.49	237.67	0.89	0.99	11.24	2.57	7.85	205.45	0.48	0.50	4.17
Moderate												
S_D (g)	0.76	2.18	186.84	0.33	0.35	6.06	0.98	2.29	133.67	0.33	0.35	6.06
$\beta_{D\|IM}$	0.17	0.74	335.29	0.10	0.10	0.00	0.25	0.67	168.00	0.10	0.10	0.00
β_{TOT}	0.30	0.78	160.00	0.41	0.41	0.00	0.47	0.78	65.96	0.91	0.91	0.00
DMR	3.19	9.10	185.27	1.36	1.47	8.09	4.07	9.54	134.40	1.36	1.46	7.35
Extensive												
S_D (g)	1.34	3.02	125.37	0.44	0.47	6.82	2.09	3.03	44.98	0.54	0.56	3.70
$\beta_{D\|IM}$	0.34	0.91	167.65	0.12	0.12	0.00	0.57	0.86	50.88	0.14	0.14	0.00
β_{TOT}	0.57	1.02	78.95	0.42	0.42	0.00	0.70	0.95	35.71	0.86	0.86	0.00
DMR	5.58	12.58	125.45	1.85	1.95	5.41	8.71	12.62	44.89	2.25	2.35	4.44
Collapse												
S_D (g)	1.83	3.32	81.42	0.56	0.58	3.57	2.56	3.18	24.22	-	-	-
$\beta_{D\|IM}$	0.50	0.82	64.00	0.14	0.14	0.00	0.69	0.87	26.09	-	-	-
β_{TOT}	0.68	0.94	38.24	0.42	0.42	0.00	0.80	0.95	18.75	-	-	-
DMR	7.63	13.83	81.26	2.32	2.41	3.88	10.66	13.26	24.39	-	-	-

Table 3.15. Peak response history of bridge components

	Longitudinal			Transverse		
	Monolithic	Isolated	Discrepancy (%)	Monolithic	Isolated	Discrepancy (%)
Deck						
Displacement [m]	0.027	0.094	242.34	0.025	0.091	259.06
Velocity [m/s]	0.296	0.551	85.80	0.294	0.520	76.56
Abs. acceleration [g]	0.531	1.370	158.12	0.445	0.410	-7.93
Column						
Base shear [kN]	94.887	26.873	-71.68	89.310	26.07	-70.81
Base moment [kN.m]	145.083	61.440	-57.65	144.35	65.89	-54.35

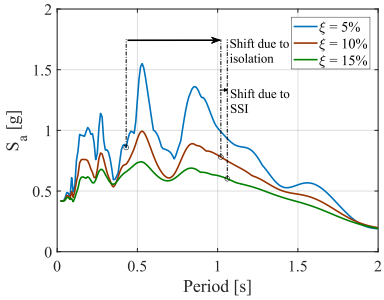

Figure 3.1. Effect of SSI on the input demand of seismically isolated structures

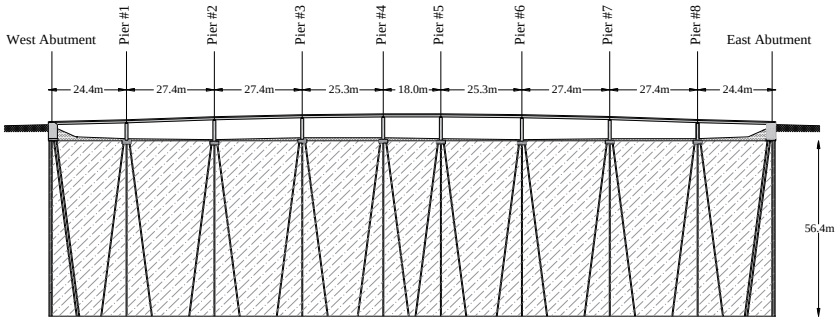

Figure 3.2. Overview of the 7th line overpass bridge

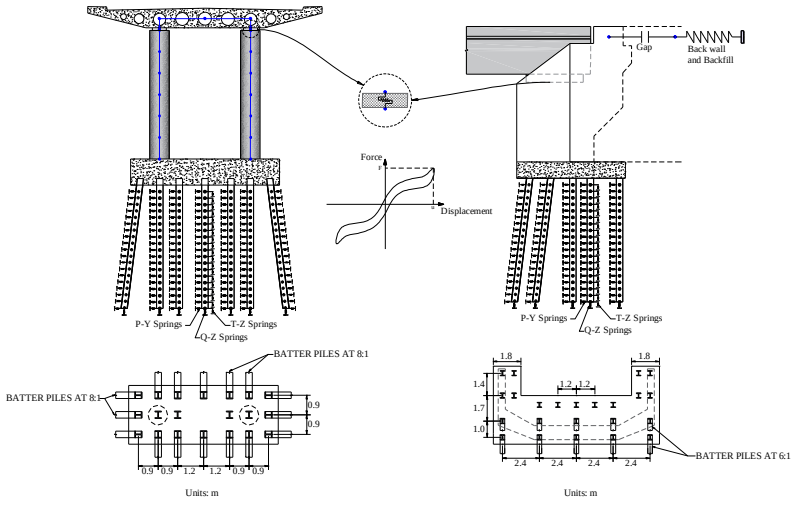

Figure 3.3. Plan and elevation view of piers, abutments, and their supporting pile groups

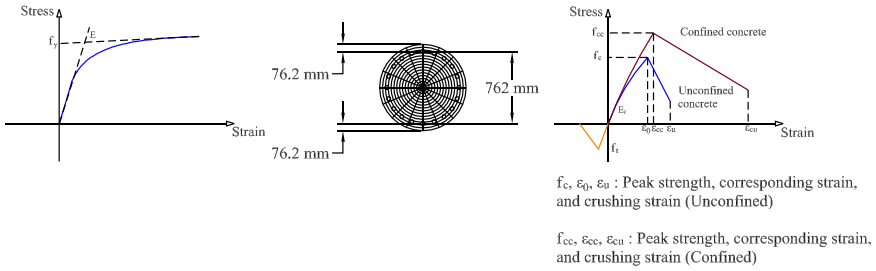

Figure 3.4. Characteristic parameters of the column fiber section

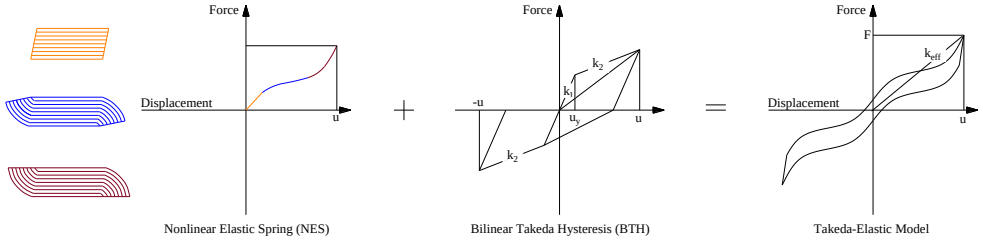

Figure 3.5. Schematic illustration of the lateral load-displacement behavior of the *Takeda-Elastic* model

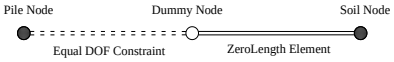

Figure 3.6. Soil spring connectivity in pile-soil interface

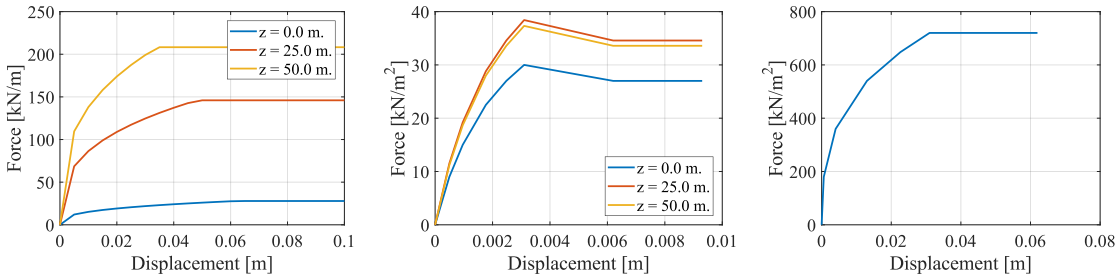

(a) (b) (c)

Figure 3.7. (a) p-y (b) t-z and (c) q-z backbone curves

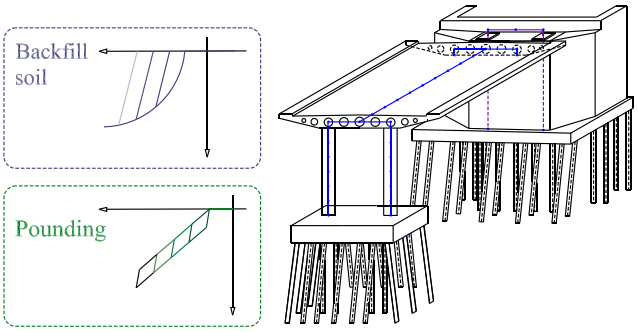

Figure 3.8. Configuration of bridge elements

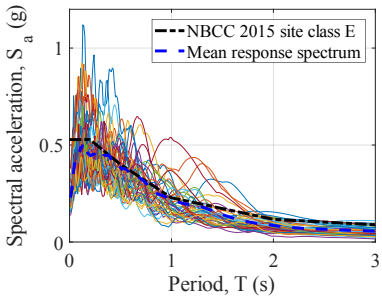

Figure 3.9. Acceleration response spectra of the ground motion records

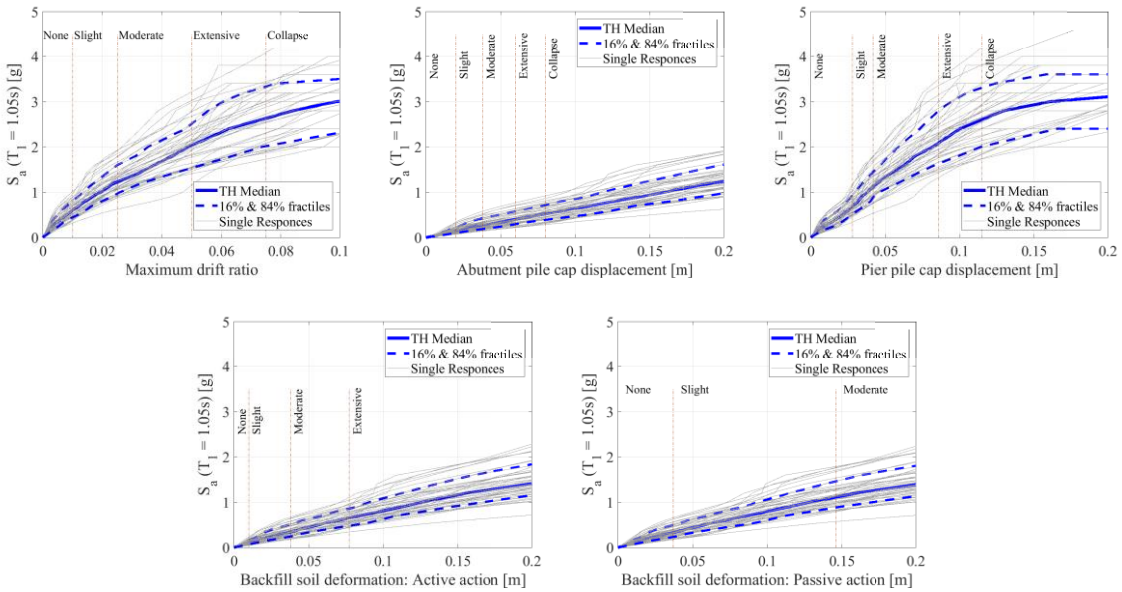

Figure 3.10. Summarized IDA curves of the monolithic bridge in longitudinal direction

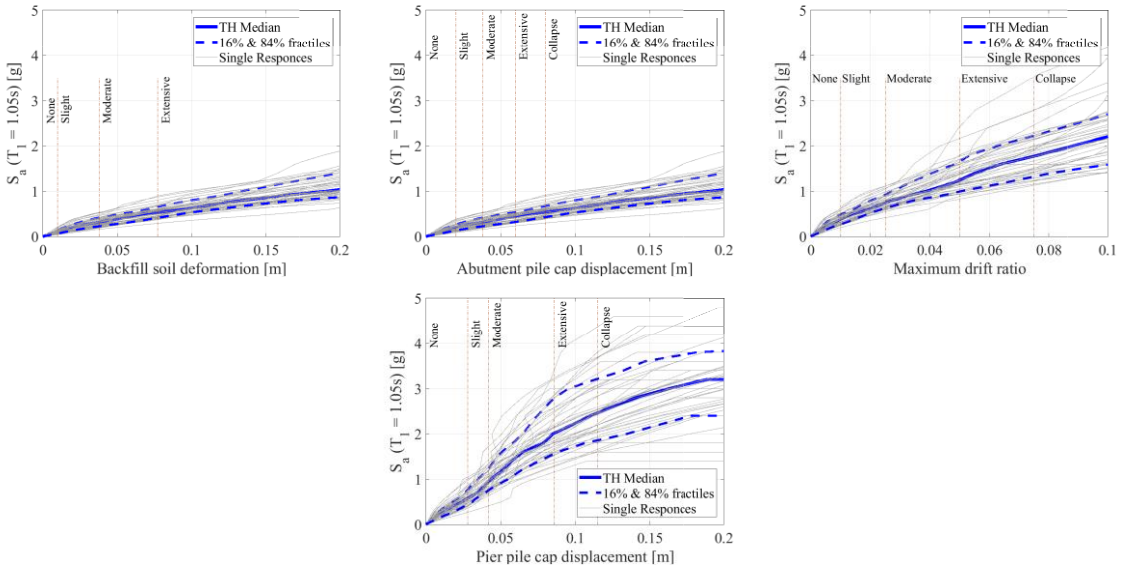

Figure 3.11. Summarized IDA curves of the monolithic bridge in transverse direction

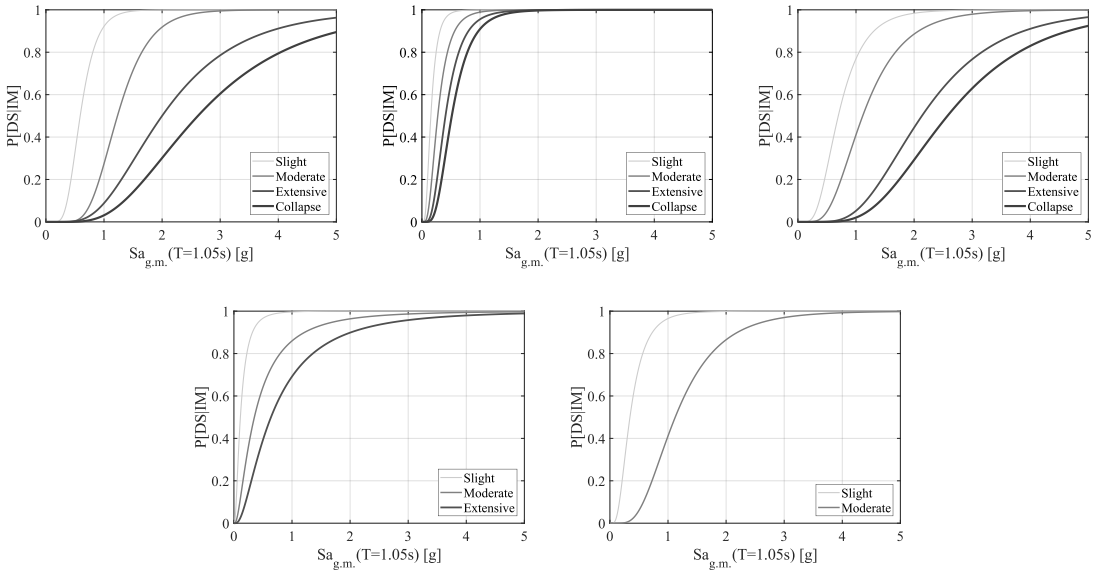

Figure 3.12. Component fragility curves of monolithic bridge in longitudinal direction

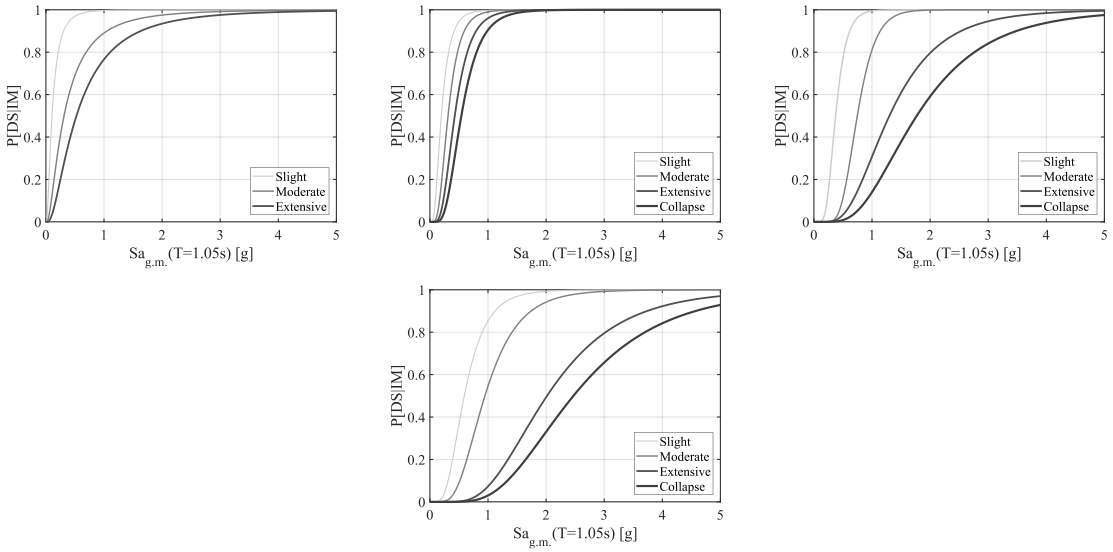

Figure 3.13. Component fragility curves of monolithic bridge in transverse direction

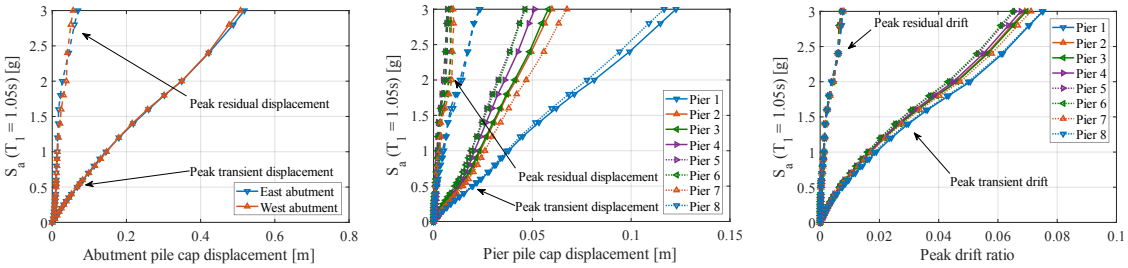

Figure 3.14. Peak transient and residual response of the monolithic bridge components in longitudinal direction

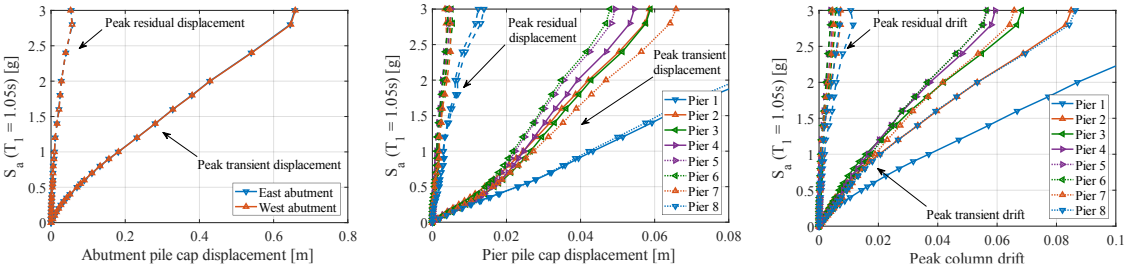

Figure 3.15. Peak transient and residual response of the monolithic bridge components in transverse direction

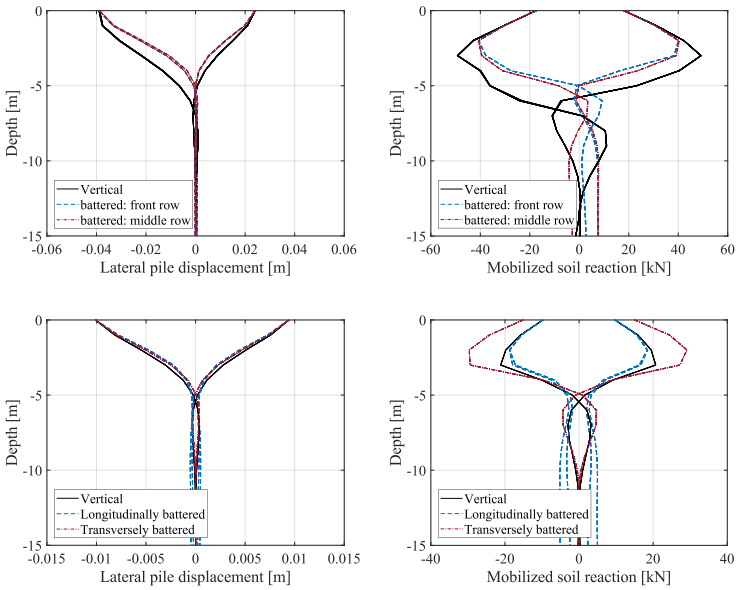

Figure 3.16. Peak lateral displacement and reaction of (a) abutment and (b) pier pile groups of monolithic bridge at MCE level in longitudinal direction

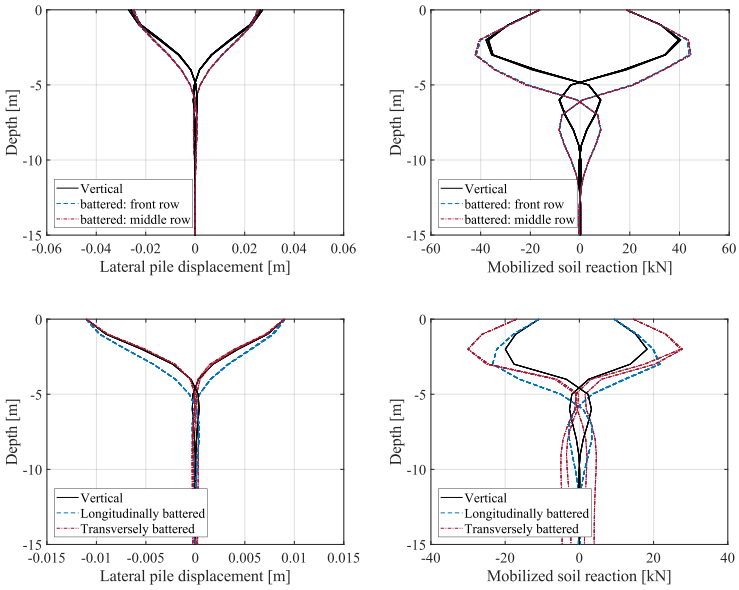

Figure 3.17. Peak lateral displacement and reaction of (a) abutment and (b) pier pile groups of monolithic bridge at MCE level in transverse direction

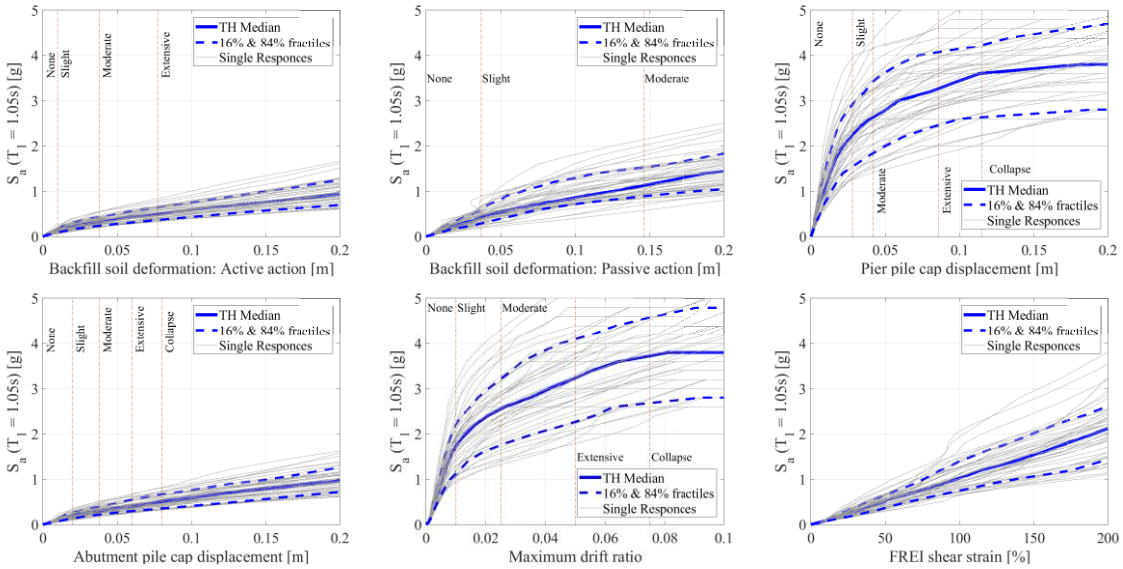

Figure 3.18. Summarized IDA curves of the isolated bridge in longitudinal direction

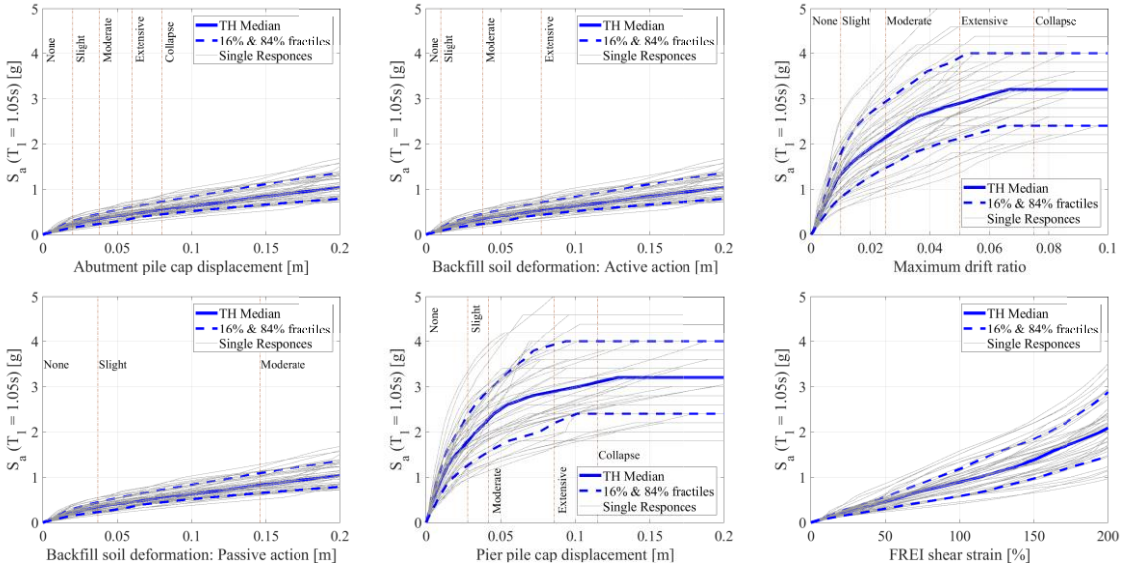

Figure 3.19. Summarized IDA curves of the isolated bridge in transverse direction

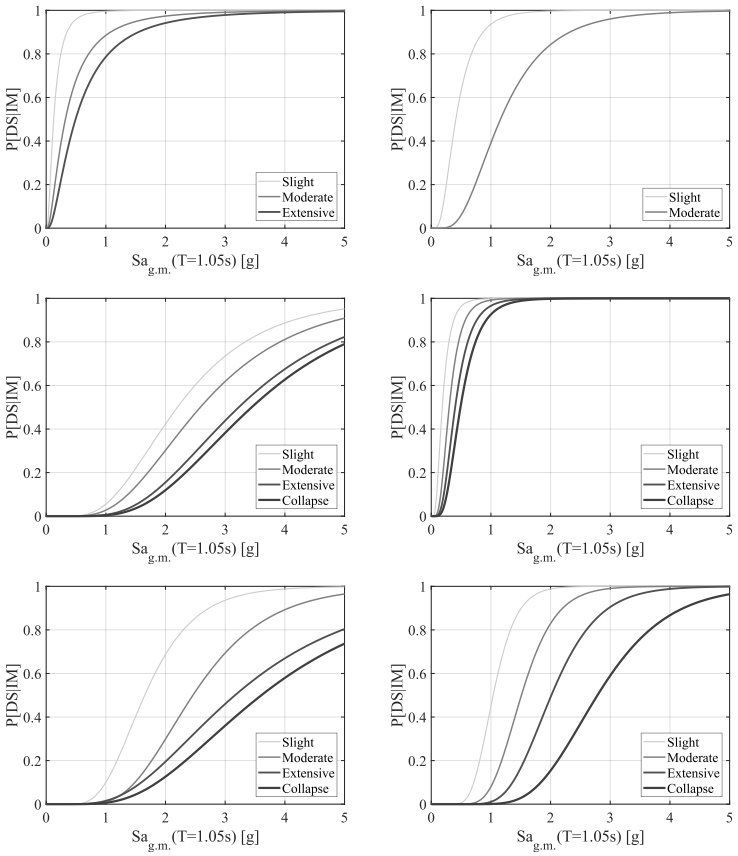

Figure 3.20. Component fragility curves of isolated bridge in longitudinal direction

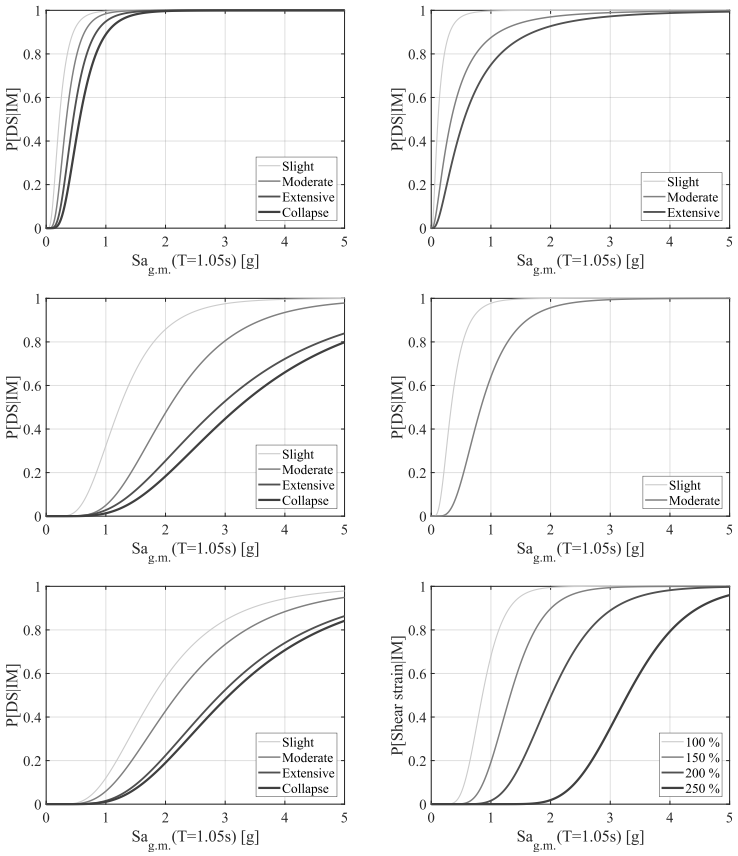

Figure 3.21. Component fragility curves of isolated bridge in transverse direction

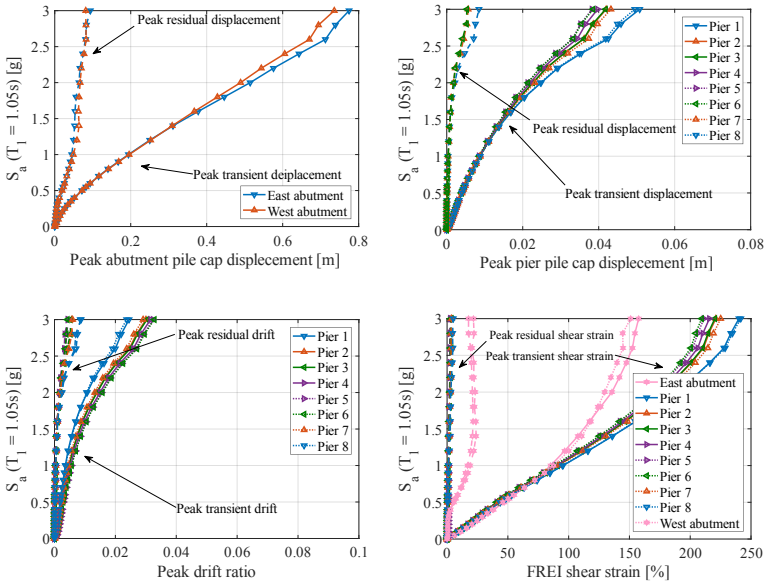

Figure 3.22. Peak transient and residual response of the isolated bridge components in longitudinal direction

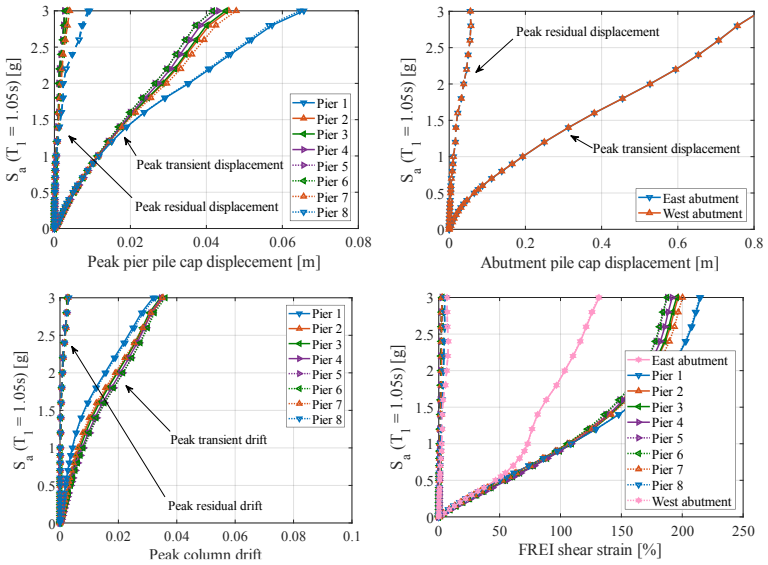

Figure 3.23. Peak transient and residual response of the isolated bridge components in transverse direction

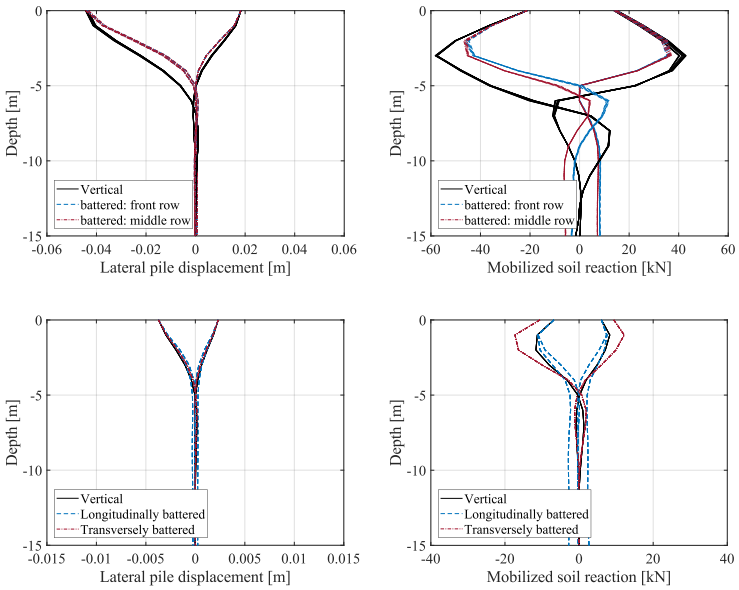

Figure 3.24. Peak lateral displacement and reaction of (a) abutment and (b) pier pile groups of isolated bridge at MCE level in longitudinal direction

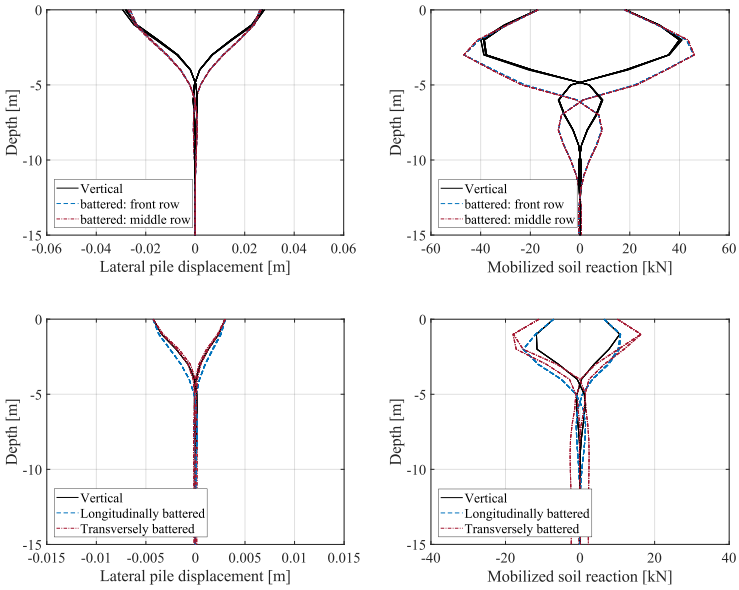

Figure 3.25. Peak lateral displacement and reaction of (a) abutment and (b) pier pile groups of isolated bridge at MCE level in transverse direction

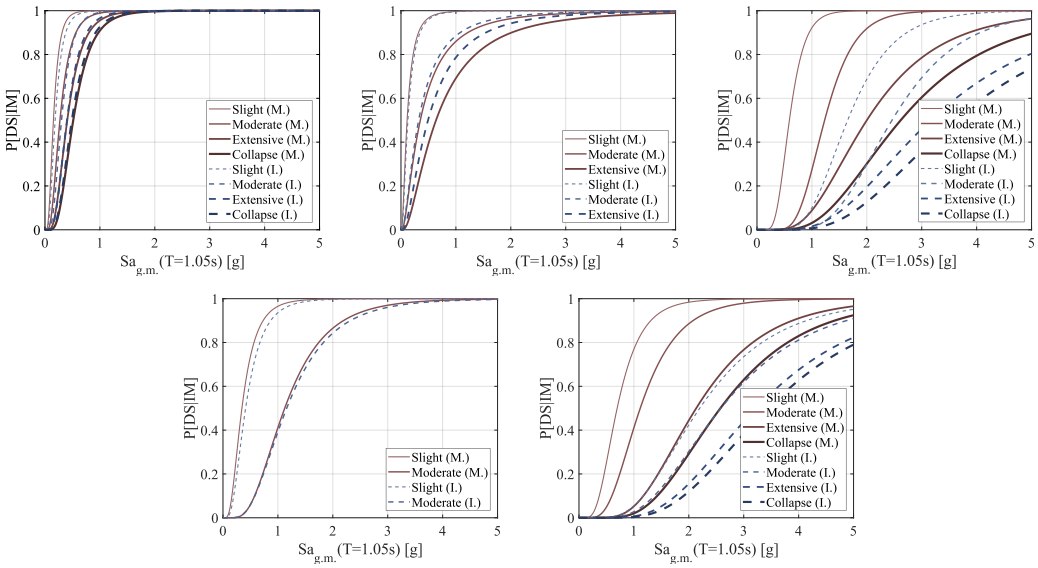

Figure 3.26. Comparison of seismic fragility curves of the monolithic and isolated bridge in longitudinal direction

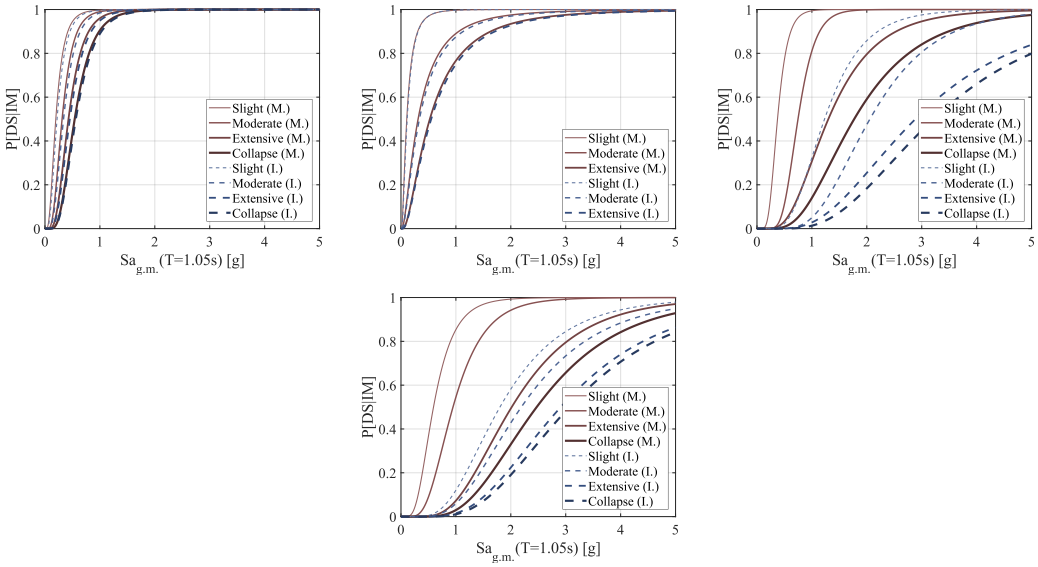

Figure 3.27. Comparison of seismic fragility curves of the monolithic and isolated bridge in transverse direction

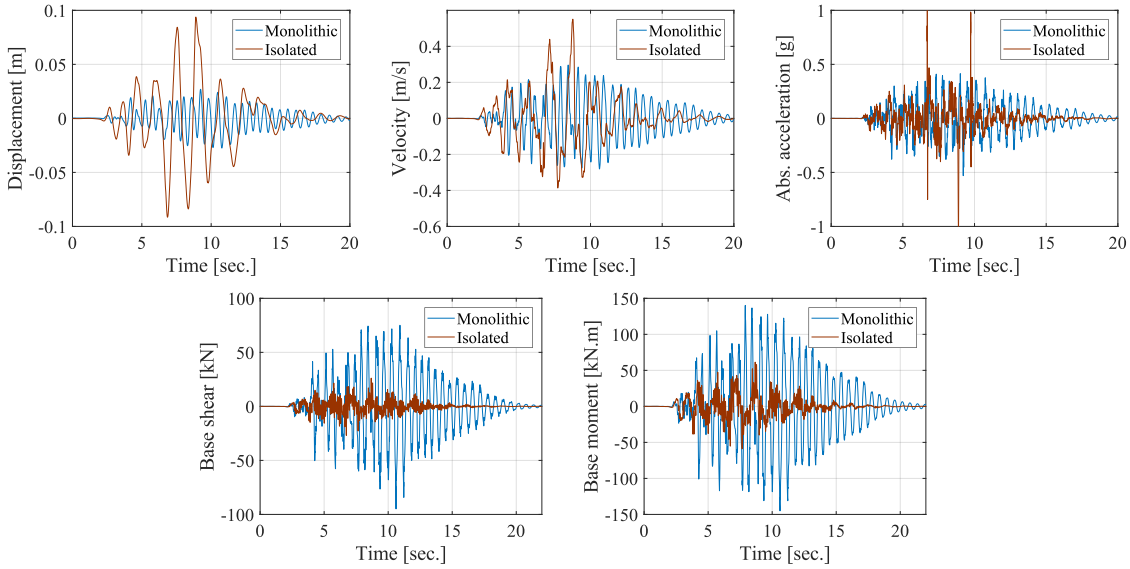

Figure 3.28. Comparison of the component response histories at MCE level in longitudinal direction

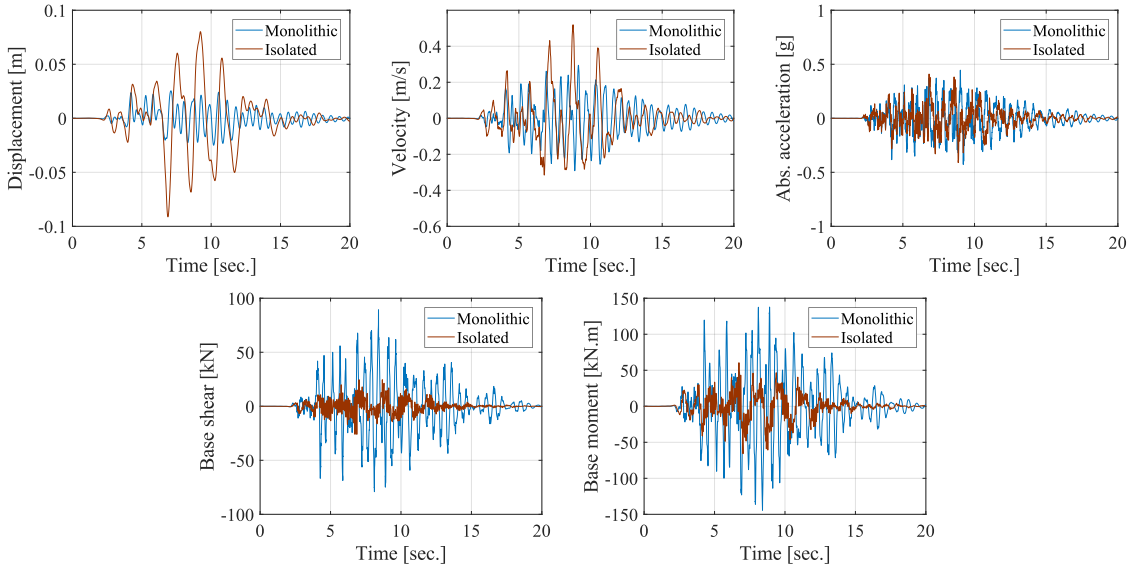

Figure 3.29. Comparison of the component response histories at MCE level in transverse direction

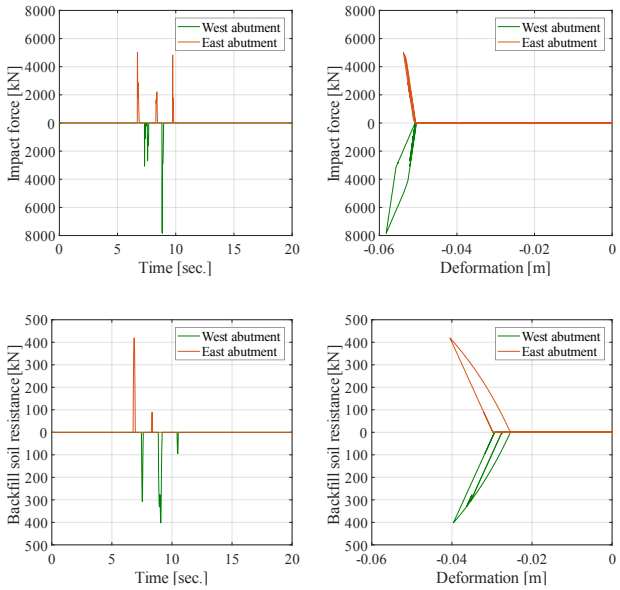

Figure 3.30. Pounding and backfill soil response history at MCE level

4 Seismic Fragility Analysis of Bridge-Isolator-Foundation-Soil Systems in Subfreezing Temperatures

Abstract

Several cold regions around the world are in seismic active zones. Seasonal freezing can significantly affect the seismic performance of complex bridge-isolator-foundation-soil systems by inducing brittle failure and premature collapse due to a combination of load reversals and cold temperature behavior of the bridge material. In cold conditions, constitutive material of bridge components, namely, concrete, steel reinforcement, rubber, and supporting soil undergo substantial stiffening which afflicts the ductility capacity of bridges. This study investigates the seismic performance of four bridge cases, namely, isolated bridge supported by pile groups, monolithic bridge supported by pile groups, isolated fixed-base bridge, and monolithic fixed-base bridge at room and subfreezing temperatures to unmask the effectiveness of using Fiber Reinforced Elastomeric Isolator (FREI) as a retrofit measure and to evaluate the performance of bridges at temperatures ranging from room (i.e. 20°C) to -37°C. To this end, an analysis matrix is developed based on the climatic condition of the bridge site along with the code provisions. A seismic fragility analysis is carried out in the context of Incremental Dynamic Analysis (IDA) using a set of synthetic ground motion records for longitudinal and transverse directions of the bridge, independently. It is shown that while the seismic isolation system can effectively mitigate the probability of damage to the bridge at room temperatures, isolated bridges demonstrated an acceptable behavior at subfreezing temperatures.

Keywords: Seismic isolation, Low temperature, SU-FREI, Seismic fragility, SSI, IDA

4.1 Introduction

Highway bridges serve as a foundation for infrastructure development by facilitating an efficient flow of commerce and commuting across cities. Continuous exposure of these structures to various types of natural hazards (e.g. earthquakes, hurricanes, etc.) and environmental stressors (e.g. subfreezing temperatures, scouring, etc.) during their life cycle entails seismic risk assessment and retrofit prioritization plans to mitigate the probability of damage to the bridge components as well as potential life and monetary losses. Statistical investigation of recent seismic events reveals that major earthquakes have occurred in subfreezing conditions, namely, 1811-1812 Midwest at New Madrid in the United States, the 1935 Timiskaming earthquake (M_W = 6.1) in Canada, 1964 Prince William Sound earthquake (M_W = 9.2) in Alaska, and 2011 Tohoku earthquake in Japan (M_W = 9.0). The likelihood of seismic events during cold temperatures is quite significant for particular regions of North America such as Ottawa, Canada where the minimum mean daily temperature can either drop as low as -35.3°C at least once a year or maintain -10°C for fourteen consecutive days within a year (Guay & Bouaanani, 2016). The engineering properties of constitutive materials of different bridge components such as foundation soil, concrete, steel reinforcement bars, and rubber are subject to change under such freezing conditions. Therefore, the risk of brittle failure due to a combination of extreme cyclic load reversals and freezing temperatures should be taken into account. The effect of seasonal freezing on lateral response of integrated bridge column-foundation systems is investigated experimentally by Suleiman et al. and it is shown that subfreezing temperatures as low as -10°C increases the effective elastic stiffness of the foundation shaft and its average lateral

force resistance, and reduces the length of the plastic region in the shaft (Suleiman, Sritharan, & White, 2006). Sritharan et al. have interrogated the impact of different subfreezing temperatures from -1°C to -20°C on the lateral load response of a bridge column supported by a cast-in-drilled-hole foundation shaft and have confirmed the results obtained by Suleiman et al. (Sritharan, Suleiman, & White, 2007). Seasonal frost effect on a soil-foundation-structure interaction system in Anchorage, Alaska, is studied by Yang et al. (Yang, Dutta, Zhu, Marx, & Biswas, 2007) via monitoring the bridge response to ambient noises, traffic-induced vibrations, and small magnitude earthquakes over more than a one-year period and developing a finite element model. The results demonstrated that the environmental variables can significantly alter the dynamic properties of the bridge system by modifying the bridge stiffness. Billah and Todorov scrutinized the effect of cold temperatures on the seismic performance of a Lead Rubber Bearing (LRB) isolated bridge in Montreal, Quebec, by developing a finite element model being exposed to two temperature variations of +35°C and -35°C (Billah & Todorov, 2019). Results demonstrate that the reduced stiffness of LRB results in higher shear forces and smaller displacement ductility in the bridge piers. Nassar et al. (Nassar, Guizani, Nollet, & Tahan, 2019, 2022) have developed a probability-based reliability assessment approach for seismic base-isolated bridges in cold regions and evaluated the seismic performance of a two span bridge in Quebec isolated with LRB. Deng et al. (Deng, Gan, Hayashikawa, & Matsumoto, 2020) have evaluated the seismic response of highway viaducts equipped with lead-rubber bearings under low temperature and demonstrated that cold temperature has a detrimental effect of the performance of LRB, particularly, for smaller size LRB where plastification

due to cold temperature is more severe. Recently, Fosoul and Tait (A. S. Fosoul & Tait, 2021) evaluated the cold-temperature seismic performance of a multi-span concrete bridge retrofitted with SU-FREI and Bandini et al. used fragility surfaces to predict the cold-temperature probability of damage of bridges retrofitted with bonded natural rubber isolators (Bandini, Siqueira, Padgett, & Paultre, 2022). Although different studies are available in the literature on evaluating the effect of cold temperature on the mechanical behavior of materials and seismic performance of individual bridge components, a comprehensive seismic assessment of a bridge-isolator-foundation-soil system at subfreezing temperature has not been conducted yet.

This study aims to investigate the effect of subfreezing temperature on the seismic performance of a bridge-isolator-foundation-soil system by performing an IDA and developing seismic fragility curves for different bridge components. A conventionally designed bridge in Ottawa, Ontario, is adopted and its detailed comprehensive three-dimensional finite element model is generated in OpenSees. The effect of cold temperature on concrete, reinforcing rebars, rubber, and the supporting soil is taken into account to investigate the impact of cold-temperature behavior of different bridge components on the bridge fragility. Four bridge cases are considered herein; first, a fixed-base monolithic bridge; second, a fixed-base retrofitted bridge isolated with a novel type of elastomeric isolator called Stable Unbonded-Fiber Reinforced Elastomeric Isolator (SU-FREI); third, a monolithic bridge supported by the underlying soil; and forth, a retrofitted bridge using SU-FREI supported by the underlying soil. The analysis matrix shown in Table 4.1 is adopted to evaluate the seismic performance of the bridge under real climatic conditions in

Ottawa, namely, 1 day at -37°C, 1 day at -26°C, 3 days at -18°C, and 14 days at -10°C, as well as, the AASHTO requirements for permitting the use of elastomeric isolators such as 28 days at -37°C, 21 days at -26°C, 14 days at -18°C, and 7 days at -10°C.

4.2 Influence of low temperature on seismic behavior of materials

4.2.1 Concrete

Past studies on the mechanical behavior of concrete indicate that subfreezing temperature has a remarkable impact on its compressive strength (Browne & Bamforth, 1981; A Filiatrault & M Holleran, 2001; Lee, Shih, & Chang, 1988a, 1988b; Rostásy & Pusch, 1987; Sho Yamane & Toru). As temperature drops below freezing, saturated concrete stiffens to a larger extent with respect to partially dried concrete, but even oven-dried concrete will experience a degree of stiffening (Luis Alberto Montejo, 2008). This increase is attributed to a kind of prestressing that is occurred in the concrete due to filling capillary pores and micro-cracks by expanded water that has been turned into ice (Manuel & Jaime). Several researchers have proposed equations for estimating the compressive strength of concrete at low temperatures as a function of compressive strength at room temperature and concrete moisture content (Goto & Miura, 1979; Okada & Iguro, 1978; Sehnal, Kronen, & Marshall, 1983; A. T. Shelman, 2013). A comparison of these predictive equations in Figure 4.1 demonstrates that although different linear or polynomial fashions have been adopted for predicting the cold temperature compressive strength of concrete, they have a negligible discrepancy within the temperature range under investigation in this study. Therefore, Equation (4.1) proposed by Browne and Bamforth (Browne & Bamforth, 1981) is adopted.

$$f_c'(T) = f_c'(20^\circ C) - \frac{T.w}{12} \quad (4.1)$$

In this equation, T and w are representing subfreezing temperature and concrete moisture content, respectively. Montejo has shown that this equation provides the closest prediction to experimental data while it is simple enough for manipulation (Luis Alberto Montejo, 2008). The unconfined and confined compressive strains of concrete at low temperatures are adopted from a study by Shelman and are shown in Equations (4.2) and (4.3), respectively (A. T. Shelman, 2013).

$$\varepsilon_{co} = 6.9\times10^{-6}[T(^\circ C)] + 1.86\times10^{-3} \quad (4.2)$$

$$\varepsilon_{cc} = \varepsilon_{cc,room}\left(-0.0034[T(^\circ C)] + 1.086\right) \quad (4.3)$$

Past studies have shown that the Poisson's ratio of concrete can be taken as 0.2 regardless of the temperature, whereas Lee et al. have reported that Poisson's ratio will increase at extremely low temperatures (Lee et al., 1988a). For the cold temperature range considered in this study, it is assumed that the Poisson's ratio will remain unaffected. Modulus of elasticity also increases with low temperatures, however, Montejo has shown that the conventional relation of $E = k\sqrt{f_c'}$ is still applicable to cold temperatures given that the corresponding low-temperature compressive strength is used (Luis Alberto Montejo, 2008).

4.2.2 Steel reinforcing bars

Previous studies have demonstrated that the yield and ultimate strength of steel rebar increase when they are subjected to cold temperatures, whereas the modulus of elasticity and ductility remain unaffected (Sleigh, 1981; Whiteley, Armstrong, & Welburn, 1982).

Filiatrault and Holleran (A. Filiatrault & M. Holleran, 2001) have investigated the combined effect of strain rate and low temperature on a set of steel rebar and confirmed that the yield and tensile strength have increased by 22% and 12%, respectively, when the temperature has dropped from 20°C to -40°C, whereas the Young's modulus and the ultimate tensile strain have changed negligibly. Likewise, Sloan (Sloan, 2005) has explored the effect of low temperature and strain rate on a set of 13 specimens and confirmed that low temperature increases both yield and ultimate strength of the steel. Based on a statistical investigation of the abovementioned results, Montejo et al. (Luis A. Montejo, Sloan, Kowalsky, & Hassan, 2008) proposed that the yield and ultimate strengths of reinforcing steel within a cold temperature range of -40°C to -25°C can be approximated to be about 10-12% of those in room temperature. These two parameters linearly decrease to zero at 0°C as shown in Equations (4.4) and (4.5). These equations are the basis for determining the cold temperature behavior of the reinforcing steel in this study. It is shown by other researchers that the yield strength of the reinforcing steel increases in a polynomial (mostly quadratic) fashion as shown in Figure 4.1-a. However, the discrepancy between these approaches is less than 10%.

$$f_s = \left(1 - 0.004T(^{\circ}C)\right) \times f_s^{20^{\circ}C} \qquad 0^{\circ}C > T > -25^{\circ}C \tag{4.4}$$

$$f_s = 1.1 \times f_s^{20^{\circ}C} \qquad -25^{\circ}C > T > -40^{\circ}C \tag{4.5}$$

4.2.3 Lateral stiffness and damping of SU-FREI

Elastomeric isolators can mitigate the seismic demand on the superstructure by decoupling the bridge deck from the input base excitation. The elastomer used in this study is natural

rubber, which is the main constituent of these isolators is sensitive to temperature and is found to stiffen under low temperatures (Murray & Detenber, 1961; Stevenson, 1986; Yakut, 2000; Yakut & Yura, 2002). As the temperature drops below zero, rubber undergoes two successive phases of stiffening called instantaneous thermal stiffening and crystallization. The former refers to a stage in which an immediate change in the stiffness of the elastomer occurs and the latter refers to a phase transition stage from an amorphous to a crystalline state after the elastomer was exposed to cold temperature for a sufficiently long time (Bukhina, Bukhina, & Kurlyand, 2007).

The effect of temperature on the lateral, vertical, and rotational response of SU-FREI is extensively scrutinized by Sciascetti and Tait (Sciascetti & Tait, 2019) by performing a set of experimental tests at subfreezing temperatures from -18°C to -37°C. It is demonstrated that while no delamination occurs between the fiber and elastomer layers, cold temperature lateral, vertical, and rotational stiffness of the FREI increases up to 6, 2.5, and 2.5 times those of room temperature, respectively. Moreover, the cold temperature has a negligible effect on the energy dissipation ratio in the vertical and rotational directions, whereas it can increase the lateral damping ratio up to 2.5 times that of room temperature (Figure 1-b).

4.2.4 Lateral resistance of soil

The ice matrix formed in the frozen soil has a significant impact on the stress-strain behavior of soil (Andersland & Ladanyi, 2003). In an early study, Tsytovich (Tsytovich, 1975) investigated the increase in the ultimate compression strength of a wide range of soil types, including quartz sand, silty sandy loam, and clay, subjected to freezing temperatures. Akili (Akili, 1971) scrutinized the subfreezing stress-strain behavior and strength of fine

soils (clay and clayey silt) where Sayles (Sayles, 1974) and Jones and Parameswaran (Jones & Parameswaran, 1983) focused on those of frozen Ottawa sand. The ultimate strength of remolded seasonally frozen silty soil and permafrost is investigated by Haynes and Karalius (Haynes & Karalius, 1977) and Zhu and Carbee (Zhu & Carbee, 1984). More recently, Shelman et al. (A. Shelman, Levings, & Sritharan, 2010) conducted an experimental study on five types of soil common to the state of Alaska to characterize the subfreezing mechanical properties for seismic design of foundations. Mechanical properties of undisturbed naturally frozen soil were explored by Yang et al. (Yang, Still, & Ge, 2015). Figure 4.1-c demonstrates the ultimate compressive strength of soil obtained from the conducted experiments on fine soil. The discrepancy between the curves is negligible.

In the context of Beam-on-Nonlinear-Winkler Foundation (BNWF) (Boulanger, Curras, Kutter, Wilson, & Abghari, 1999), lateral resistance of soil is typically demonstrated by p-y curves. Several p-y curves have been developed for modelling different soil types in warm weather conditions (Matlock, 1970; Reese, Cox, & Koop, 1974, 1975; Welch, 1972). However, limited p-y curves have been developed for cold wintry conditions based on field experiments on full-sized piles (Li & Yang, 2017). Crowther (Crowther, 1990) proposed characteristic parameters for developing p-y curves based on the shape of frozen soil stress-strain curves. Shelman (A. Shelman et al., 2010) developed a p-y model based on the experimental tests of different soil types including alluvial deposits, glacial till and clay. Yang (Yang et al., 2015) proposed parameters for constructing p-y curves of ice-rich frozen silt based on the results of an experimental test on the mechanical properties of natural

seasonally frozen silt. Various linear, quadratic, and exponential equations have been developed for estimating the unconfined compressive strength and undrained shear strength of the frozen soil. Since the upper layer of the underlying soil in this study is composed of 2.0 m. deep deposit of alluvium, the undrained shear strength is determined using a linear equation fitted over the results of the conducted test by Shelman (A. Shelman et al., 2010) over alluvial deposits. Using the obtained undrained shear strength and corresponding strain value (ε_{50}), the p-y curves are developed as shown in Figure 4.1-c. It should be pointed out that the frost penetration for the location of the bridge is 0.5-1.0 m. according to the contour maps shown in Figure 4.2 developed by Armstrong and Csathy (Armstrong & Csathy, 1963) based on the climatic data for southern Ontario.

4.3 Analytical modeling of the case study bridge

The bridge under investigation in this study is a highway bridge located in Ottawa, Canada. The bridge (constructed in 1969) is selected as a testbed for this study because it is representing about 42% of the bridges in the province of Ontario that are constructed prior to 1970 and are not designed in accordance with the modern ductile design requirements. Furthermore, the latest version of the National Building Code of Canada, NBCC 2015 (*National Building Code of Canada, 2015*, 2015), has updated the seismic hazard from seismic events with a 475-year return period to those with a 2475-year return period which underlines the need for reevaluation of the seismic performance of conventionally designed structures.

As shown in Figure 4.3, this bridge is a nine-span reinforced concrete bridge with an overall length of 236.0 m. supported by eight pairs of reinforced concrete columns and two seat-type abutments with no skewness.

The superstructure is composed of a nine-cell continuous post-tensioned cast-in-place voided slab rested on fixed pot bearings on top of the intermediate columns and end abutments. Therefore, it is assumed that the superstructure and columns are monolithically connected in the as-built configuration of the bridge to maximize the shear force demand on the columns. Alternatively, SU-FREI is designed according to the provisions of CHBDC (*Canadian Highway Bridge Design Code*, 2019) for bridge applications in a way that the average pressure of the isolator under both service and ultimate load does not exceed the code specified values. Additionally, the combined induced shear strain including compression, rotation, and shear is maintained at less than the code specified value of 5.5 (*Canadian Highway Bridge Design Code*, 2019). Meeting these requirements, an isolator comprised of eight natural rubber layers (six intermediate and two cover layers) with a hardness of 55 durometers, Shore A (*Standard Test Method for Rubber Property--Durometer Hardness*, 2005) is designed. The vertical stiffness of the SU-FREI is determined to be 274×10^6 kN/m using the following equation:

$$K_v = \frac{E_c \times A}{t_r} \tag{4.6}$$

where E_c, the compression modulus of the SU-FREI, is determined to be 102 MPa using the following relation

$$E_c = 96 \times G \times S^2 \times \left(2 + \frac{a}{b}\right)^2 \times \left[\sum_n \left[\frac{1}{\left(\alpha_1^2 + \beta_1^2\right) \times \left(2 + \frac{a}{b}\right)^2 + n^2 \times \pi^2} \times \frac{1}{n^2 \times \pi^2} \times \left(1 - \frac{\tanh\left(\lambda_1(n)\right)}{\lambda_1(n)}\right)\right]\right] \quad (4.7)$$

where α_1, β_1, and λ_1 are obtained from the following relations

$$\alpha_1 = \sqrt{\frac{24 \times G \times S^2 \times t}{E_f \times t_f}} \quad (4.8)$$

$$\beta_1 = \sqrt{\frac{12 \times G \times S^2}{K_{bulk}}} \quad (4.9)$$

$$\lambda_1(n) = \frac{\sqrt{\left(\alpha_1^2 + \beta_1^2\right) \times \left(2 + \frac{a}{b}\right)^2 + n^2 \times \pi^2}}{\frac{a}{b}} \quad n = 1, 3, ..., 99999 \quad (4.10)$$

Finally, the horizontal stiffness of the SU-FREI is determined to be 2.18×10^6 using the following equation

$$K_h = \frac{G \times A}{t_r} \quad (4.11)$$

All other parameters are defined in Table 4.2.

The substructure consists of eight circular reinforced concrete column pairs with a transverse center-to-center distance of 4.3 m., a diameter of 0.914 m., and unequal height with an average of 6.1 m. Columns are reinforced with 20 # 14 longitudinal steel rebars with a nominal diameter of 43 mm producing a longitudinal reinforcement ratio of 4.4%

confined with #5 spirals with a nominal diameter of 16 mm and a 50 mm pitch. It should be mentioned that in the absence of pier caps, the superstructure is directly rested on the columns.

The columns and end abutments are supported by reinforced concrete rectangular pile caps with a dimension of 7.0×2.75×1.2 m. and 11.0×5.1×0.75 m. for pier pile caps and abutment pile caps, respectively. Pile groups under intermediate piers are comprised of 20 HP 12×74 steel sections including four vertical piles in the middle, six longitudinally battered and 10 transversely battered perimeter piles whereas the pile groups under end abutments are composed of 23 piles including 13 vertical and 10 longitudinally battered piles as shown in Figure 4.3. The H-shaped steel pile sections are driven friction with a total length of 56.4 m.

The underlying soil domain is comprised of relatively thick deposits of sensitive marine clay, silt, and silty clay that were deposited within the Champlain sea basin (Chapman & Putnam, 1984). Geotechnical tests on the soil of the bridge site have demonstrated that the average shear wave velocity in the upper 30 m. of the subsurface stratigraphy is 127 m/s which corresponds to soil class E according to CHBDC site classification for the seismic response. The structural and mechanical properties of the bridge components are presented in Table 4.2.

4.3.1 Finite element modeling of bridge components

A detailed nonlinear 3-D finite element model of the case study bridge-isolator-pile-soil system is created in OpenSees (OpenSees, 2013). To this end, first, four previously

mentioned bridge cases are generated, independently. Investigating the seismic performance of these four counterparts shed light on the current performance of the bridge, the effectiveness of SU-FREI as a means of isolation system, the effect of considering Soil-Structure-Interaction (SSI) on the seismic performance of the bridge, and the seismic behavior of the bridge at subfreezing temperatures. The finite element model of the bridge is generated using the original construction drawings and is calibrated with previously performed experiments. The detailed information on the analytical modeling of the bridge components is provided, accordingly.

4.3.1.1 Superstructure

The superstructure is modeled using a spine-line method in which the deck is represented by a single line located at the centroid of the deck cross-section. This method outperforms the grillage method where the abutments are not skewed (Aviram, Mackie, & Stojadinović, 2008). Since the deck is expected to remain fully elastic during and after an earthquake, an *elasticBeamColumn* element with lumped translational and rotational masses is adopted. Following the recommendation by Aviram (Aviram et al., 2008) to discretize the frame elements to a minimum of five equally spaced elements, each deck span is divided into 10 equal segments.

4.3.1.2 SU-FREI

The proposed retrofit technique in this study is isolating the superstructure from the ground motion vibrations utilizing SU-FREI. This type of isolator exhibits a unique successive softening and stiffening regime under lateral displacements that makes it a viable alternative for conventional SREI. Under relatively small amplitudes where the top and

bottom faces of SU-FREI are in full contact with supports, SU-FREI demonstrates a linear behavior like SREI. Increasing the lateral displacements initiates rollover where the top and bottom faces start gradually to lose contact with supports. As a result of this decrease in the shear area, lateral shear stiffness of the isolator decreases resulting in a softening regime in the SU-FREI behavior. This softening continues up until the onset of full rollover where a complete loss of contact between the top and bottom faces of the isolator with supports occurs. Thereafter, initially vertical faces of the isolator reach full contact with the supports increasing in the shear area and stiffness, consequently. Osgooei et al. (Osgooei, Tait, & Konstantinidis, 2017) have developed a non-iterative rate-independent model that takes advantage of the available material libraries embedded in OpenSees. As shown in Figure 4.3, the Takeda-Elastic model is comprised of a Takeda-based bilinear plastic model (Takeda, Sozen, & Nielsen, 1970) in parallel with a nonlinear elastic spring model where the former considers the hysteresis aspect of the model and the latter dictates the softening and stiffening regimes. The shear forces accommodated by the Takeda-Elastic model can be presented using the following equations:

$$F_{TE} = k_1 u \qquad u < u_y \tag{4.12}$$

$$F_{TE} = k_1 u + k_2 \left(u - u_y\right) \qquad u > u_y \tag{4.13}$$

where k_1, k_2, u_y and u are initial stiffness, post-yield stiffness, yield displacement, and lateral displacement, respectively. The shear forces accommodated by the nonlinear elastic spring is represented using a fifth-order polynomial as follows:

$$F_{NES} = a_1 u + a_2 u^3 + a_3 u^5 \tag{4.14}$$

where a_i are the polynomial parameters. Finally, effective stiffness and damping of SU-FREI can be calculated by combining equations (4.12) to (4.14) as follows

$$\begin{aligned} K_{eff} &= k_1 + a_1 + a_2 u^2 + a_3 u^4 && u < u_y \\ K_{eff} &= [k_1 - k_2]\frac{u_y}{u} + k_2 + a_1 + a_2 u^2 + a_3 u^4 && u > u_y \end{aligned} \tag{4.15}$$

$$\beta_{eff} = \frac{1}{4\pi}\left[\frac{\left[k_1 u + k_2\left(u - u_y\right)\right] + 2\left[u - \dfrac{k_1 u + k_2\left(u - u_y\right)}{k_1}\right]}{K_{eff} u^2}\right] \tag{4.16}$$

The SU-FREI characteristic parameters (i.e. k_1, k_2, u_y, a_1, a_2, and a_3) are quantified utilizing a minimization technique (e.g. least square method) by minimizing the error between the effective stiffness and damping obtained from equations (4.15) and (4.16) and those obtained from the experimental tests. In this study, these characteristic parameters of the SU-FREI springs are calibrated using a set of experimental results obtained from a study by Sciascetti and Tait (Sciascetti & Tait, 2019) conducted on a set of quarter-scale SU-FREIs. The model parameters are then updated to match the SU-FREI designed specifically for this bridge. These parameters are used to implement the Takeda-Elastic model in OpenSees, where the Takeda and Nonlinear Elastic springs are represented using *Hysteretic* and *ElasticMultiLinear* materials, respectively. As shown in Figure 4.4, validation of the numerical model developed in OpenSees against the experimental data demonstrates that this model can readily simulate the lateral behavior of SU-FREI. The mechanical and geometrical properties of the designed SU-FREI are presented in Table 4.2 and the characteristic parameters are tabulated in Table 4.3.

To take the effect of subfreezing temperatures into account, the characteristic parameters need to be updated. To this end, two sets of intersecting equations that model the low-temperature behavior of full-scale SU-FREI are developed by Sciascetti (Sciascetti, 2017). These sets of equations are given as coefficients that are substituted into one of the following relations where equations (4.17) and (4.18) describe effects of instant thermal stiffening and crystallization, respectively. In these equations, P, T, and D are placeholders for each of the characteristic parameters, temperature, and day where coefficients a are presented in Table 4.3.

$$P_{\text{Temperature}} = a_{T_0} + a_{T_1} T \qquad -18^{\circ}\text{C} > T > -37^{\circ}\text{C} \tag{4.17}$$

$$P_{\text{Duration}} = a_{T_0} + a_{D_1} D \qquad 1\text{day} > D > 28\text{days} \tag{4.18}$$

4.3.1.3 Piers

3-D *nonlinearBeamColumn* elements have been used to capture any probable nonlinearity or damage in the columns under seismic actions. For this purpose, column sections have been discretized into fibers to represent the material's nonlinearity along the length and cross-section of the member. Each column is discretized into eight equal segments. The stress-strain behavior of confined and unconfined concrete is modeled using a linear tension softening model called *Concrete02* developed by Hisham and Yassin (Hisham & Yassin, 1994) where a uniaxial Giuffre-Menegotto-Pinto (Filippou, Bertero, & Popov, 1983) relationship with isotropic strain hardening called *steel02* is adopted for reinforcing rebars. The stress-strain constitutive models of concrete and steel are demonstrated in Figure 4.3.

4.3.1.4 Pile groups and soil domain

Supporting piles groups consist of HP 12×74 driven friction steel profiles with a total height of 0.31 m. and a total length of 56.4 m. Similar to columns, pile sections are modelled using a *nonlinearBeamColumn* element with spread plasticity to capture potential plastic hinge formations along the length of piles. The pile steel sections are discretized into fibers represented by *steel02* material in OpenSees characterized by uniaxial Giuffre-Menegotto-Pinto (Filippou et al., 1983) relationship with isotropic strain hardening constitutive model. Rigid frame elements are used to connect pile head nodes to column base nodes in modelling pile caps as inelastic behavior is not anticipated in foundations as per typical design provisions of bridge foundations (Ramadan, Mehanny, & Kotb, 2020).

The BNWF approach is deemed to be a computationally efficient technique for incorporating the SSI. In this context, a set of standard p-y, t-z, and q-z spring elements are developed to simulate soil lateral resistance, axial friction, and pile tip bearing, respectively. *PySimple1*, *TzSimple1*, and *QzSimple1* uniaxial materials in OpenSees are utilized to represent p-y, t-z, and q-z materials, respectively. According to an available geotechnical report for the bridge site, the underlying soil is determined to be a thick single layer of sensitive clay. Therefore, the corresponding backbone curves of the three mentioned soil springs are determined using the provisions of API (API, 2007). The lateral resistance of the individual piles are reduced to incorporate the effect of pile-pile interaction. While several methods have been developed for determining the reduction factor (P_m) for regularly-spaced rectangular pile groups (AASHTO, 2012; *Canadian Highway Bridge Design Code*, 2019; FEMA:P-751, 2012), none of them are applicable

herein since the configuration of the piles in the pile groups is neither symmetric nor rectangular. Therefore, an approach developed by Van Impe and Reese (Van Impe & Reese, 2010) is adopted by which the P_m factors are determined to be 0.81 and 0.84 for abutment pile groups in longitudinal and transverse directions, and 0.66 and 0.63 for pier pile groups in longitudinal and transverse directions, respectively. The mechanical properties of piles and the surrounding soil are presented in Table 4.2.

4.3.1.5 Abutments

The seat-type abutments of the case study bridge are simulated using a complex spring model proposed by Mackie and Stojadinovic (Mackie & Stojadinovic, 2006). As shown in Figure 4.3, this model is composed of a set of zero-length springs connected to the abutment nodes representing, the pounding between deck and abutment, and mobilized abutment backfill soil. In this system, superstructure forces are transmitted to the SU-FREI and supporting abutment, accordingly, which triggers the backfill soil resistance after the deck lateral displacements exceed the gap between the deck and abutment. Pounding between deck and abutment is implemented in OpenSees using an *ImpactMaterial* proposed by Muthukumar and DesRoches (Muthukumar & DesRoches, 2006) that simulates the pounding using a bilinear Hertz contact element. The backfill soil resistance is modeled using a backfill stiffness model developed by Shamsabadi et al. (Shamsabadi, Rollins, & Kapuskar, 2007) and implemented in OpenSees using a *HyperbolicGap* material.

4.4 IDA-based seismic fragility analysis

To assess the seismic fragility of the case study bridge components under a vast range of earthquake intensities, an IDA was carried out in the longitudinal and transverse directions of the bridge axis, independently. The independence stems from the lack of an available bidirectional model for SU-FREI and the complicated nature of three-dimensional wave propagation. Therefore, it is assumed that the bridge must be able to equally resist the seismic input excitations from all possible directions (Aviram et al., 2008). A set of monotonically increasing ground motion records are applied to the bridge, peak component responses are recorded, IDA curves and percentiles are determined, and the prescribed performance criteria are applied to develop the fragility curves. The Intensity Measure (IM) used herein for scaling ground motion records is the spectral acceleration at the fundamental period of the bridge, $S_a(T_1)$, and the monitored Engineering Demand Parameters (EDP) are pile cap displacements under piers and abutments, column drift, and backfill soil deformation is active and passive actions.

A deaggregation analysis is carried out for the bridge site to determine the contribution of events to the seismic hazard. As a result, Seismic hazard, mean magnitude (M_w), and mean distance for the fundamental period of the bridge (T_1 = 1.0 sec.) are determined to be 0.125g, 6.9, and 63 km for a 2% in 50 years probability of exceedance and soil class C. However, the available records of real ground motions in eastern Canada are not sufficient and using synthetic records is inevitable (Siqueira, Sanda, Paultre, & Padgett, 2014; Tavares, Padgett, & Paultre, 2012). Therefore, a suite of 10 synthetic accelerograms developed by Atkinson (Atkinson, 2009) is adopted in accordance with the given

magnitude and site to source distance. It should be noted that according to a geotechnical report for a nearby site, the shear wave velocity for the upper 30 m. of the soil layer beneath the bridge is approximately 127 m/s that corresponds to soil class E and the soil is not liquefiable. Therefore, the response spectrum is updated to match NBCC (*National Building Code of Canada*, 2015) where the spectral acceleration for the fundamental period of the retrofitted bridge, S_a (T_1 = 1.0 sec.) is 0.24g.

The prescriptive damage states (DS) in this study are adopted from HAZUS-MH (FEMA, 2003) by which the qualitative damage states for the bridge structure are divided into four states, namely, slight, moderate, extensive, and collapse as presented in Table 4.4. These qualitative DS have been translated into quantitative measures by different researchers described by means of a median value for damage S_c, and its corresponding logarithmic standard deviation β_c. As presented in Table 4.5, various EDPs have been considered in this study. Damage to columns is quantified by monitoring the column drift. Due to the relatively large longitudinal reinforcing ratio and low spiral pitch, a quantitative DS for seismically designed columns is adopted according to a study by Dutta and Mander (Dutta & Mander, 1998). For backfill soil deformation in active, passive, and transverse directions, Nielson (Nielson, 2005) has proposed different DS using a combination of available damage states and survey-based results being updated using a Bayesian updating approach. Abutment and pier pile cap DS are adopted from a study by Aygun (Aygün, Dueñas-Osorio, Padgett, & DesRoches, 2010). It is worth mentioning that SU-FREI will not experience damage under excessive shear strains up to 250% according to the experimental tests performed by different researchers (Al-Anany, Van Engelen, & Tait,

2017; Losanno, Sierra, Spizzuoco, Marulanda, & Thomson, 2019; Russo, Pauletta, & Cortesia, 2013).

Finally, seismic fragility defined as the conditional probability of a structural system or its comprising components reaching or exceeding a certain DS for a given IM is expressed as

$$F = P\left(DS \mid IM = y\right) \tag{4.19}$$

where y is a given intensity of IM. The component-level fragilities can be expressed using the following relations where a lognormal distribution is assumed for the damage states and the seismic demand

$$P\left[DS \mid IM\right] = \Phi\left[\frac{\ln \frac{S_D}{S_C}}{\sqrt{\beta_{D|IM}^2 + \beta_C^2}}\right] \tag{4.20}$$

where Φ is the standard normal cumulative function. S_D and $\beta_{D|IM}$ are the median and logarithmic standard deviation of seismic demand, respectively. Similarly, S_C and β_C are the median and logarithmic standard deviation of the component capacity, respectively.

4.5 Low-temperature effect on the seismic fragility of bridges

This section describes the seismic fragility estimates of the four previously defined bridge cases. For brevity, bridge types are denoted by IS, MS, IF, and MF, standing for Isolation+SSI, Monolithic+SSI, Isolation+Fixed-base, and Monolithic+Fixed-base, respectively. As presented in Table 4.5, six damage states are defined for different bridge components in longitudinal direction, namely, column drift, abutment soil failure in active and passive action, pile foundation failure for piers and abutments and deck unseating.

However, results showed that pier pile caps do not undergo any damage in the IS and MS cases due to the high lateral strength of soil in low temperatures as a result of the formation of an ice matrix. This desirable behavior is even more prominent in the IS bridge where the seismic isolation system effectively mitigates the seismic demand on the pier pile caps. Similarly, deck unseating did not occur even at relatively high earthquake intensities. Therefore, fragility parameters of pier pile caps and unseating are not presented here. In the same fashion, abutment and pier pile caps and deck unseating are deemed not to be a concern in the transverse direction of the bridge at subfreezing temperatures and their fragility estimates are neglected. Seismic fragility curves of the bridge components in longitudinal and transverse directions are depicted in Figure 4.5-8.

4.5.1 Column drift

As shown in Figure 4.5, the probability of damage (lower tail) to columns of the IS bridge (both longitudinal and transverse directions) at room temperature is higher than that of subfreezing temperatures at all damage states except for 21 and 28 days of exposition to -37°C at slight and moderate damage states. This behavior is in compliance with a study by Cardone and Gesualdi (Cardone & Gesualdi, 2012) where it is shown that thermal crystallization has a lower impact on the lateral stiffness of isolators at larger shear strains. In the absence of the isolation system in the MS bridge (Figure 4.6), it is observed that by stiffening the columns and their supporting soil as a result of temperature drop, the damage potential of columns decreases for both orthogonal directions. For example, probability of slight damage in the transverse direction is 13% and 3% for room and subfreezing temperatures, respectively. In the absence of the soil domain for the case of the IF bridge

in Figure 4.7, it is shown that the adverse impact of subfreezing temperatures on the probability of damage to columns is more severe in longitudinal directions with respect to the transverse direction. This observation implies that unlike the bridges that are located on soft soil, subfreezing temperature increases the seismic demand on the columns of bridges located on hard rock or stiff soil. The fragility curves of the MF bridge in Figure 4.8 demonstrate that these bridges are not sensitive to subfreezing temperatures because the only source of stiffening in these bridges are the reinforced concrete columns. For relatively smaller earthquake amplitudes (slight and moderate damage states), it is shown that subfreezing temperature reduces the damage potential of columns in both orthogonal directions whereas for larger amplitudes (moderate and collapse damage states) the probability of damage has increased, in part.

Comparing the medians of damage in Figure 4.9 – a depicts that the MF bridge has the lowest median of damage for all damage states. This can be attributed to the monolithic connection of deck and columns, which maximizes the deformation demand on the columns and makes this component more vulnerable. Introducing the isolation system to the fixed-base bridge has improved the median of damage by reducing shear forces in the columns. As the temperature drops from -10°C to -37°C and maintains this temperature for up to 28 days, the median of damage decreases for slight and moderate damage states and increases for extensive and collapse. In the presence of the soil domain (i.e. for IS and MS bridge cases), the median of damage to the columns of the MS bridge has increased by decreasing the temperature as a result of the stiffening of the underlying soil along with concrete and steel bars. Similar to the IF bridge, the median of slight and moderate damage

of the MS bridge decreased whereas it is increased for extensive damage and collapse. While isolated bridges were expected to demonstrate higher dispersion in their structural response due to the introduction of a highly nonlinear component (e.g. SU-FREI), Figure 4.9 – b exhibits that fixed-base bridges have higher dispersion in the column drift over the entire subfreezing temperature range. This relatively larger dispersion is due to the larger transferred shear forces from the superstructure for monolithic bridges that caused nonlinear behavior of the columns to a larger extent. It should be pointed out that subfreezing temperature reduces the dispersion in the structural response, particularly for higher damage states.

Figure 4.10-a demonstrates that monolithic bridges (MS and MF) exhibit a smaller median of damage for all damage states in the transverse direction due to the absence of an isolation system. As shown in this figure, the IF bridge has a smaller median of damage with respect to the IS bridge, which highlights the desirable behavior of bridge columns even for a bridge that is supported by soft soil. Like the longitudinal direction, the dispersion in the column response decreases with decreasing temperature.

4.5.2 Abutment soil failure in active action

Retrofitting bridges using isolation systems results in an increase in the damage potential of abutments due to excessive lateral deck displacements. Figure 4.5 to Figure 4.8 reveal that the IF bridge has the largest probability of damage within a range of 100%-40% for slight to extensive damage states whereas the MF bridge exhibits the smallest probabilities of damage within 48% to 1.6% that accentuates the presence of the isolation system in increasing the probability of damage to abutments. Moreover, it is demonstrated that for

all bridge cases, decreasing the temperature from room temperature to -37°C results in decreasing the probability of damage to abutments due to excessive active deformation. Figure 4.9-a demonstrates that the monolithic bridges have the highest median of damage to abutments over all subfreezing temperatures. This can be attributed to the monolithic deck-column connection that prevents the deck from excessive displacements. Figure 4.9-b shows that abutment backfill deformation in active action has the highest dispersion with respect to other bridge components which leads to a higher probability of damage. Moreover, it is shown that subfreezing temperatures have a negligible impact on the dispersion of the active soil deformation at end abutments.

4.5.3 Abutment soil failure in passive action

Investigating Figure 4.5 to Figure 4.8 reveals that subfreezing temperature has a larger impact on the probability of damage to abutments of the bridges supported by soil domain (e.g. IS and MS). For the IS bridge the probability of slight and moderate damage is decreased from 17.6% and 1.8% to zero whereas for the IF bridge, these probabilities decrease from 80% and 7.5% to 9% and 0.1%, respectively. As shown in Figure 4.9-a, IF, MF, MS, and IS bridges have the least median of damage within the entire temperature rage, respectively. Moreover, where the fixed-base bridges deemed to be relatively insensitive to cold temperatures, IS and MS bridge exhibit an increase in their median of damage as temperature drops from room temperature to -37°C. It should be pointed out that damage to the abutments due to active and passive actions is not of concern since these damages are mostly cosmetic and will not cause any traffic disruption. It is shown in Figure 4.9-b that the dispersion in the response is also insensitive to temperature change.

4.5.4 Abutment soil failure in transverse action

Figure 4.5 to Figure 4.8 demonstrate that subfreezing temperature has a desirable impact on the probability of damage to abutments particularly for the MS bridge where the probabilities of slight, moderate, and extensive damage has been reduced from 83%, 36%, and 17% at room temperature to zero at subfreezing temperatures. Moreover, abutments of the IF bridge are most fragile in room temperature with damage probabilities within 94% to 31% for slight to extensive damage states, whereas the MF bridge is most fragile at cold temperatures with damage probabilities within 67% to 5.3% at -37°C and 28 days. At subfreezing temperatures, the IS and MS bridges will not experience moderate and extensive damage and for temperatures under -18°C. This is due to the fact that supporting soil under the bridge stiffens exponentially at cold temperatures and prevents abutment from excessive deformations. Figure 4.10 demonstrates that while the MF and IF bridges are almost insensitive to cold temperatures, the IS and MS bridges experience a monotonic increase in their median of damage for slight damage state. Moreover, the dispersion in the response of abutment is almost independent of the temperature.

4.5.5 Pile foundation failure at abutments

As shown in Figure 4.5 and Figure 4.6, using SU-FREI for isolating the superstructure at room temperature has decreased the probability of damage to abutment pile caps by 14%, 21%, and 4% for slight, moderate and extensive damage states, respectively, and increased the probability of collapse by 17%. At relatively small or intermediate lateral displacements, there may be minor, if any, pounding between the superstructure and end abutments resulting in lower induced forces in abutment pile caps. By increasing the

earthquake intensity, this pounding is severe and abutment pile caps experience larger displacements and accelerations. As the temperature drops below subfreezing ranges, the ice matrix formed in the soil domain increases the lateral stiffness of the soil resulting in a lower probability of damage at all damage states.

As Figure 4.9 demonstrates, the medians of damage to abutment pile caps are monotonically increasing by decreasing the temperature. This monotonic behavior is due to monotonic increase in the concrete, reinforcing steel, and the soil domain, independent of the duration of exposure to cold temperatures. While the IS bridge exhibits a similar fashion, it is shown that the effect of crystallization in the SU-FREI plays an important role in the seismic response of abutment pile caps. Similar to the dispersion of column drift fragilities, the MS bridge exhibited larger dispersion in the seismic response of abutment pile caps due to the highly nonlinear response of the soil domain as a result of deck excessive deformations.

4.6 Low-temperature effect on the seismic response of bridges

4.6.1 SU-FREI shear strain

As mentioned previously, SU-FREI does not exhibit any damage for shear strains up to 250%. While there is not a consensus on the effectiveness of isolation system for retrofitting bridges located on soft soil, Figure 4.11-a reveals that incorporating the SSI can mitigate the seismic demand on the isolation system (i.e. SU-FREI) for both room and subfreezing temperatures which complies with findings of Fosoul and Tait (Fosoul & Tait, 2021). Moreover, it is demonstrated that the isolator barely reaches 250% shear strain and the assumption of no damage is valid. Additionally, Figure 4.11-a shows that for a certain

intensity level, it is less likely for the SU-FREI in the transverse direction to experience larger shear strains with respect to the longitudinal direction. As shown in Figure 4.11-b, the hysteretic behavior of SU-FREI for room and subfreezing temperatures demonstrates that as temperature decreases, the effective stiffness and damping of SU-FREI increases.

4.6.2 Displacement, velocity, and acceleration of bridge deck

Figure 4.12 to Figure 4.15 demonstrate bridge response histories in longitudinal direction at MCE level. As expected, isolated bridges exhibit larger deck displacements with respect to monolithic bridges, which is in accordance with findings of Fosoul and Tait (Fosoul & Tait). As the temperature drops below subfreezing, the deck displacements of the IS, MS, IF, and MF bridges decreases from 0.09m, 0.03m, 0.09m, and 0.03m for room temperature to 0.03m, 0.01m, 0.02m, and 0.03m, respectively, for -37°C. It is also shown that the presence of soil domain mitigates the lateral displacement of the superstructure that accordingly leads to less damage to supporting columns and end abutments.

While incorporating the effect of SSI at subfreezing temperatures resulted in a decrease in deck velocity, deck velocity of fixed-base bridges is observed to be less sensitive to cold temperatures. The velocity of the MS and MF bridge decks are almost independent of the subfreezing temperatures. On the other hand, the deck velocity of isolated bridges decreases up to -37°C where an increase is observed as a consequence of increasing the duration of conditioning from 1 to 28 days.

The absolute acceleration of the bridge deck is a function of the induced inertial forces due to seismic excitation. While the isolation system aims to mitigate the bridge deck

acceleration, it is shown that the deck of the IS bridge experiences accelerations up to 1.37g, 1.72g, and 1.27g for room temperature, -10°C, and -37°C, respectively. These relatively high accelerations are due to the pounding between the deck and abutments at the time of 6.5 seconds of the earthquake. It is shown that the deck absolute acceleration of the MF bridge is independent of subfreezing temperatures whereas the MS bridge exhibits a mild decrease in the deck acceleration at -37°C.

4.6.3 Base shear and moment in columns

Retrofitting bridges with seismic isolation systems is perceived to be an effective technique for reducing base shear and moments in bridge columns. However, it is of high importance to evaluate the effectiveness of isolation systems in subfreezing temperatures where their lateral stiffnesses are subject to increase. Figure 4.12 to Figure 4.15 demonstrate the column base shear and moments for room and cold temperatures. A comparison between the IS and MF bridges reveals that using SU-FREI as a retrofit technique along with the incorporation of SSI leads to a decrease in both base shear and moment of columns within a range of 88%-98%. Additionally, it is shown that isolating the superstructure using SU-FREI can effectively mitigate the base shear and moment at all subfreezing temperatures whereas the base shear response histories of monolithic bridges are less sensitive to subfreezing temperatures.

4.6.4 Pounding and backfill soil

Figure 4.16 depicts pounding and backfill soil response histories of the IS bridge for room temperature, -10°C, and -18°C. At room temperature, the bridge deck impacts the east and

west abutments three times during the earthquake resulting in considerable energy dissipation and triggering the soil embankment to resist excessive lateral displacements. Although the deck impacts the abutments at -10°C and -18°C, the induced displacement is not sufficiently large to trigger the backfill soil resistance. As temperature decreases from -26°C to -37°C, the stiffened SU-FREI prevents the deck from impacting the end abutments resulting in lower deck accelerations.

4.7 Conclusion

This study evaluates the seismic performance of four bridge cases located in Ottawa, Ontario, namely, a fixed-base monolithic bridge, a fixed-base retrofitted bridge isolated with SU-FREI, a monolithic bridge supported by the underlying soil, and a retrofitted bridge using SU-FREI supported by the underlying soil. Seismic fragility estimates of different bridge components along with response histories of critical bridge components are presented in room and subfreezing conditions. Subfreezing mechanical behavior of constitutive material of bridge components including concrete, reinforcing steel, rubber, and soil is simulated and an IDA is conducted using 10 synthetic ground motion records developed specifically for eastern Canada. Based on the numerical analysis, the following conclusions are drawn:

- The isolation system effectively mitigates the damage potential of columns and pier foundations by altering the load transfer mechanism from columns to end abutments. Accordingly, soil deformation in active, transverse and passive actions are observed to be fragile components. A comparison of pile-supported bridges

reveals that the isolated bridge exhibited less damage to columns and pier pile caps and larger damage to the end abutments and their supporting pile groups. This failure mechanism is deemed to be favorable since it does not disrupt the traffic flow and retains the bridge functionality.

- Extremely low temperature has an adverse effect on the seismic fragility estimates of the bridge columns due to brittle behavior of concrete. Increased stiffness of the underlying soil prevents the pier and abutment pile caps from inordinately large lateral displacements, particularly for seismically isolated bridges where less shear force is transferred to the pile caps.
- It is shown that neglecting SSI results in an immense overestimation of base shear and moment in both summer and winter conditions. By decreasing the temperature from room to -37°C, all bridge components stiffen resulting in a decrease in deck displacement, an increase in deck acceleration, and an increase in column base shear and moment.
- Even at extremely cold temperatures (e.g. -37°C) and long durations of exposure (e.g. 28 days), SU-FREI demonstrates an acceptable behavior in terms of its experienced shear strain and its effectiveness in preventing critical bridge components (e.g. columns, pier and abutment pile caps) from damage. From the results obtained from the systems investigated in this study, it can be concluded that the cold temperature provisions developed by AASHTO are conservative and bridges can still demonstrate acceptable performance under large earthquakes.

4.8 Acknowledgments

The authors would like to express their gratitude for the financial support provided by the Ministry of Transportation Ontario (MTO) through the Highway Infrastructure Innovation Funding Program (HIIFP) and the Natural Sciences and Engineering Research Council (NSERC).

References

A. S. Fosoul, S., & Tait, M. (2021). *Seismic fragility assessment of isolated bridges in cold regions: A case study for eastern Canada*. Paper presented at the 17th World Conference on earthquake Engineering, Sendai, Japan.

AASHTO. (2012). American Association of State Highway and Transportation Officials. *Washington, DC*.

Akili, W. (1971). Stress-strain behavior of frozen fine-grained soils. *Highway Research Record*(360).

Al-Anany, Y., Van Engelen, N., & Tait, M. (2017). Vertical and Lateral Behavior of Unbonded Fiber-Reinforced Elastomeric Isolators. *Journal of Composites for Construction, 21*(5), 04017019.

Andersland, O. B., & Ladanyi, B. (2003). *Frozen ground engineering*: John Wiley & Sons.

API. (2007). American petroleum institute recommended practice for planning, designing and constructing fixed offshore platforms—working stress design. *American Petroleum Institute, Washington Google Scholar*.

Armstrong, M. D., & Csathy, T. I. (1963). Frost design practice in canada-and discussion. *Highway Research Record*(33).

Atkinson, G. M. (2009). Earthquake time histories compatible with the 2005 National building code of Canada uniform hazard spectrum. *Canadian Journal of Civil Engineering, 36*(6), 991-1000.

Aviram, A., Mackie, K. R., & Stojadinović, B. (2008). *Guidelines for nonlinear analysis of bridge structures in California*: Pacific Earthquake Engineering Research Center.

Aygün, B., Dueñas-Osorio, L., Padgett, J. E., & DesRoches, R. (2010). Efficient longitudinal seismic fragility assessment of a multispan continuous steel bridge on liquefiable soils. *Journal of Bridge Engineering, 16*(1), 93-107.

Bandini, P. A. C., Siqueira, G. H., Padgett, J. E., & Paultre, P. (2022). Seismic Performance Assessment of a Retrofitted Bridge with Natural Rubber Isolators in Cold Weather Environments Using Fragility Surfaces. *Journal of Bridge Engineering, 27*(6), 04022040. doi:doi:10.1061/(ASCE)BE.1943-5592.0001873

Billah, A. H. M. M., & Todorov, B. (2019). Effects of subfreezing temperature on the seismic response of lead rubber bearing isolated bridge. *Soil Dynamics and Earthquake Engineering, 126*, 105814. doi:https://doi.org/10.1016/j.soildyn.2019.105814

Boulanger, R. W., Curras, C. J., Kutter, B. L., Wilson, D. W., & Abghari, A. (1999). Seismic soil-pile-structure interaction experiments and analyses. *Journal of geotechnical and geoenvironmental engineering, 125*(9), 750-759.

Browne, R., & Bamforth, P. (1981). *The use of concrete for cryogenic storage: A summary of research, past, and present.* Paper presented at the Proc., 1st Int. Conf. on Cryogenic Concrete.

Bukhina, M. F., Bukhina, M. a. F., & Kurlyand, S. K. (2007). *Low-temperature behaviour of elastomers* (Vol. 31): Brill.

Canadian Highway Bridge Design Code. (2019). Canadian Standard Association.

Cardone, D., & Gesualdi, G. (2012). Experimental evaluation of the mechanical behavior of elastomeric materials for seismic applications at different air temperatures. *International Journal of Mechanical Sciences, 64*(1), 127-143.

Chapman, L., & Putnam, D. (1984). The Physiography of Southern Ontario, Ontario Geological Survey Special. *Queen's Printer, Toronto, Ontario, 270*.

Crowther, G. S. (1990). Analysis of laterally loaded piles embedded in layered frozen soil. *Journal of Geotechnical Engineering, 116*(7), 1137-1152.

Deng, P., Gan, Z., Hayashikawa, T., & Matsumoto, T. (2020). Seismic response of highway viaducts equipped with lead-rubber bearings under low temperature. *Engineering Structures, 209*, 110008. doi:https://doi.org/10.1016/j.engstruct.2019.110008

Dutta, A., & Mander, J. (1998). *Seismic fragility analysis of highway bridges.* Paper presented at the Proceedings of the INCEDE-MCEER center-to-center project workshop on earthquake engineering Frontiers in transportation systems.

FEMA. (2003). Multi-hazard loss estimation methodology, earthquake model *Washington, DC, USA: Federal Emergency Management Agency*.

FEMA:P-751. (2012). NEHRP Recommended Seismic Provisions: Design Examples: FEMA P-751: Washington, DC.

Filiatrault, A., & Holleran, M. (2001). *Characteristics of reinforced concrete bridge components under seismic strain rates and low temperatures.* Paper presented at the Proc., 18th US–Japan Bridge Engineering Workshop.

Filiatrault, A., & Holleran, M. (2001). Stress-strain behavior of reinforcing steel and concrete under seismic strain rates and low temperatures. *Materials and Structures, 34*(4), 235-239. doi:10.1007/BF02480594

Filippou, F. C., Bertero, V. V., & Popov, E. P. (1983). Effects of bond deterioration on hysteretic behavior of reinforced concrete joints.

Fosoul, S. A. S., & Tait, M. J. Seismic Performance Assessment of An Existing Multi-span Bridge in Eastern Canada Retrofitted with Fiber Reinforced Elastomeric Isolator. *Canadian Journal of Civil Engineering, In press*. doi:10.1139/cjce-2021-0344

Fosoul, S. A. S., & Tait, M. J. (2021). Soil-pile-structure interaction effects on seismic demands and fragility estimates of a typical Ontario highway bridge retrofitted with fiber reinforced elastomeric isolator. *Soil Dynamics and Earthquake Engineering, 151*, 106967. doi:https://doi.org/10.1016/j.soildyn.2021.106967

Goto, Y., & Miura, T. (1979). Experimental studies on properties of concrete cooled to about minus 160 C. *Technology Reports, 44*(2), 357-385.

Guay, L.-P., & Bouaanani, N. (2016). Assessment of low temperature exposure for design and evaluation of elastomeric bridge bearings and seismic isolators in Canada. *Canadian Journal of Civil Engineering, 43*(9), 851-863.

Haynes, F. D., & Karalius, J. A. (1977). *Effect of temperature on the strength of frozen silt*. Retrieved from

Hisham, M., & Yassin, M. (1994). Nonlinear analysis of prestressed concrete structures under monotonic and cycling loads. *University of California, Berkeley. Ph. D. thesis*.

Jones, S., & Parameswaran, V. (1983). *Deformation behavior of frozen sand-ice materials under triaxial compression.* Paper presented at the Fourth International Conference on Permafrost, Fairbanks, Alaska.

Lee, G. C., Shih, T. S., & Chang, K. C. (1988a). Mechanical Properties of Concrete at Low Temperature. *Journal of Cold Regions Engineering, 2*(1), 13-24. doi:doi:10.1061/(ASCE)0887-381X(1988)2:1(13)

Lee, G. C., Shih, T. S., & Chang, K. C. (1988b). Mechanical Properties of High Strength Concrete at Low Temperature. *Journal of Cold Regions Engineering, 2*(4), 169-178. doi:doi:10.1061/(ASCE)0887-381X(1988)2:4(169)

Li, Q., & Yang, Z. (2017). P–Y approach for laterally loaded piles in frozen silt. *Journal of geotechnical and geoenvironmental engineering, 143*(5), 04017001.

Losanno, D., Sierra, I. E. M., Spizzuoco, M., Marulanda, J., & Thomson, P. (2019). Experimental assessment and analytical modeling of novel fiber-reinforced isolators in unbounded configuration. *Composite Structures, 212*, 66-82.

Mackie, K., & Stojadinovic, B. (2006). *Seismic vulnerability of typical multiple-span California highway bridges.* Paper presented at the Fifth National Seismic Conference on Bridges & Highways Multidisciplinary Center for Earthquake

Engineering ResearchCalifornia Department of Transportation Federal Highway Administration Transportation Research Board.

Manuel, E., & Jaime, P. Measurement of Tensile Strength of Concrete at Very Low Temperatures. *ACI Journal Proceedings, 79*(3). doi:10.14359/10898

Matlock, H. (1970). Correlations for design of laterally loaded piles in soft clay. *Offshore Technology in Civil Engineering Hall of Fame Papers from the Early Years*, 77-94.

Montejo, L. A. (2008). Seismic behavior of reinforced concrete bridge columns at sub-freezing temperatures.

Montejo, L. A., Sloan, J. E., Kowalsky, M. J., & Hassan, T. (2008). Cyclic Response of Reinforced Concrete Members at Low Temperatures. *Journal of Cold Regions Engineering, 22*(3), 79-102. doi:doi:10.1061/(ASCE)0887-381X(2008)22:3(79)

Murray, R., & Detenber, J. (1961). First and second order transitions in neoprene. *Rubber chemistry and technology, 34*(2), 668-685.

Muthukumar, S., & DesRoches, R. (2006). A Hertz contact model with non-linear damping for pounding simulation. *Earthquake Engineering & Structural Dynamics, 35*(7), 811-828.

Nassar, M., Guizani, L., Nollet, M.-J., & Tahan, A. (2019). A probability-based reliability assessment approach of seismic base-isolated bridges in cold regions. *Engineering Structures, 197*, 109353. doi:https://doi.org/10.1016/j.engstruct.2019.109353

Nassar, M., Guizani, L., Nollet, M.-J., & Tahan, A. (2022). Effects of temperature, analysis and modelling uncertainties on the reliability of base-isolated bridges in Eastern Canada. *Structures*, *37*, 295-304. doi:https://doi.org/10.1016/j.istruc.2022.01.023

National Building Code of Canada. (2015). National Research Council of Canada.

National Building Code of Canada, 2015. (2015).

Nielson, B. G. (2005). *Analytical fragility curves for highway bridges in moderate seismic zones*. Georgia Institute of Technology.

Okada, T., & Iguro, M. (1978). Bending behaviour of prestressed concrete beams under low temperature. *J. Jpn. Prestressed Concr. Eng. Assoc*, *208*, 15-17.

OpenSees. (2013). Open system for earthquake engineering simulation: Pacific Earthquake Engineering Research Center, University of California Berkeley, CA.

Osgooei, P. M., Tait, M. J., & Konstantinidis, D. (2017). Non-iterative computational model for fiber-reinforced elastomeric isolators. *Engineering Structures*, *137*, 245-255.

Ramadan, O. M., Mehanny, S. S., & Kotb, A. A.-M. (2020). Assessment of seismic vulnerability of continuous bridges considering soil-structure interaction and wave passage effects. *Engineering Structures*, *206*, 110161.

Reese, L. C., Cox, W. R., & Koop, F. D. (1974). *Analysis of laterally loaded piles in sand.* Paper presented at the Offshore Technology Conference.

Reese, L. C., Cox, W. R., & Koop, F. D. (1975). *Field testing and analysis of laterally loaded piles in stiff clay.* Paper presented at the Offshore technology conference.

Rostásy, F. S., & Pusch, U. (1987). Strength and deformation of lightweight concrete of variable moisture content at very low temperatures. *International Journal of Cement Composites and Lightweight Concrete, 9*(1), 3-17. doi:https://doi.org/10.1016/0262-5075(87)90033-9

Russo, G., Pauletta, M., & Cortesia, A. (2013). A study on experimental shear behavior of fiber-reinforced elastomeric isolators with various fiber layouts, elastomers and aging conditions. *Engineering Structures, 52*, 422-433.

Sayles, F. H. (1974). *Triaxial constant strain rate tests and triaxial creep tests on frozen Ottawa sand*: Corps of Engineers, US Army Cold Regions Research and Engineering Laboratory.

Sciascetti, A. (2017). *The Effect of Temperature on Unbonded Fiber-Reinforced Elastomeric Isolators.*

Sciascetti, A., & Tait, M. (2019). Effect of Temperature on the Response of Unbonded Fiber-Reinforced Elastomeric Isolators. *Journal of Structural Engineering, 145*(11), 04019124. doi:doi:10.1061/(ASCE)ST.1943-541X.0002401

Sehnal, Z., Kronen, H., & Marshall, A. (1983). *Factors influencing the low temperature strength of concrete.* Paper presented at the Proceedings 2 nd international conference on cryogenic concrete, Amsterdam.

Shamsabadi, A., Rollins, K. M., & Kapuskar, M. (2007). Nonlinear soil–abutment–bridge structure interaction for seismic performance-based design. *Journal of geotechnical and geoenvironmental engineering, 133*(6), 707-720.

Shelman, A., Levings, J., & Sritharan, S. (2010). Seismic design of deep bridge pier foundations in seasonally frozen ground.

Shelman, A. T. (2013). Advancing the seismic design of reinforced concrete bridge columns.

Sho Yamane, H. K., & Toru, O. Properties of Concrete at Very Low Temperatures. *ACI Symposium Publication, 55*. doi:10.14359/6615

Siqueira, G. H., Sanda, A. S., Paultre, P., & Padgett, J. E. (2014). Fragility curves for isolated bridges in eastern Canada using experimental results. *Engineering Structures*, *74*, 311-324.

Sleigh, G. (1981). *'The Behaviour of Steel at Low Temperatures.* Paper presented at the Proceedings of the 1st International Conference on Cryogenic Concrete, Construction Press, Newcastle upon Tyne, UK, 167.

Sloan, J. E. (2005). The seismic behavior of reinforced concrete members at low temperatures.

Sritharan, S., Suleiman, M. T., & White, D. J. (2007). Effects of seasonal freezing on bridge column–foundation–soil interaction and their implications. *Earthquake Spectra*, *23*(1), 199-222.

Standard Test Method for Rubber Property--Durometer Hardness. (2005). American Society for Testing Materials.

Stevenson, A. (1986). *Low Temperature Stiffening of Structural Rubber Bearings.* Paper presented at the Proceedings of the International Rubber Conference.

Suleiman, M. T., Sritharan, S., & White, D. J. (2006). Cyclic Lateral Load Response of Bridge Column-Foundation-Soil Systems in Freezing Conditions. *Journal of Structural Engineering, 132*(11), 1745-1754. doi:doi:10.1061/(ASCE)0733-9445(2006)132:11(1745)

Takeda, T., Sozen, M. A., & Nielsen, N. N. (1970). Reinforced concrete response to simulated earthquakes. *Journal of the Structural Division, 96*(12), 2557-2573.

Tavares, D. H., Padgett, J. E., & Paultre, P. (2012). Fragility curves of typical as-built highway bridges in eastern Canada. *Engineering Structures, 40*, 107-118.

Tsytovich, N. A. (1975). *Mechanics of frozen ground*: Scripta Book Co.

Van Impe, W. F., & Reese, L. C. (2010). *Single piles and pile groups under lateral loading*: CRC press.

Welch, R. C. (1972). *Lateral load behavior of drilled shafts*: The University of Texas at Austin.

Whiteley, J., Armstrong, B., & Welburn, R. (1982). Reinforcing and prestressing steels for cryogenic applications. *Cryogenic Concrete*, 252-279.

Yakut, A. (2000). *Performance of elastomeric bridge bearings at low temperatures.* Citeseer.

Yakut, A., & Yura, J. A. (2002). Evaluation of elastomeric bearing performance at low temperatures. *Journal of Structural Engineering, 128*(8), 995-1002.

Yang, Z. J., Dutta, U., Zhu, D., Marx, E., & Biswas, N. (2007). Seasonal Frost Effects on the Soil-Foundation-Structure Interaction System. *Journal of Cold Regions Engineering, 21*(4), 108-120. doi:doi:10.1061/(ASCE)0887-381X(2007)21:4(108)

Yang, Z. J., Still, B., & Ge, X. (2015). Mechanical properties of seasonally frozen and permafrost soils at high strain rate. *Cold regions science and technology*, *113*, 12-19.

Zhu, Y., & Carbee, D. L. (1984). Uniaxial compressive strength of frozen silt under constant deformation rates. *Cold regions science and technology*, *9*(1), 3-15.

Table 4.1. Cold temperature analysis matrix

Temp/duration	1 day	3 day	7 day	14 day	21 day	28 day
-37°C	Ottawa				AASHTO	AASHTO
-26°C	Ottawa			AASHTO		
-18°C		Ottawa	AASHTO			
-10°C				Ottawa		

Table 4.2. Mechanical properties of bridge components

Component	Material model	Details
Deck	3D nonlinear beam-column element	Total length = 236 m Maximum thickness = 0.91 m Concrete compressive strength, f_{ck} = 35 MPa Mass density, ρ = 2400 kg/m^3 Cross sectional area, A = 6 m^2 Moment of inertia along the y-axis, I_y = 51 m^4 Moment of inertia along the z-axis, I_z = 0.4 m^4
Isolator	A non-iterative rate-independent *Takeda-Elastic* model	Width, a = 850 mm Length, 2b = 850 mm Rubber thickness (cover layer) = 5 mm Rubber thickness (intermediate layer) = 43.16 mm Reinforcement fiber thickness = 0.51 mm Total rubber thickness, t_r = 269 mm Total fiber thickness, t_f = 3.57 mm Total height of bearing, h = 272.5 mm
Pier	3D fiber-section forced-based beam-column element with nonlinear fiber materials	Diameter = 0.91 m Cover = 76.2 mm Yield strength, $f_y = 2.75\times10^5$ kPa Young's modulus, $E_s = 2\times10^8$ kPa Strain hardening ratio, b = 0.01
Piles	3D fiber-section forced-based beam-column element with nonlinear fiber materials	Modulus of elasticity, $E_p = 2\times10^8$ kPa Cross-sectional area, A = 0.0141 m^2 Depth, d = 0.308 m Width, w = 0.31 m Moment of inertia along the x-axis, $I_x = 23.7\times10^7$ mm^4 Moment of inertia along the y-axis, $I_y = 7.74\times10^7$ mm^4
Pile-soil interface	BNWF nonlinear springs	Undrained cohesion (top) = 30 kN/m^2 Undrained cohesion (bottom) = 80 kN/m^2 Unit weight, γ = 15.2 kN/m^3

Table 4.3. Characteristic parameters of the Pivot-Elastic model with intercept and slope coefficients for low-temperature equations

Parameter	Room value	Temperature		Duration	
		a_{T0}	a_{T1}	a_{D0}	a_{D1}
Bilinear Takeda					
K_1 (N/m)	6727	-15719.2	-1359.6	33345.2	924.8
K_2 (N/m)	557	210.5	-5.2×10^{-1}	240.1	-10.9
u_y (m)	0.0087	8.3×10^{-1}	3.7×10^{-3}	6.5×10^{-1}	2.8×10^{-2}
Nonlinear Elastic Spring					
a_1 (N/m)	2043.4	814.3	6.1	557.8	27.5
a_3 (N/m^3)	-50.1	-4.8×10^{-2}	-1×10^{-3}	-6.1×10^{-3}	-5.5×10^{-3}
a_5 (N/m^5)	1.61×10^{-8}	1.4×10^{-6}	-1.2×10^{-3}	1.2×10^{-6}	2.6×10^{-7}

Table 4.4. Qualitative description of damage states

Damage state	Description of the damage state
None	No damage to the bridge
Minor/Slight	Minor cracking or spalling of concrete in the abutments, hinges, columns (superficial damage), or minor cracking to the deck
Moderate	Any column experiencing moderate cracking (shear cracks) and spalling (column structurally still sound), moderate movement of the abutment (<50 mm), keeper bar failure without unseating,
Major/Extensive	Any column degrading without collapse (column structurally unsafe), significant residual displacement at connections, vertical offset of the abutment
Complete/Collapse	Any column collapsing which may result in immediate deck collapse or tilting of the substructure due to foundation failure

Table 4.5. Quantitative description of damage states

Failure mode	Corresponding bridge component	Slight		Moderate		Extensive		Collapse		Reference
		S_c	β_c	S_c	β_c	S_c	β_c	S_c	β_c	
Column failure	Drift (%)	1	0.25	2.5	0.25	5	0.46	7.5	0.46	(Dutta & Mander, 1998)
Abutment soil failure in passive action	Abutment soil deformation (mm)	37	0.46	146	0.46	N/A*	N/A*	N/A*	N/A*	(Nielson, 2005)
Abutment soil failure in active action	Abutment soil deformation (mm)	9.8	0.7	37.9	0.9	77.2	0.85	N/A*	N/A*	(Nielson, 2005)
Abutment soil failure in transverse action	Abutment soil deformation (mm)	9.8	0.7	37.9	0.9	77.2	0.85	N/A*	N/A*	(Nielson, 2005)
Pile foundation failure at abutments	Pile cap displacement (mm)	20	0.4	38	0.4	60	0.4	80	0.4	(Aygün, Dueñas-Osorio, Padgett, & DesRoches, 2010)
Pile foundation failure at piers	Pile cap displacement (mm)	28	0.4	42	0.4	86	0.4	115	0.4	(Aygün et al., 2010)
Unseating of the deck at abutment	Displacement of the deck relative to the abutment (m)	N/A	N/A	N/A	N/A	N/A	N/A	1.37	0	-

* Padgett and DesRoches determined that severe damage to abutments does not essentially result in a global collapse (Padgett & DesRoches, 2007)

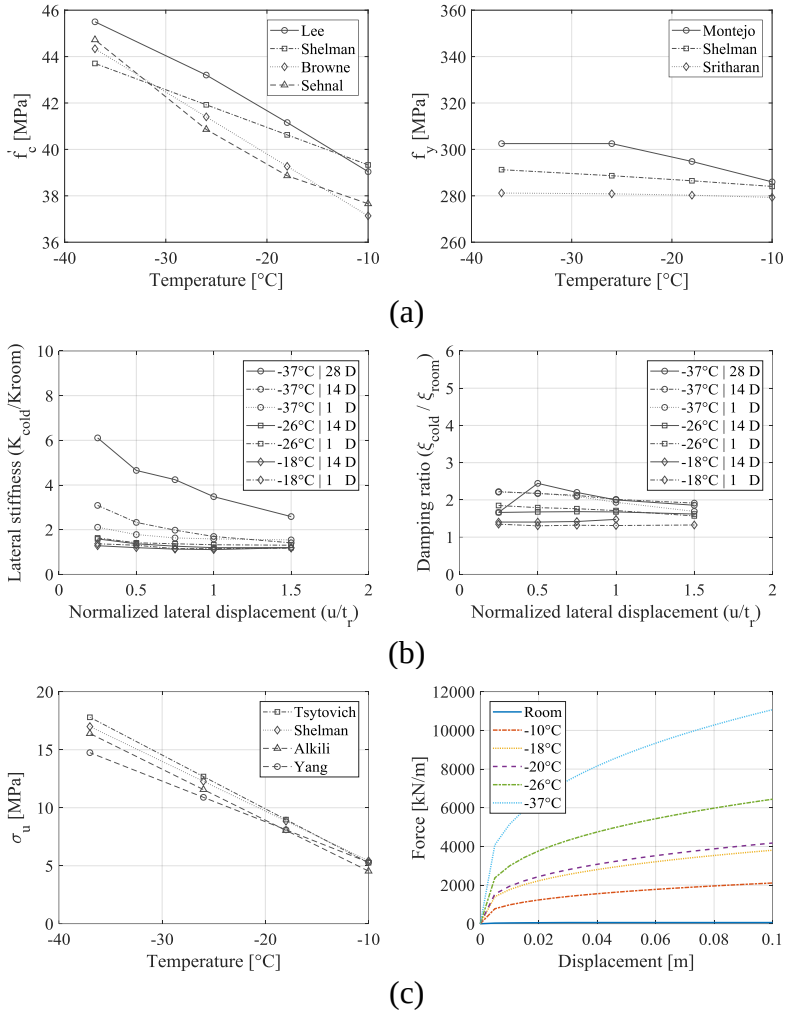

Figure 4.1. Cold temperature behavior of (a) concrete and reinforcing steel, (b) SU-FREI, and (c) Supporting soil in lateral direction (p-y spring)

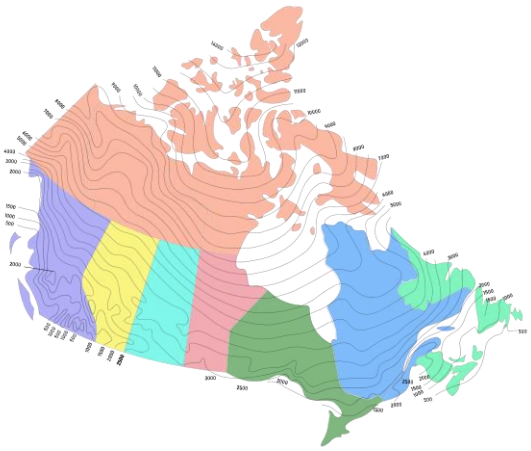

Figure 4.2. Freezing indexes in Canada

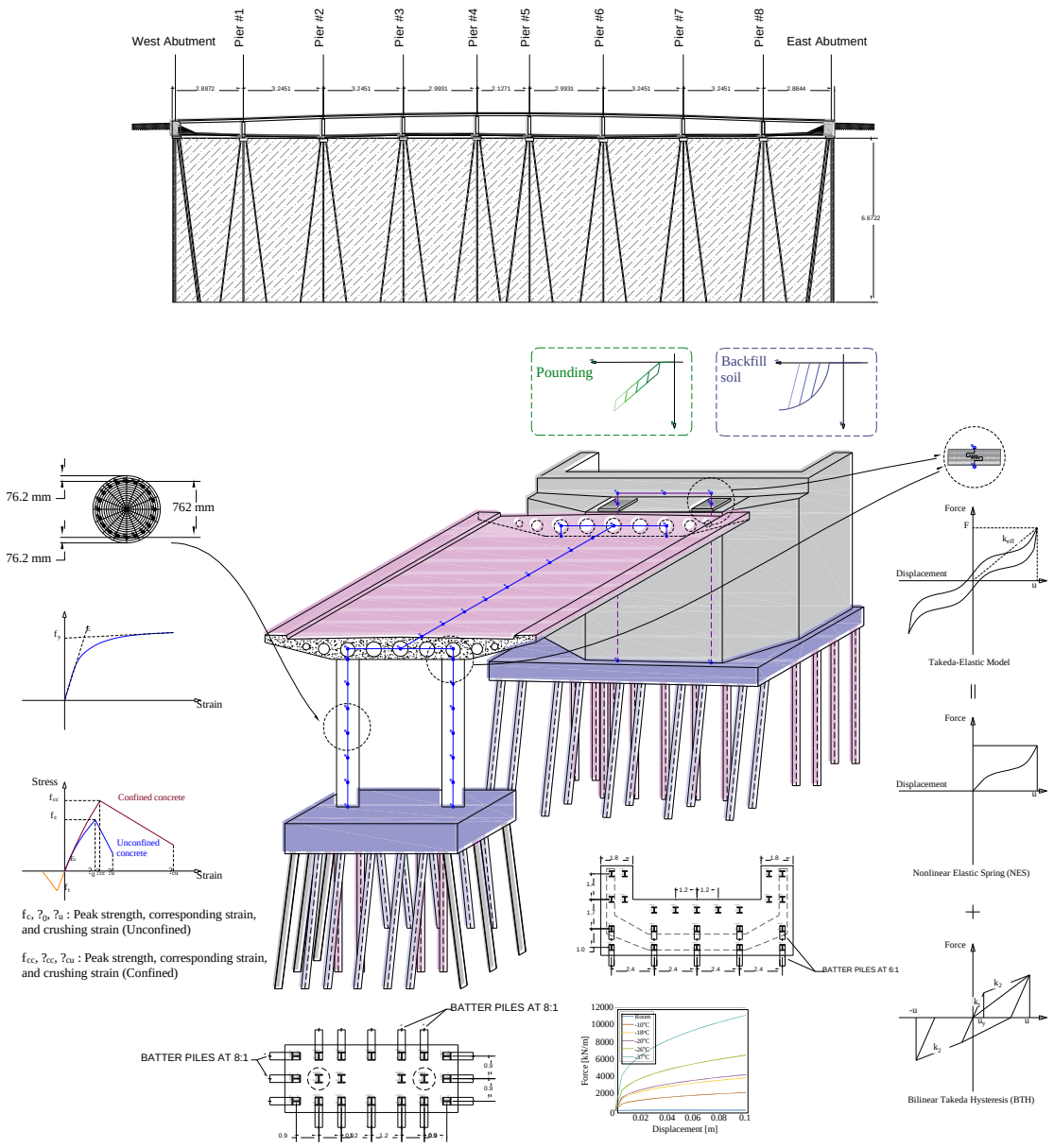

Figure 4.3. Elevation and isometric view of piers, abutments, and the supporting pile group, schematic illustration of lateral load-displacement behavior of Takeda Elastic model (Osgooei, Tait, & Konstantinidis, 2017), and characteristic parameters of the column fiber section

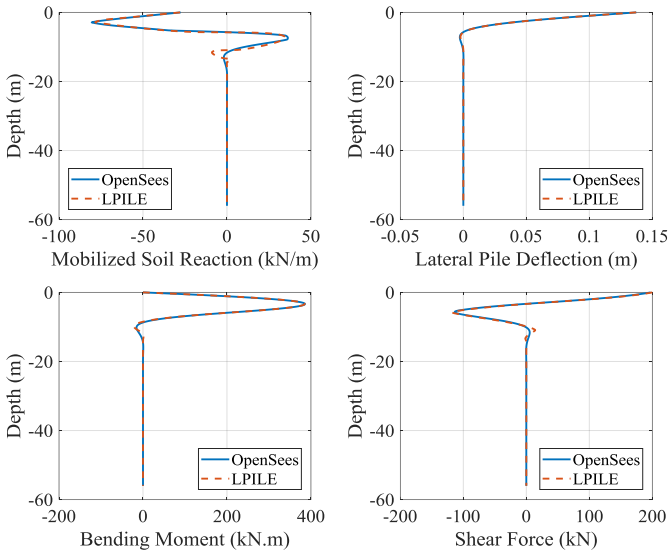

(a)

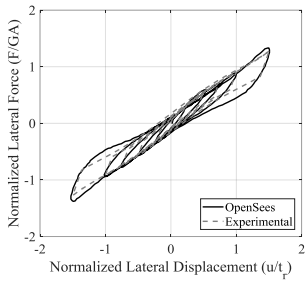

(b)

Figure 4.4. Validation of (a) lateral behavior of a single vertical pile (A. S. Fosoul & Tait, 2021) and (b) SU-FREI (Sciascetti, 2017)

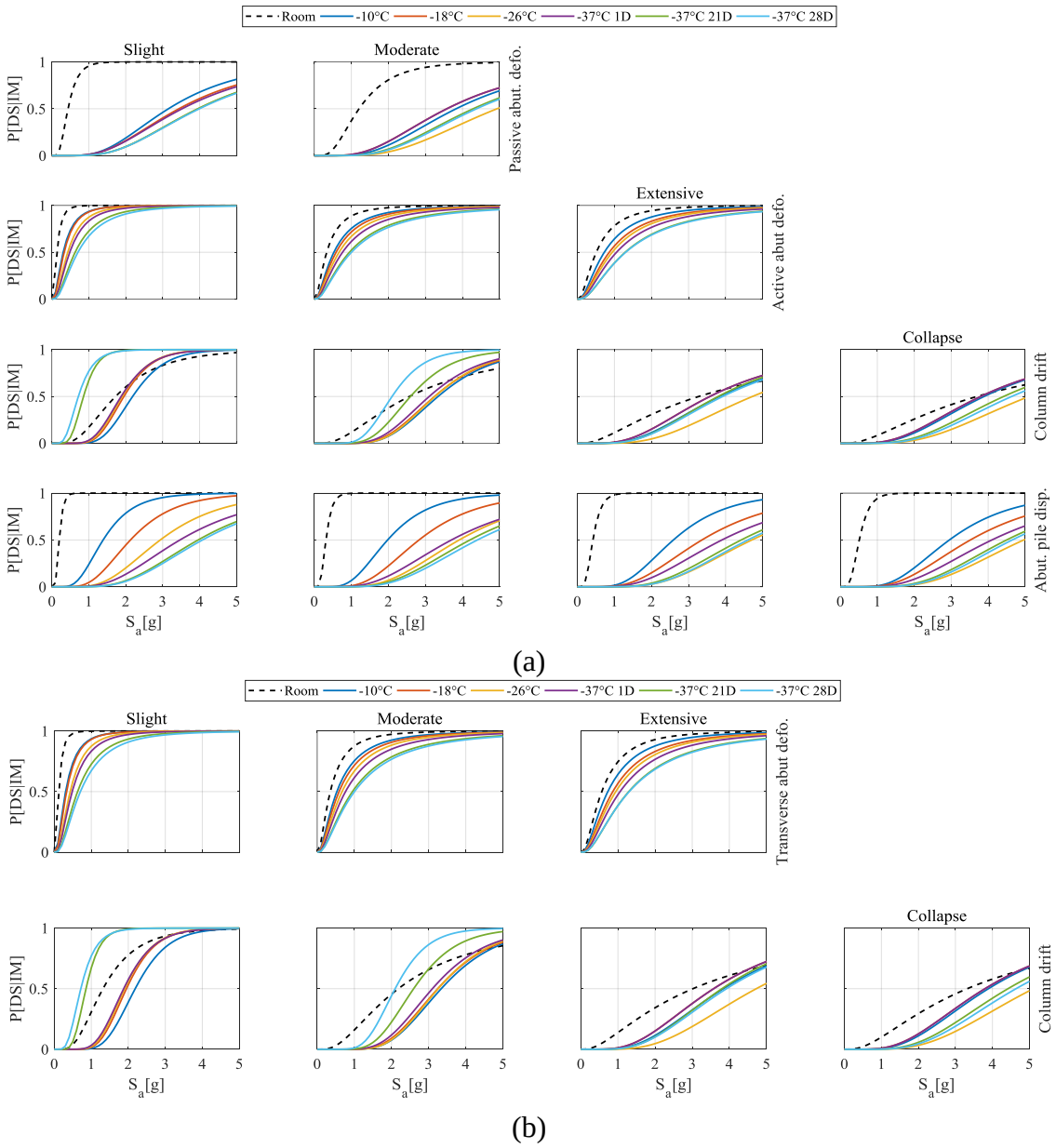

Figure 4.5. Component fragility curves of IS bridge for (a) longitudinal and (b) transverse direction

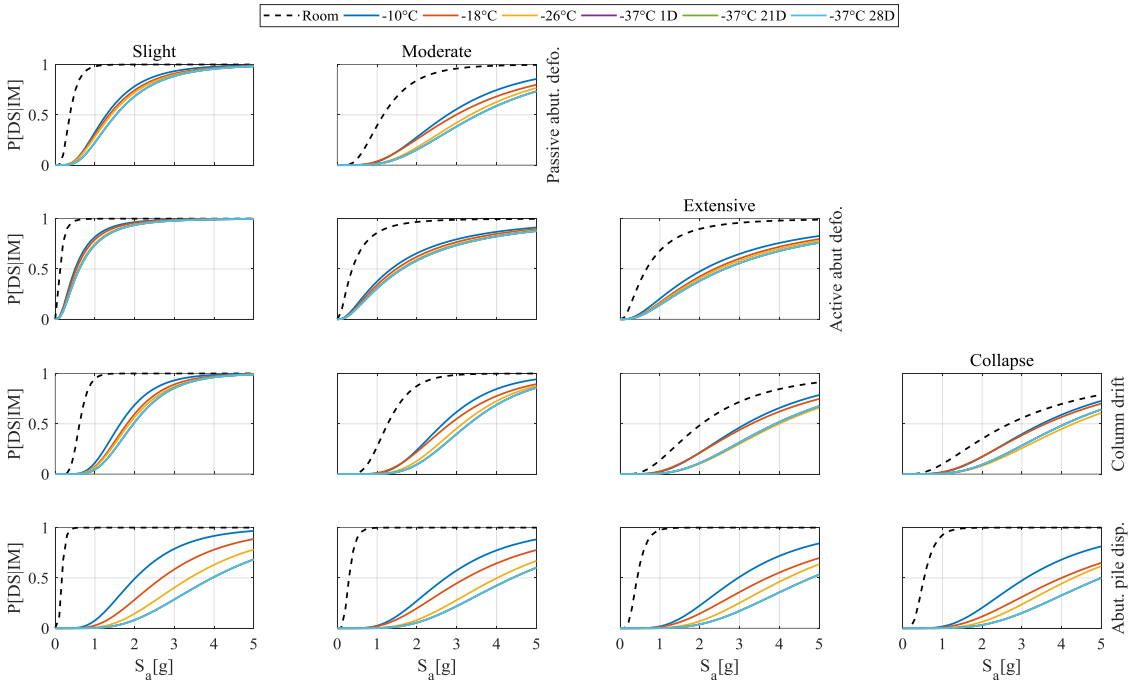

(a)

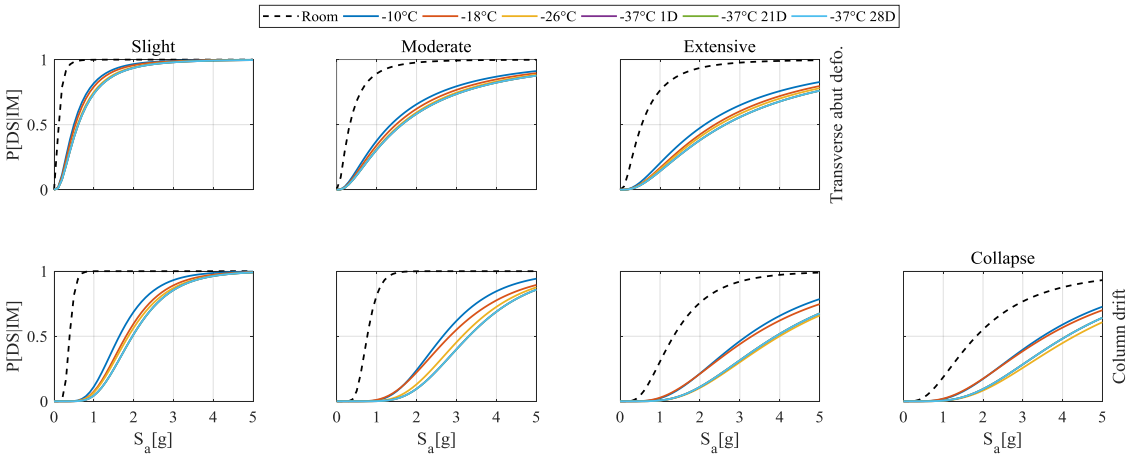

(b)

Figure 4.6. Component fragility curves of MS bridge for (a) longitudinal and (b) transverse direction

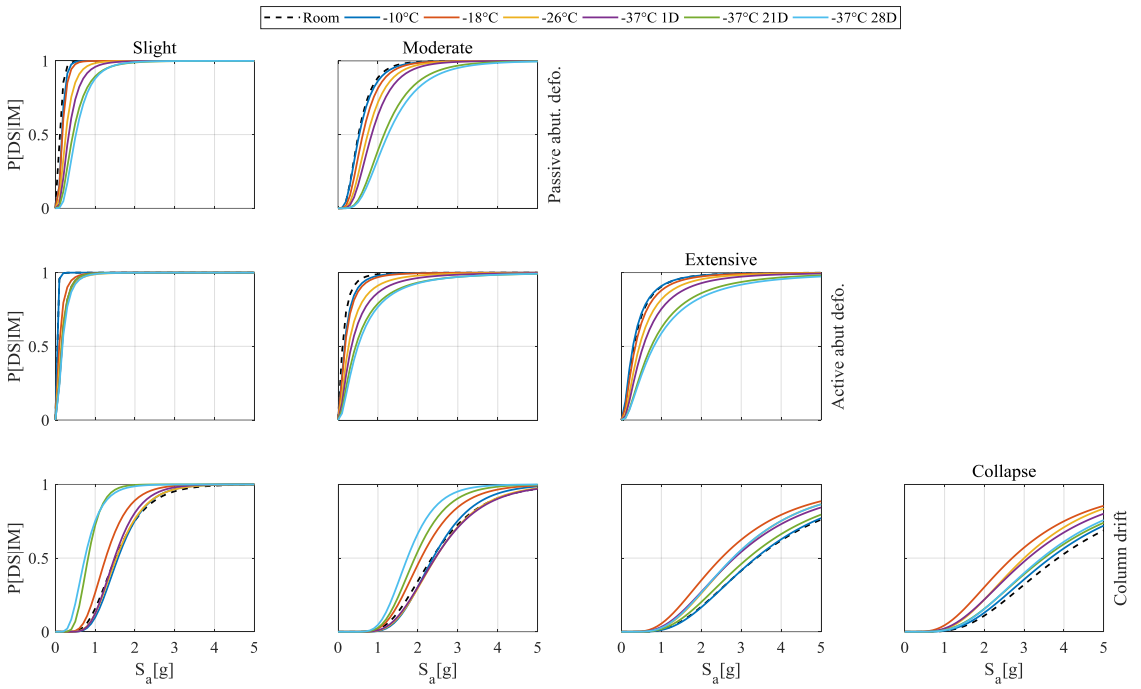

(a)

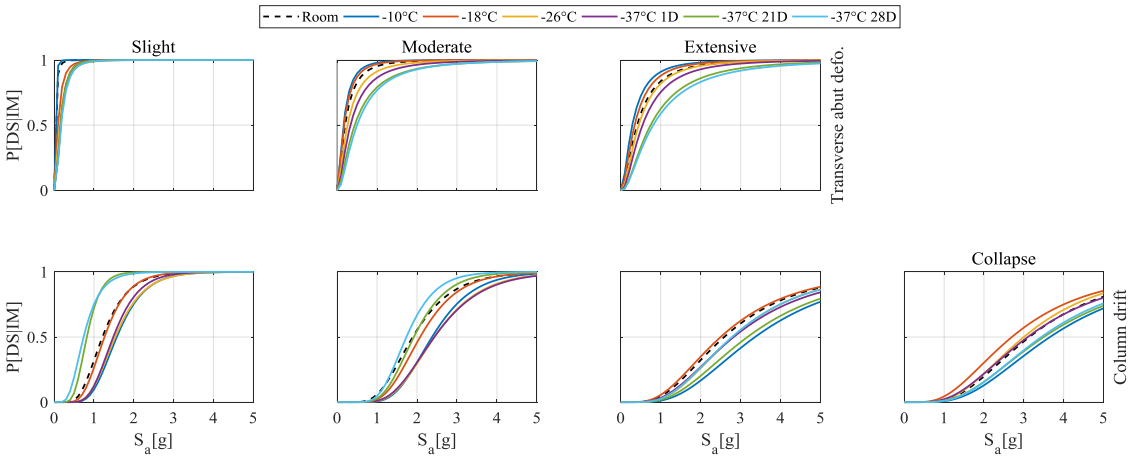

(b)

Figure 4.7. Component fragility curves of IF bridge for (a) longitudinal and (b) transverse direction

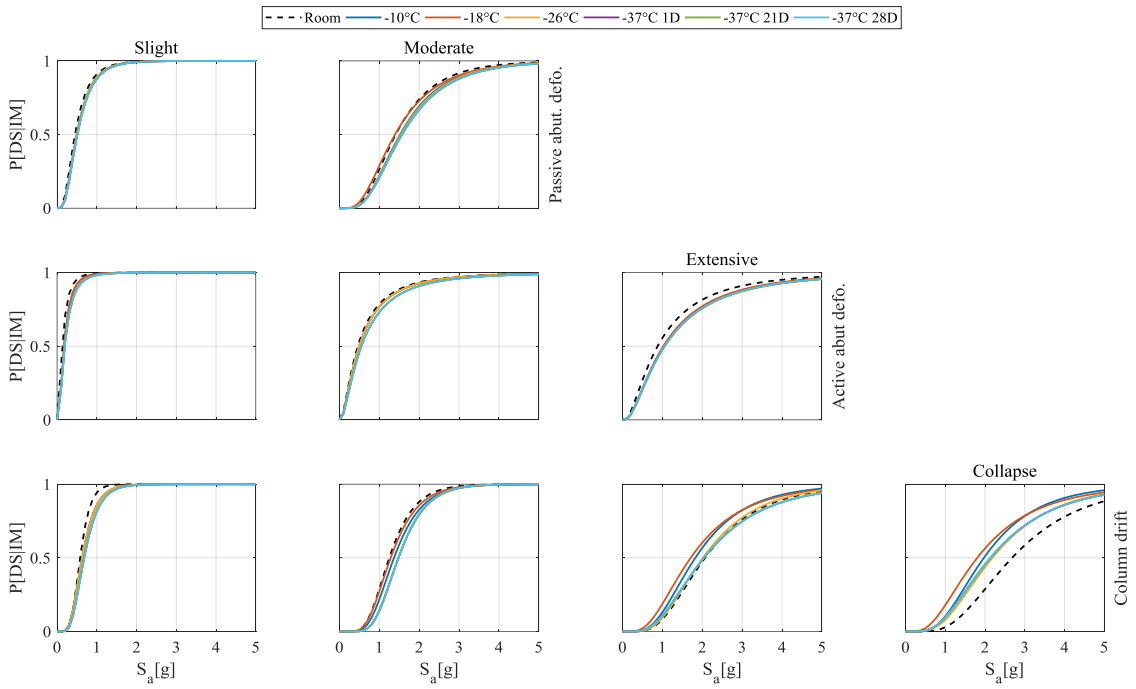

(a)

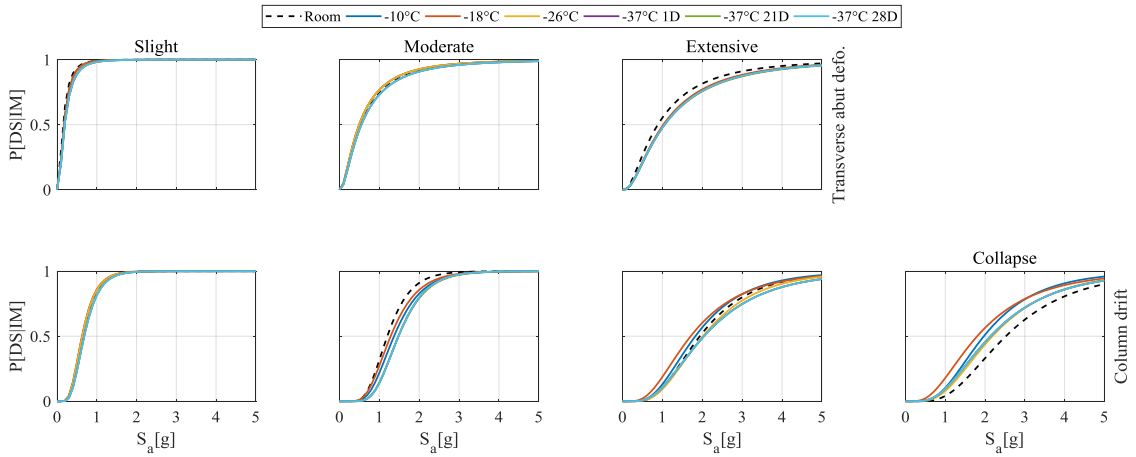

(b)

Figure 4.8. Component fragility curves of MF bridge for (a) longitudinal and (b) transverse direction

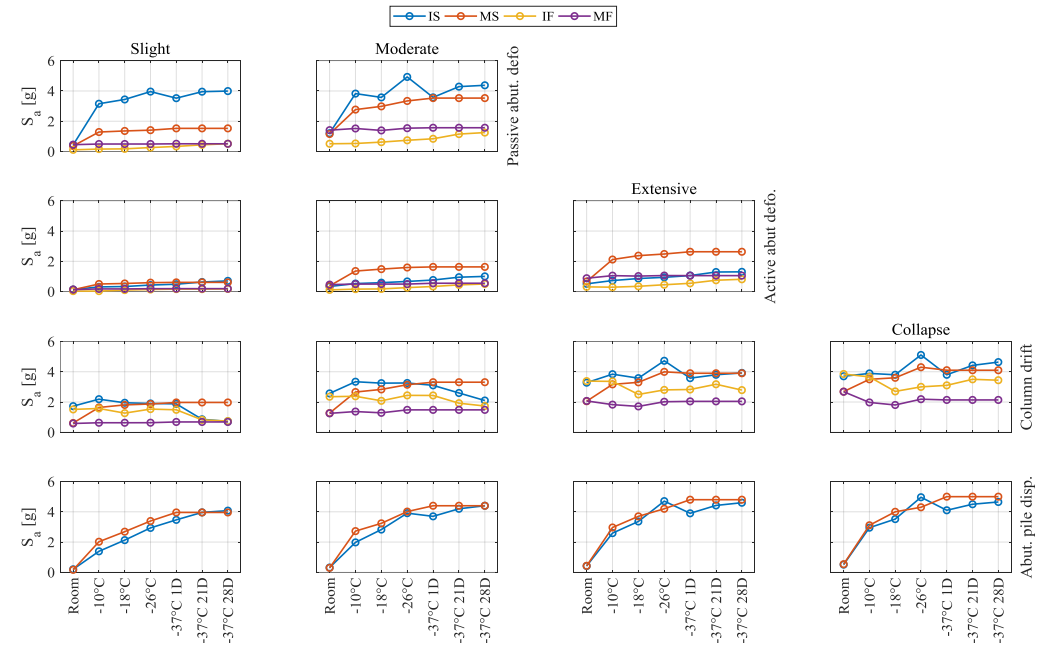

(a)

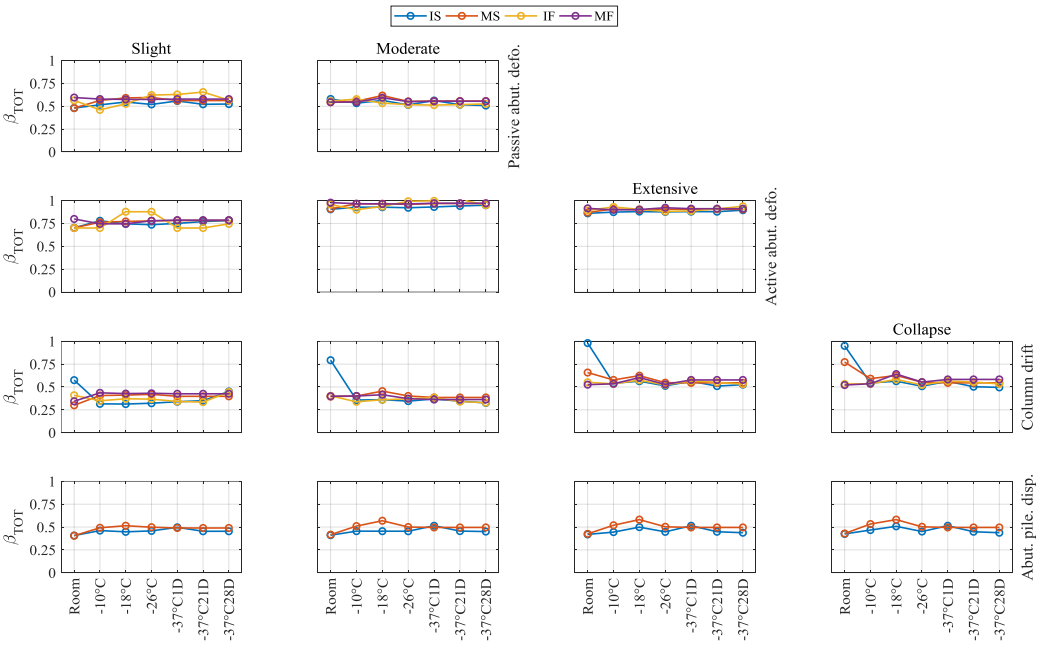

(b)

Figure 4.9. (a) Median of damage and (b) dispersion in longitudinal direction

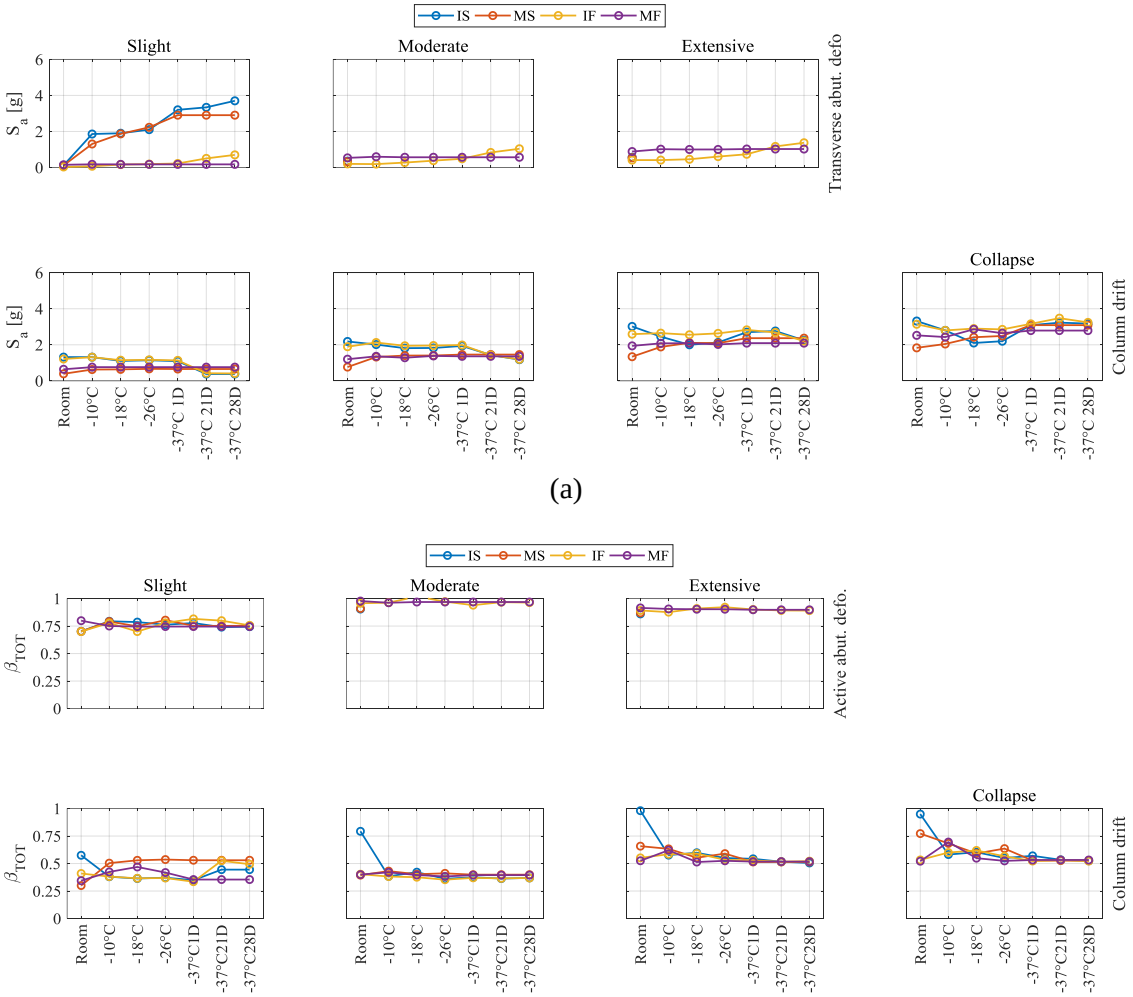

(a)

(b)

Figure 4.10. (a) Median of damage and (b) dispersion in transverse direction

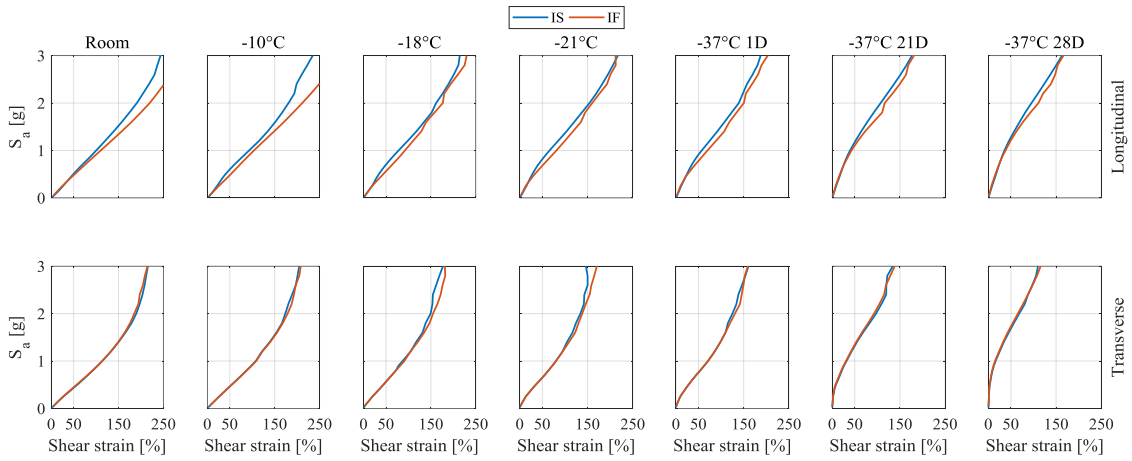

(a)

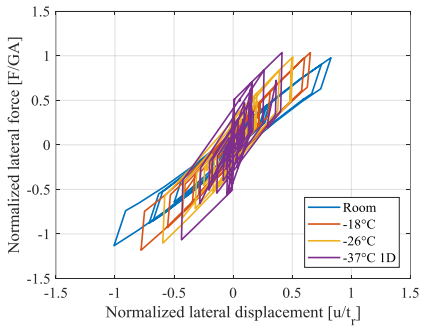

(b)

Figure 4.11. (a) Median response of FREI and (b) Hysteresis behavior of FREI under subfreezing temperatures

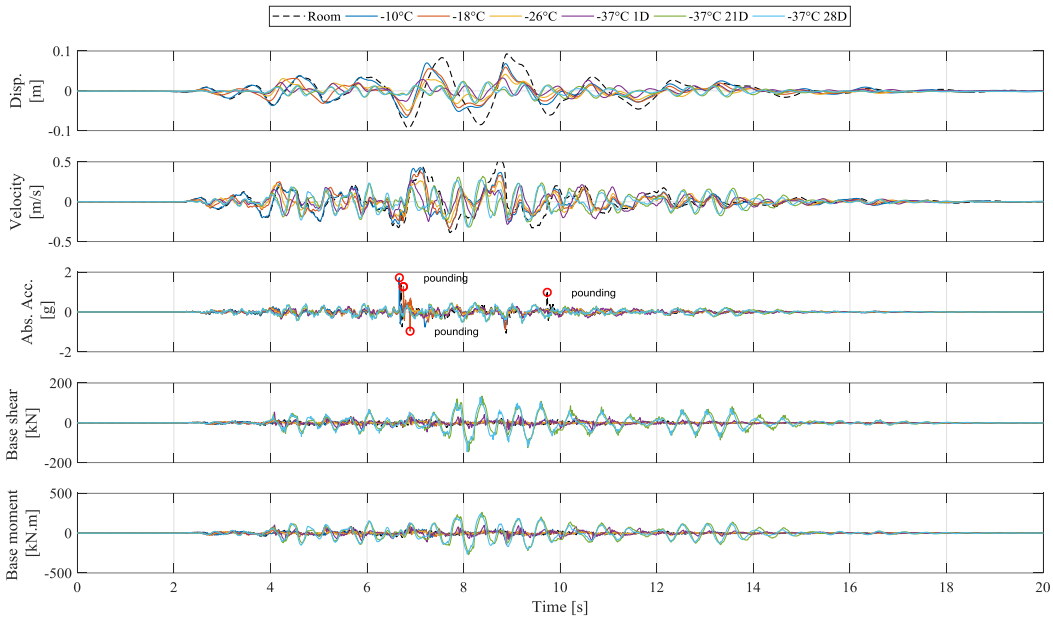

Figure 4.12. Response histories of the IS bridge at MCE level

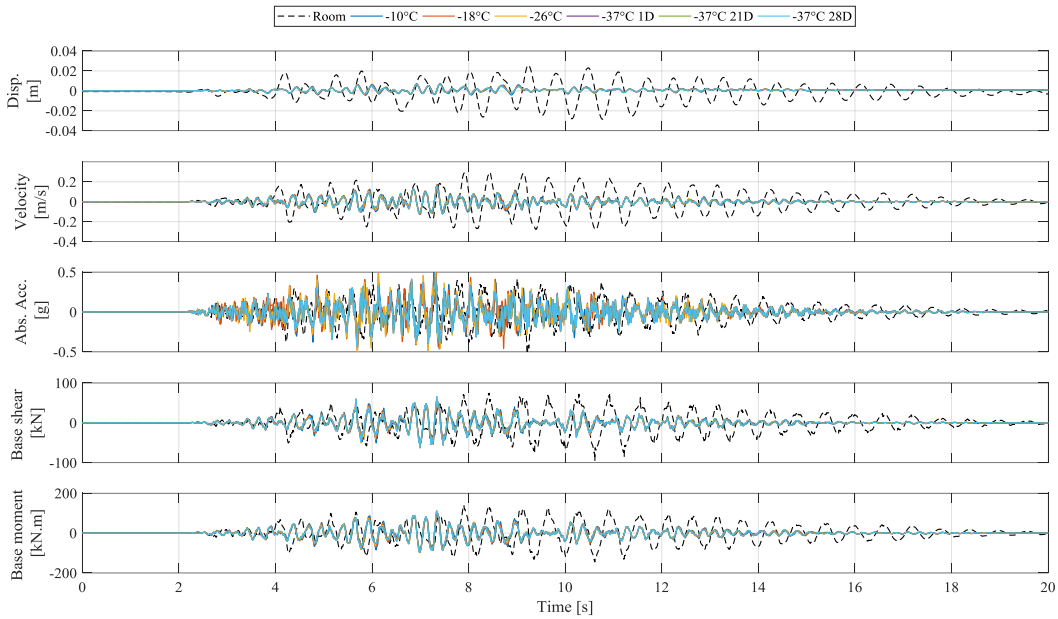

Figure 4.13. Response histories of the MS bridge at MCE level

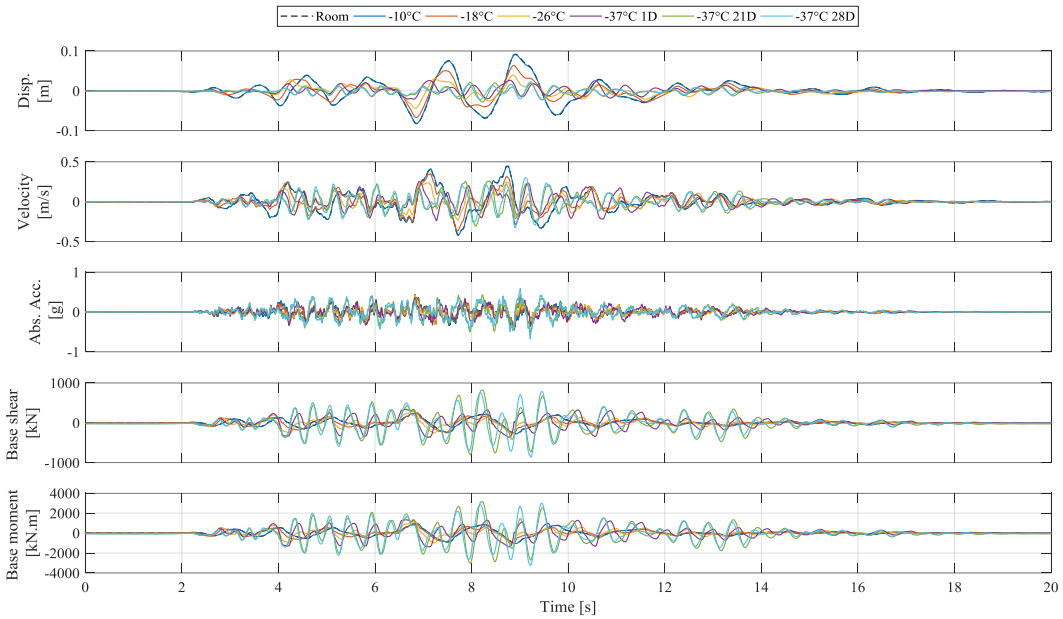

Figure 4.14. Response histories of the IF bridge at MCE level

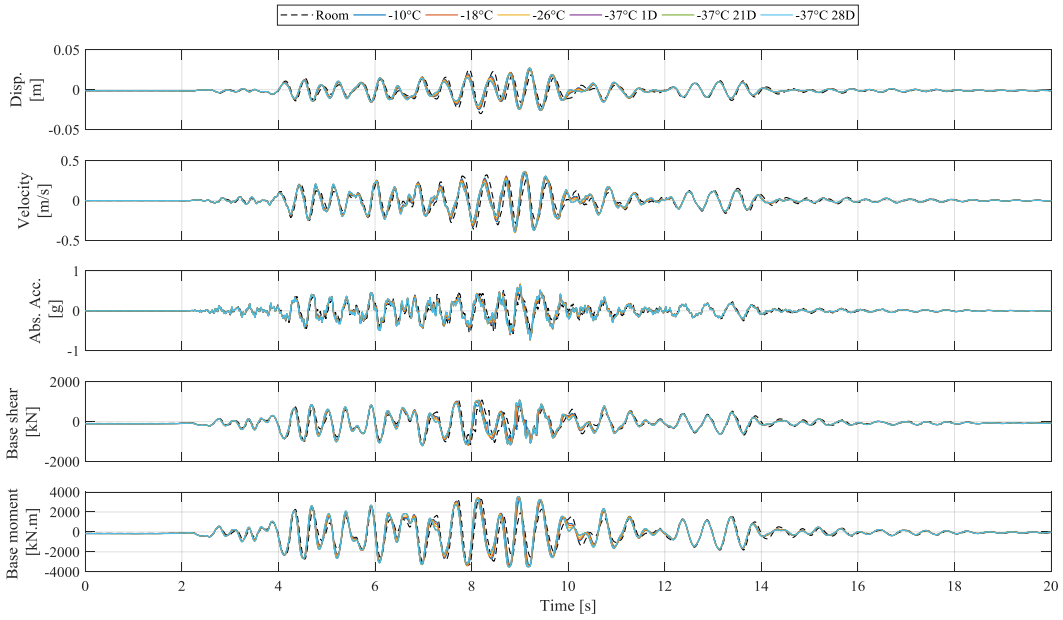

Figure 4.15. Response histories of the MF bridge at MCE level

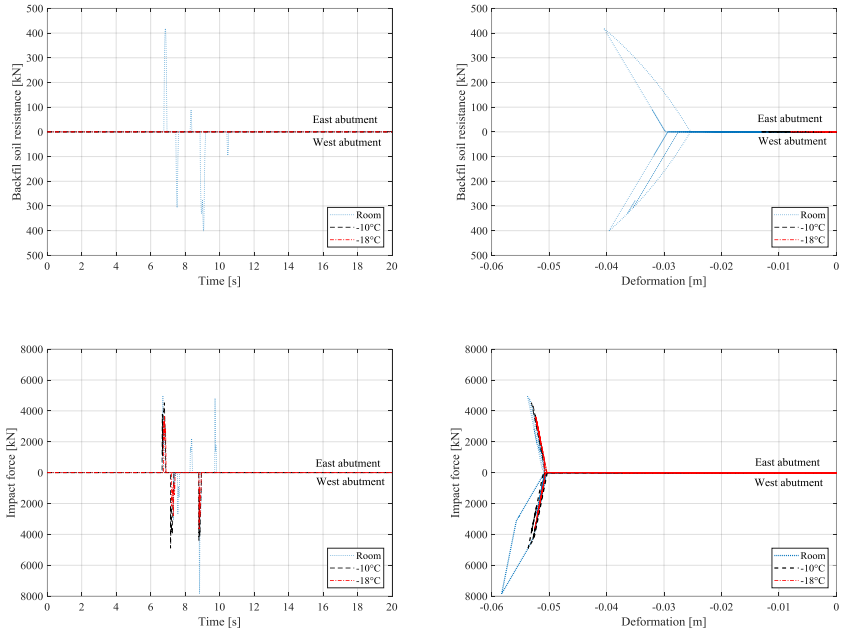

Figure 4.16. Pounding and backfill soil response history at MCE level

5 Summary, Conclusion, and Recommendations

Based on the research objectives outlined in the introductory chapter, a research program was completed and presented in a sandwich thesis format where each chapter comprises an article or manuscript that addresses one of the research objectives. This chapter completes the thesis by highlighting important findings of this work and recommends areas for further research on multi-hazard seismic performance assessment of bridges.

5.1 Summary

Seismic fragility analysis is a well-established tool for evaluating damage potential of bridge components. While researchers have utilized this tool for quantifying the seismic response of bridge systems, most of these studies are focused on generic bridges and fragility estimates of real bridges are limited. Furthermore, few studies have focused on seismically isolated bridges. Most of the seismically isolated bridges being investigated to date, use simplistic models for lead rubber bearings, friction bearings or steel reinforced elastomeric isolators, and to the author's knowledge, no studies have been conducted on real bridges retrofitted with fiber reinforced elastomeric isolators. To fill this gap, this thesis explored the seismic performance of a real bridge by constructing a comprehensive three dimensional model of the bridge, including all bridge components, namely, deck, abutments, columns, isolators, and pile groups, along with necessary interactions, such as abutment-embankment, soil-pile, and pile-soil-pile interactions. Based on the thesis objective three successive stages are completed to scrutinize the damage potential of bridge components and evaluate the effectiveness of the retrofit technique being applied. In the first stage, the bridge is modeled in its as-built condition in order to evaluate its seismic

performance and identify its most fragile components. A seismic isolation system is then introduced to the system to improve the seismic performance of the bridge and mitigate the seismic demand. Fragility curves are developed and compared for both systems and the effectiveness of the SU-FREI is investigated. In the second stage, the SSI effects are taken into account to address the coupled bridge-isolator-foundation-soil problem. To this end, pile groups under piers and abutments are added to the previously constructed numerical models (i.e. as-built and retrofitted bridges) to gauge the impact of the lateral behavior of soft soil on the seismic performance of bridges. Since the pile groups under piers and abutments are comprised of multiple closely-spaced vertical and battered piles, it is of high importance to consider the pile-soil-pile interaction in the lateral behavior of pile groups by applying reduction factors for the group effect and also the effect of batter. IDA is conducted and fragility estimates of different bridge components are evaluated and compared. In the final stage, the bridge models developed in the previous steps are exposed to a vast range of subfreezing temperatures and different durations of exposure in order to evaluate the seismic performance of bridges in cold temperature. The cold temperature behavior is extremely important for the Canadian cities which experience subfreezing temperatures for a significant number of days during a year. The cold temperature behavior of different constitutive materials of bridge components such as concrete, reinforcing steel, rubber, and soil are taken into account and the material behavior of these materials are altered in the numerical model to reflect the subfreezing behavior. Seismic fragility assessment is carried out in the context of IDA and damage potential of different bridge cases are evaluated. The findings of the work presented in this thesis and potential areas

for future research and development of bridge evaluation are outlined in the following sections.

5.2 Conclusions

5.2.1 Seismic performance of as-built and retrofitted bridges with fixed supports

Seismic performance of a conventionally designed bridge is evaluated by performing an IDA using 45 synthetic ground motion records in two orthogonal bridge directions, independently. Spectral acceleration at the fundamental period of the bridge ($S_a(T_1)$) is considered as the intensity measure (IM) and engineering demand parameters (EDPs) such as column drift, backfill soil deformation in active and passive actions, abutment deformation in transverse direction, and deck unseating are monitored. Two bridge cases are developed in this study; first, the as-built bridge which is referred to as the monolithic bridge because it is assumed that the deck and columns are connected monolithically, and second, the isolated bridge which is the bridge with SU-FREI installed between the deck and columns and deck and end abutments.

For the as-built bridge, backfill soil deformation in active action is the most fragile component by demonstrating a probability of damage from 78% to 8% from slight to extensive damage states. The second most fragile component is determined to be the backfill soil deformation in the transverse direction with damage probabilities ranging from 73% to 7.5% from slight to extensive damage states. Backfill soil deformation in passive action is the next fragile component by probabilities of damage within 14.5% to zero from slight to moderate damage states. Column drifts in both orthogonal bridge directions are observed not be prone to any damage by demonstrating a negligible probability of damage

at all damage states. Since damage to abutments are commonly cosmetic and do not result in bridge closure, it is concluded that the bridge has an acceptable behavior for the MCE hazard level in the region. The analysis also demonstrates that the residual displacements for all columns and abutments are within an acceptable range and do not result in considerable damage. However, reported deficiencies in column bases and foundation capacities necessitate evaluating the bridge performance retrofitted with SU-FREI.

Seismic isolation using SU-FREI resulted in a low probability of damage to columns in both the longitudinal and transverse directions for all damage states, whereas the probability of damage to abutments increased. Using SU-FREI has a relatively larger impact on the slight damage state and a smaller impact the on collapse damage state. The isolated bridge exhibited an increased median damage capacity of column drift in the longitudinal direction between 160% for slight to 44% for collapse damage state where this increase is 90% to 25% for the transverse direction. On the contrary, backfill soil deformation in active, passive, and transverse directions were found to have a decrease in their median damage capacity within a range of 80% to 54%. As expected, introducing the isolation system with a relatively low lateral stiffness permits the deck to experience larger displacements and as such, larger damage to abutments are anticipated. While the residual deformation of backfill soil in the isolated bridge is relatively larger with respect to the monolithic bridge, it is still within an acceptable range and does not jeopardize the bridge functionality.

For the MCE hazard level, it is demonstrated that seismic isolation using SU-FREI resulted in a 221% and 197% increase in the peak deck displacement in the longitudinal and

transverse directions, respectively, whereas its corresponding acceleration is decreased by 23% and 35%. Moreover, column base shear and moment decreased by 76% and 69% in the longitudinal and 81% and 71% in the transverse direction. Overall, isolation using FREI is demonstrated to be an effective approach for mitigating the column demands and reducing the acceleration of the superstructure. Therefore, it is shown that seismic isolation of the bridge can mitigate the seismic demand on the column bases and foundations.

5.2.2 Seismic performance of as-built and retrofitted bridges including the SSI effects

The previously modeled bridges are expanded on by introducing the pile groups under piers and abutments in order to evaluate the seismic performance of bridges on soft soil. In seismically isolated bridges, the effectiveness of the isolation system is a function of the relative stiffness of soil, columns, and the isolation system. As a result, there is no consensus in the literature whether isolating bridges located on soft soil improves or aggravates the seismic performance of those bridges (Jeremić, Kunnath, & Xiong, 2004; Mylonakis & Gazetas, 2000; Zhang & Makris, 2002). A Beam on Nonlinear Winkler Foundation (BNWF) method is implemented in order to simulate the lateral and vertical behavior of piles. In the lateral direction, p-y springs are utilized in both orthogonal directions of the bridge where forces were reduced to consider the effect of pile group and also to include the effect of batter for battered piles. In the vertical direction, the effect of skin friction is included using t-z springs to address any probable rocking or tipping of the pile group. In addition, a q-z spring is used to simulate the behavior of pile tip. The IM considered in this study is $S_a(T_1)$ and column drift, abutment soil failure in passive, active,

and transverse directions, pile foundation failure at piers and abutments, and unseating are the used EDPs. Seismic fragility assessment is carried out using IDA and 45 synthetic ground motion records.

While unseating did not take place in the monolithic bridge, the most fragile components are determined to be abutments due to their relatively large probability of damage as a result of abutment deformation in the transverse direction, abutment deformation in active action, abutment pile cap displacement in longitudinal direction, abutment pile cap displacement in the transverse direction, and abutment deformation in active action, respectively. The vulnerability of abutments stems from the relatively large masses of these components, which results high inertial forces in addition to the induced displacements from the deck. Column drifts and pier pile cap displacements in both orthogonal bridge directions demonstrated a negligible probability of damage. In the longitudinal direction and under the MCE hazard level, abutment pile caps experienced a maximum displacement of 0.04 m where vertical piles underwent larger lateral displacement with respect to battered piles. Moreover, a maximum mobilized soil reaction determined to be 50 kN and 40 kN in vertical and bettered piles, respectively. Pier pile caps demonstrated a maximum of 0.01 m where both vertical and battered piles exhibited the same response. However, the mobilized soil reaction of the transversely battered piles is larger with that of vertical and longitudinally battered piles by a factor of 50%. In the transverse direction, the pile cap displacements of both piers and abutments has decreased by a factor of 50%. It is shown that battered piles of the abutment pile groups experience a larger force with respect

to vertical piles. In the same fashion, transversely battered piles, longitudinally battered piles and vertical piles experienced the largest forces, respectively.

Like the monolithic bridge, abutments are the most fragile components of isolated bridge where all the corresponding probabilities of damage are increased due to the larger deck displacements. Abutment deformation in the transverse direction, abutment deformation in active action, abutment pile cep displacement in longitudinal direction, abutment pile cep displacement in the transverse direction, and abutment deformation in passive action are the most fragile components of abutments, respectively. On the other hand, columns and pier pile caps are completely prevented from excessive lateral displacements and the probability of damage to these components is zero for all damage states. In the longitudinal direction and under the MCE hazard level, abutment pile caps exhibited similar behavior to the monolithic bridge by experiencing a maximum displacement of 0.04 m where vertical piles undergo larger displacement. However, maximum mobilized soil reaction has increased by 20%, which was anticipated due to larger shear forces transferred from the deck to abutments. Piles under piers demonstrated a negligible displacement and shear force. While the piles under piers and abutments withstood smaller displacements and forces in the transverse direction in comparison with the monolithic bridge, their diagrams are following a same trend.

Overall, seismic isolation results in increasing the median of damage to columns within 182% to 38% in the longitudinal direction and within 234% to 81% in the transverse direction. Moreover, the median of pier pile cap displacement has increased within a range of 217% to 34% in the longitudinal direction and in a range of 203% to 25% in the

transverse direction. Similarly, median backfill soil deformation in passive action and in transverse direction are increased within 20% to 4.5% and within 10% to 4%, respectively. Where the transverse response of abutment piles is also improved by implementing the isolation system, the only adverse impact of this system is on the median of abutment pile cap displacement in longitudinal direction by 5%.

In terms of peak response history of the deck and columns, using the isolation system has increased the deck peak displacement by 242% and 260% in longitudinal and transverse directions, respectively. while the deck acceleration is decreased by 8% in the transverse direction, it is increased by 158% in the longitudinal direction due to the pounding of the deck and abutment. Peak base shear and moment of columns are also decreased by 71% and 56%, respectively.

5.2.3 Seismic performance of bridges in subfreezing temperatures

To address the third objective of thesis, seismic performance of the previously modeled bridges is investigated in the subfreezing temperature. To this end, the material properties of all mentioned bridges, namely, monolithic fixed base (MF), isolated fixed base (IF), monolithic with SSI effects (MS), and isolated with SSI effects (IS) are set to subfreezing temperatures. A cold temperature analysis matrix comprising a range of cold temperatures from -10ºC to -37ºC and different exposition durations in a range of 1 day to 28 days is developed. This matrix is developed based on the cold temperature provisions outlined in AASHTO (AASHTO, 2016) along with the climatic data of the region under study. A set of eight IDA is conducted in two orthogonal bridge directions by setting the material properties of constituent bridge components, such as concrete, steel, rubber, and soil, to

subfreezing temperatures and fragility curves are developed. While there is a limited number of studies on the seismic performance of bridges, none has investigated seismic performance on a coupled bridge-isolator-foundation-soil system. The IM considered in this study is $S_a(T_1)$ and column drift, abutment soil failure in passive, active, and transverse directions, pile foundation failure at piers and abutments, and unseating are the EDPs used.

Fundamentally, all constitutive materials of bridge components stiffen in cold temperatures. Concrete stiffens due to prestressing occurs due to filling capillary pores and micro-cracks by expanded water that has been turned into ice. Cold temperature yield and ultimate strengths of reinforcing steel can be approximated to be about 10-12% of the room temperature within a temperature range of -40°C to -25°C and then linearly decrease to zero at 0°C. Rubber, the main constituent of these isolators, undergoes two successive phases of stiffening called instantaneous thermal stiffening and crystallization where the former refers to a stage in which an immediate change in the stiffness of the elastomer occurs and the latter refers to a phase transition stage from an amorphous to a crystalline state after the elastomer is exposed to cold temperature for a sufficiently long time. The ice matrix formed in the frozen soil increases its ultimate compression and shear strength.

No damage is observed in the pier pile caps due to the relatively low demand on these components along with the stiffening of the soil domain due to the formation of ice at subfreezing temperature. In the longitudinal direction, results show that the damage to columns of the MF bridge is almost insensitive to temperature fluctuations which highlights the impact of cold temperature behavior of soil and isolator on the risk potential of bridge. For the MS bridge, the median of damage to columns has monotonically

increased by dropping the temperature from room to -37ºC for 28 days. The stiffening of the SU-FREI due to crystallization (conditioning the bridge to -37ºC for 1 to 28 days) has decreased the median of damage to columns of IS and IF bridges at slight and moderate damage states and increased the median of damage for extensive and collapse damage states. the median of column damage in transverse direction follows the same fashion except that crystallization results in a decrease in the median of damage to columns of IS and IF bridges for all damage states. As anticipated, the median of damage to abutments has increased monotonically by decreasing the temperature as the lateral stiffness of soil increases significantly as the temperature drops. The median of damage to abutments due to excessive soil deformation in active action has increased by decreasing the temperature for all damage states and bridge cases. The median of damage to abutments due to excessive soil deformation in passive action follows the same trend except for -26ºC where a spike in the median of damage is observed. Where no damage observed to the abutments of the IS and MS bridge in transverse direction, the median of slight damage of those bridges increased, monotonically.

5.3 Recommendations for Future Research

Despite the comprehensive nature of the work presented in this thesis, several aspects of multi hazard seismic performance assessment of bridges still require future study. It should be pointed out that the effect of different epistemic uncertainties is not considered in this study and this effect may be explored in future research. Potential areas for further research identified through the completion of this work are as follows:

- The findings observed from this thesis are based on a case study of a multi-span continuous reinforced concrete bridge in eastern Canada. To better study the detrimental effect of the isolation system on the abutment foundation, a more complex and physics-based spring system should be considered in future studies to better capture the dynamic interactions of abutment-embankment and abutment-foundation.
- This thesis is focused on seismic performance evaluation of a regular multi span continuous reinforced concrete bridge with straight deck and no skewness in the abutments. To quantify the effectiveness of isolating the superstructure using SU-FREI, a range of different bridges shall be investigated. These bridges include multi span simply supported bridges, steel bridges, bridges with irregularities, curved decks, and skewed abutments.
- Since a bidirectional numerical model of SU-FREI is not available, an experimental study may be conducted to develop bidirectional backbone curve for the SU-FREI and then the effects of bidirectional excitation of ground motions could be studied directly by applying the pairs of ground motions, simultaneously.
- Vertical ground motions records are excluded from the IDA and vertical contact behavior at the soil- structure interface have been simplified by q-z and t-z springs. Given the fact that SU-FREI is installed unbonded, it is possible that the seismic fragility is underestimated because of exclusion of vertical components of ground motions from the nonlinear dynamic analysis. Further investigations

should be conducted to evaluate the bridge performance under vertical ground motions.

- This thesis is focused on seismic risk assessment due to main-shock ground motions and does not account for the sequence of main-shock after-shock, aging and deterioration. The effect of aftershock, aging and deterioration, and material degradation should be investigated further.
- Although the effect of uncertainties on the fragility estimates of bridge components are taken into account to some extent, other factors of uncertainty such as material properties, geometric properties, etc. could be included in the future studies to obtain more accurate fragility estimates.

References

AASHTO. (2016). M 251-06 Standard Specification for Plain and Laminated Elastomeric Bridge Bearings: American Association of State Highway and Transportation Officials.

Jeremić, B., Kunnath, S., & Xiong, F. (2004). Influence of soil–foundation–structure interaction on seismic response of the I-880 viaduct. *Engineering Structures, 26*(3), 391-402. doi:https://doi.org/10.1016/j.engstruct.2003.10.011

Mylonakis, G., & Gazetas, G. (2000). Seismic soil-structure interaction: Beneficial or detrimental? *Journal of Earthquake Engineering, 4*(3), 277-301. doi:10.1080/13632460009350372

Zhang, J., & Makris, N. (2002). Kinematic response functions and dynamic stiffnesses of bridge embankments. *Earthquake Engineering & Structural Dynamics, 31*(11), 1933-1966. doi:10.1002/eqe.196